



Czech Technical University in Prague

Faculty of Civil Engineering

Department of Hydraulics and Hydrology

CML R-R modelling

Ing. Jaroslav Pastorek

Doctoral study programme:

Stavební inženýrství | Civil Engineering

Branch of study:

Vodní hospodářství a vodní stavby | Water Engineering and Water Management

Supervisor:

Ing. Vojtěch Bareš, Ph.D.

April 2022

Declaration

I hereby declare that this thesis has been composed by myself under the guidance of the supervisor Ing. Vojtěch Bareš, Ph.D.

I confirm that the thesis submitted is my own work and effort, except where work which has formed part of jointly-authored publications is included. My contribution and those of the other authors to such work are explicitly indicated in the thesis.

Any additional sources of information from which I have quoted or drawn reference have been referenced fully in the text and in the list of references.

.....
Jaroslav Pastorek

Acknowledgements

I would like to thank everyone who supported my work on this project. In particular, I would like to thank Vojtěch Bareš, Martin Fencl, and David Stránský from CTU in Prague, and also Jörg Rieckermann, Andreas Scheidegger, and others from Eawag.

I would also like to thank T-Mobile Czech Republic, a.s., for providing the CML data, and especially Pavel Kubík for assisting with our numerous requests. I would also like to thank Pražská vodohospodářská společnost, a.s., for providing rainfall data from their rain gauge network, and Pražské vodovody a kanalizace, a.s., for carefully maintaining the flow meter and the rain gauges inside the experimental catchment.

I would like to thank the team around the `ctuthesis LATEX` package which provided a template for this document.

The work on the thesis was supported by:

- the Czech Science Foundation (GAČR) under the projects no.
 - 14-22978S
 - 17-16389S
 - 20-14151J
- the Grant Agency of the Czech Technical University in Prague under the projects no.
 - SGS16/057/OHK1/1T/11
 - SGS17/064/OHK1/1T/11
 - SGS18/053/OHK1/1T/11
 - SGS19/045/OHK1/1T/11
 - SGS20/050/OHK1/1T/11

I owe a special thank you to Deep Thought for the answer to the ultimate question of life, the universe, and everything.

Abstract

We develop ...

Keywords:

Abstrakt

Rozvíjíme ...

Klíčová slova:

Překlad názvu: nejaký český text

Contents

1 Introduction	1	5.1 Introduction	32
1.1 Thesis outline	2	5.2 Methods	32
2 Rainfall monitoring for urban hydrology	5	5.3 Results	38
2.1 Requirements on rainfall data for urban hydrology	5	5.4 Discussion	41
2.2 Rainfall data retrieval and availability	6	5.5 Conclusions	42
2.3 Rainfall retrieval from commercial microwave links.....	8		
2.4 CML QPE uncertainties	9	6 The effect of link characteristics and their position on runoff simulations	45
2.5 Hydrological potential of CML QPEs	13	6.1 Introduction	46
3 Evaluation of rainfall data for urban hydrology	15	6.2 Methods	47
3.1 Prediction uncertainty quantification in hydrology	16	6.3 Results	50
3.2 Explicit statistical consideration of model bias	18	6.4 Discussion	55
3.3 Rainfall-runoff modelling performance assessment	22	6.5 Conclusions	58
4 Material	25		
4.1 Data retrieval and availability ..	26	7 Practical Approaches to Wet-Antenna Correction	61
4.2 Rainfall-runoff model and its reliability	28	7.1 Introduction	62
5 On the value of CML QPEs for urban rainfall-runoff modelling: The pilot study	31	7.2 Methods	63
		7.3 Results	68
		7.4 Discussion	73
		7.5 Conclusions	75
		8 On the value of CML QPEs for urban rainfall-runoff modelling: The final study	77
		8.1 Introduction	77
		8.2 Methods	78

8.3 Results	84
8.4 Discussion	90
9 Conclusions	91
9.1 bla	91
Appendix	93
Bibliography	97

Chapter 1

Introduction

As the driving phenomenon of runoff mechanisms, rainfall plays an essential role in urban hydrology (Berne et al., 2004). Due to high degrees of imperviousness, relatively small scales, and high land-use spatial variability in urban areas, small-scale spatial and temporal rainfall variability can affect the hydrological response in terms of the hydrograph shape, peak flows, and their timing (Cristiano et al., 2017; Ochoa-Rodriguez et al., 2015; Rico-Ramirez et al., 2015). Thus, when used as input for urban hydrological models, rainfall data represent one of the most prominent sources of uncertainty in the modelling process (Schellart et al., 2012; Thorndahl et al., 2008). Therefore, there are high requirements on the resolution of rainfall data for urban hydrology.

Operational management of the quantity and quality of urban stormwater runoff is a serious concern nowadays as excessive amounts of stormwater can overload drainage systems and cause urban pluvial flooding and health risks due to pathogens, decrease the efficiency of wastewater treatment plants, or impact the aquatic biota of receiving waters through hydraulic stress and pollution (Tsihrintzis & Hamid, 1997). The mitigation of such negative effects often relies on methods and concepts requiring operational rainfall products which are not only available in high spatial and/or temporal resolution, but also in real time (Einfalt et al., 2004).

Commercial microwave links (CMLs) are pairs of telecom antennas which operate at frequencies where radio signal is attenuated by rainfall droplets. The difference between the transmitted and received signal levels can be used to derive path-integrated quantitative precipitation estimates (QPEs). As a crucial part of telecom networks, CMLs densely cover urban areas around the world. Moreover, they can provide data in high temporal resolutions which are accessible in (near) real time from network operation centers either through network monitoring systems or specifically designed server-sided applications (Chwala et al., 2016). Therefore, QPEs derived from CMLs represent a very

promising rainfall data source for urban hydrological modelling. However, systematic errors often associated with CML QPEs, e.g. due to inaccurate wet antenna attenuation (WAA) estimation (Leijnse et al., 2008; Fencl et al., 2017), compromise their value for applications where volume is of high importance. Uncertainties associated with such errors thus represent a major challenge to be overcome.

Over the last decade, many research studies have addressed the uncertainties in the retrieval of CML QPEs. Thanks to the innovations introduced, CML QPEs have proven to provide valuable rainfall information which could complement traditional observations with rain gauges and weather radars (Chwala & Kunstmann, 2019; Gosset et al., 2016; Imhoff et al., 2020; Rios Gaona et al., 2018; Uijlenhoet et al., 2018). However, to date, only a few studies investigated the ability of QPEs derived from real-world CML networks for quantitative hydrology, either for rural (Brauer et al., 2016; Cazzaniga et al., 2020; Smiatek et al., 2017) or urban catchments (Disch et al., 2019; Stránský et al., 2018). This gap is addressed within the presented thesis.

■ 1.1 Thesis outline

This thesis is an extensive but not exhaustive presentation of research efforts conducted by Jaroslav Pastorek as part of his doctoral studies. The principal aim of these efforts was to robustly evaluate the potential of QPEs from CMLs for hydrological modelling in small urban catchments. In order to reach the highest quality of CML QPEs, possibilities of reducing the uncertainties in the CML QPE retrieval were also intensively studied.

First, in chapter 2, the thesis provides an overview of recent developments and the current state of rainfall monitoring in urban areas for quantitative hydrological purposes. Retrieving QPEs from CMLs is introduced as a promising way of obtaining high-resolution rainfall measurements, which, however, is associated with considerable uncertainties. Recent approaches to reducing these uncertainties are reviewed while acknowledging space for further improvements.

Different approaches to assessing the value of given rainfall data for urban hydrology are analyzed in chapter 3. A special attention is payed to the importance of robust uncertainty evaluation when performing hydrological modelling. The model output uncertainty quantification method which is to be applied within the presented research is described in detail.

Material used when performing simulations and analyses which resulted in this thesis is presented in chapter 4. This includes an extensive data set

spanning over three years and containing both rainfall and runoff observations as well as a calibrated well-performing rainfall-runoff model.

Chapter 5 presents a study which explores whether QPEs obtained from CMLs can be regarded as a viable source of rainfall data in the field of urban rainfall-runoff modelling. This study can be understood as "the pilot study" which foreshadows the direction of the subsequent research endeavors. This chapter represents a synthesis of two studies first published in Pastorek et al. (2017) and Pastorek et al. (2018).

Chapter 6 presents a study which addresses the ability of individual CMLs to provide relevant QPEs for urban rainfall-runoff modelling. It investigates in how far CML instrumental parameters (path length, transmission frequency) and network topology influence the rainfall-runoff modelling performance. This study was first published in Pastorek et al. (2019b).

Chapter 7 contains a study which analyzes how, when deriving CML QPEs, WAA can be estimated without dedicated rainfall monitoring. Various WAA estimation models, including a newly proposed one, based on considerably different assumptions are tested. The transferability of WAA model parameters among CMLs of various characteristics is also addressed. This study was first published in Pastorek et al. (2022)

Chapter 8 introduces a study which explores the possibility to calibrate WAA estimation models using data that could be commonly available to many urban hydrology specialists. This investigation is then leveraged to derive state-of-the-art CML QPEs, the suitability of which for urban rainfall-runoff modelling is then to be robustly evaluated by means of model output uncertainty quantification.

The bulk of the research presented in this thesis has been originally published in peer-reviewed journal or conference papers over the course of the past few years. Thus, the thesis also partially documents the development in the current state of knowledge in the area. Therefore, especially when the chapters 5 and 6 are considered, the reader is kindly asked to perceive the presented research in the context of the time when it was first published.

Chapter 2

Rainfall monitoring for urban hydrology

2.1 Requirements on rainfall data for urban hydrology

From the hydrological point of view, urban catchments differ from natural ones in two fundamental aspects. Firstly, scales of areas examined in urban and natural catchment hydrology typically differ in orders of magnitude. Secondly, urban areas are covered by a high ratio of impermeable surfaces that not only limit rainfall infiltration, but also lead to more surface runoff (e.g. causing higher peak flows) and a faster response of the runoff process. Therefore, requirements on both temporal and spatial resolution of rainfall data are notably higher in urban catchments (e.g. Schilling, 1991; Berne et al., 2004). These requirements will further vary depending on the catchment size (Ochoa-Rodriguez et al., 2015), the climatic region (Berne et al., 2004), intended application (e.g. long-term analysis vs. online nowcasting Einfalt et al., 2004), or hydrological model complexity (semi- vs. fully-distributed Gires et al., 2015).

Berne et al. (2004) found that hydrological applications in urban catchments of the order of 1 km^2 require a resolution of about 3 min and 2 km. Notaro et al. (2013) concluded that temporal resolutions below 5 min and spatial resolutions of one rain gauge for each 1.7 km^2 is required. Ochoa-Rodriguez et al. (2015) recommended using rainfall temporal resolutions below 5 min and spatial resolution about 500 m for drainage areas between 1 ha and 100 ha, whereas 1-km resolution is recommended for drainage areas larger than 100 ha. Moreover, the growing interest in fully distributed and grid-based models (Ochoa-Rodriguez et al., 2015; Ichiba et al., 2018), developments in geographic information systems, ever increasing data availability and computational

power is expected to further strengthen the need for high-resolution rainfall data (Ochoa-Rodriguez et al., 2019; Salvadore et al., 2015).

Mitigation of the negative effects of urban drainage on society and the environment is nowadays often related to methods and concepts requiring operational rainfall products which are not only available in high spatial and/or temporal resolutions but as well in (near) real time (Einfalt et al., 2004). Such rainfall observations are employed in real-time control strategies to optimize treatment processes at wastewater treatment plants (Schütze et al., 2004), or to minimize the impacts of sewer overflows (Vezzaro & Grum, 2014). Furthermore, these data are used for extreme event analyses, e.g. for the evaluation of insurance damage claims (Spekkers et al., 2013) or for operational warnings (Montesarchio et al., 2009). Operational rainfall data are becoming increasingly important because of the ongoing climate change (van der Pol et al., 2015) as the intensity and frequency of heavy rainfall in many areas around the world are expected to increase (Willems et al., 2012).

2.2 Rainfall data retrieval and availability

Tipping bucket rain gauges represent the traditional way of retrieving precipitation measurements in urban areas. These devices provide relatively accurate rainfall estimates near the ground surface. On the other hand, they are prone to considerable uncertainties due to wind (Nešpor & Sevruk, 1999) and, especially relevant in urban conditions, obstructions by surrounding objects. Moreover, rain gauge records are in general representative only for a limited spatial extent. For instance, in a case study in northern Israel, Peleg et al. (2013) found that at least three rain stations in a specific configuration are needed to represent the rainfall data from a radar pixel of roughly 1.5 km² with a temporal resolution of about 3 min. Thus, due to their low densities, rain gauge networks very often fail to provide sufficient information on the rainfall with high spatiotemporal variability (Villarini et al., 2008). Moreover, these errors resulting from approximating an areal estimate using point measurements increase substantially with the decreasing aggregation time (Wood et al., 2000).

The development and use of weather radar quantitative precipitation estimates (QPEs) for hydrological applications has increased in recent decades (Berne & Krajewski, 2013; Thorndahl et al., 2017). Radars can survey large areas while providing rainfall data in resolutions of 500–2000 m every 5–15 min (Thorndahl et al., 2017). New generation X-band radars (e.g. Chen & Chandrasekar, 2015; Schleiss et al., 2020) can measure at even higher resolutions, but with a shorter range. However, weather radars provide indirect rainfall estimates measured hundreds of meters above ground relatively far away from the radar itself. Due to these inherent limitations of radar as a

rainfall measurement tool, the accuracy of radar measurements is in general insufficient, particularly in the case of extreme rainfall magnitudes (Bárdossy & Pegram, 2017; Thorndahl et al., 2017). Therefore, radar QPEs require adjustment to ground observations obtained typically from rain gauge networks (Harrison et al., 2009), although other data including urban stormwater runoff measurements have been employed as well (Ahm & Rasmussen, 2017).

The usage of weather radars for urban water management applications has been extensively investigated in the past decades and substantial progress has been made towards reliable high-quality data, however, many challenges remain unresolved. For example, adjusting radar data in an operational mode is both a methodological and technical challenge because rain gauge data are often delivered with a delay. Similarly, it is difficult to quantify uncertainty arising from the discrepancy between the catch area of a rain gauge (in the order of 10^{-2} m²) and the area of a radar pixel (in the order of 10^4 – 10^6 m²) (e.g. Anagnostou et al., 1999). Nevertheless, many innovative radar-rain gauge merging techniques, which aim at combining the advantages while partially overcoming the individual weaknesses of the two data sources, have been recently developed (McKee & Binns, 2016). Such methods seem to have the potential to significantly improve the quality and applicability of radar and rain gauge rainfall estimates for hydrological tasks, however, there are still considerable challenges specific to urban applications, such as the availability of rain gauge data (or other ground truth) in adequate resolutions (Ochoa-Rodriguez et al., 2019). Next, the small-scale spatial structure reflecting local rainfall extremes, critical for urban hydrology applications, is often not preserved after the adjustment (Wang et al., 2013; Borup et al., 2016; Ochoa-Rodriguez et al., 2019).

Lastly, the availability of weather radars is mostly limited to most developed countries, where, however, there are still observational gaps with radar observations not available in the desired spatiotemporal resolution (Heistermann et al., 2013; Saltikoff et al., 2019). The same holds also for the traditional rain gauge data, for which, moreover, a decrease in their availability has been observed in many areas around the world (Lorenz & Kunstmann, 2012; Sun et al., 2018). Actually, adequate rainfall data are in general lacking for most of the Earth's land surface. Global precipitation data sets can be obtained from satellite missions, but the accuracy and spatiotemporal resolution of these observations are still insufficient to be used in the hydrological modelling of small, mountainous or urban catchments (Kidd & Huffman, 2011). Thus, in order to increase the quality and availability of rainfall data, much effort has been invested in investigating alternative innovative data sources.

One possibility to overcome the above challenges regarding the rainfall data retrieval could be to make use of the recent development of various accessible hardware and software solutions which has made measurements with special purpose sensors widely available throughout many different fields (Swan,

2012). For example, there are numerous online amateur weather networks that aggregate and visualize citizen-contributed weather observations (Gharesifard et al., 2017; de Vos et al., 2017). However, quality control of such crowdsourced data (and associated metadata) from amateur weather stations is extremely challenging since these devices are often uncalibrated or irregularly maintained. Furthermore, as with radar rainfall observations, this kind of data is primarily available in developed regions only.

Rainfall data from new types of devices which could conveniently complement traditional precipitation observation networks and, thus, improve rainfall data availability, can also be obtained using so-called “opportunistic sensing” (Tauro et al., 2018). Opportunistic precipitation sensing can be performed using devices which are not constructed primarily for rainfall observation, e.g. telecommunication infrastructure or building automation sensors. Such devices are often connected to centralized communication infrastructure, so the data can be queried in (sub-)minute intervals. This is also the case of commercial microwave links whose millimeter-wave radio signal is attenuated by rainfall droplets and which densely cover urban areas worldwide and could, thus, provide urban hydrologists with rainfall data of high spatiotemporal resolutions.

2.3 Rainfall retrieval from commercial microwave links

Commercial microwave links (CMLs) are point-to-point radio connections widely used as cellular backhaul. A substantial part of CML networks is operated at frequencies between 20 and 40 GHz where radio wave attenuation caused by raindrops is almost proportional to rainfall intensity. These CMLs can, therefore, be used as unintended rainfall sensors providing path-integrated quantitative precipitation estimates (QPEs). Although deriving precipitation estimates from the attenuation of microwaves was originally suggested several decades ago (Atlas & Ulbrich, 1977), the idea has experienced a renaissance in recent years, thanks to the extensive growth of cellular networks (Messer et al., 2006; Leijnse et al., 2007) which frequently incorporate CMLs.

The relationship between raindrop-induced attenuation A_r [dB] and rainfall intensity R [mm/h] is robust and well-understood. For a given rainfall intensity, A_r is proportional to CML length and frequency. The relation can be expressed using the following approximation:

$$R = \alpha(A_r/L)^\beta, \quad (2.1)$$

where L [m] is the length of a given CML, and α [mm/h km $^\beta$ dB $^{-\beta}$] and β [-] are empirical parameters dependent upon CML frequency and polarization,

and drop size distribution (Olsen et al., 1978). The fraction A_r/L can be expressed as a single variable – specific raindrop attenuation γ [dB/km].

Nonetheless, A_r must be separated from other components of the difference between the transmitted and received signal levels $TRSL$ [dB], for whose purposes the following relation is often used:

$$TRSL = B + A = B + A_{wa} + A_r \quad (2.2)$$

where B [dB] represents baseline attenuation consisting of, e.g., free space loss and gaseous attenuation, A [dB] stands for observed attenuation after baseline separation, and A_{wa} [dB] represents wet antenna attenuation (WAA). Imprecise quantification of the raindrop-induced attenuation A_r due to CML rainfall retrieval uncertainties such as WAA estimation represents a considerable source of errors in CML QPEs (Chwala & Kunstmann, 2019) and a major challenge to their hydrological applications.

2.4 CML QPE uncertainties

Most uncertainties associated with the retrieval and application of CML QPEs could be categorized as either:

- Uncertainties associated with rainfall retrieval from individual CMLs; or
- Uncertainties associated with spatial information processing and its representativeness in relation to the location/area of interest.

2.4.1 Uncertainties in QPE retrieval from individual CMLs

Uncertainties in QPE retrieval from individual CMLs can be linked with $TRSL$ measurements (quantization, hardware imperfections), with the separation of raindrop-induced attenuation A_r from other sources of attenuation (Eq. 2.2), and with the transformation of the attenuation data into rainfall intensities (Eq. 2.1). The most prominent error sources include in particular: too coarse temporal sampling, quantization of $TRSL$ values, uncertainty regarding the baseline level and regarding the WAA estimation, with the latter two being most important for systematic errors (bias) in the estimated rain rates (Leijnse et al., 2010; Zinevich et al., 2010; Chwala & Kunstmann, 2019).

Baseline B can be identified by interpolating from dry-weather attenuation levels (Overeem et al., 2011; Schleiss & Berne, 2010). Alternatively, a low-pass filter of the $TRSL$ time series can be applied (Fenicia et al., 2012). Although

the latter approach has shown to improve CML QPEs when compared to using a constant baseline, it “might produce dynamics similar to the temporal evolution of an anticipated rain-rate-dependent WAA effect” (Chwala & Kunstmann, 2019), and thus interfere with the WAA estimation. Nevertheless, the baseline is relatively stable, whereas antenna wetting is a complex dynamic process which has not been yet completely understood (Schleiss et al., 2013, more in next subsection).

QPEs are more prone to be contain systematic errors for CMLs with shorter path lengths and lower frequencies (Leijnse et al., 2008). These CMLs are less sensitive to rainfall, and raindrop-induced attenuation A_r thus constitutes only a relatively small part of the observed TRSL (Eq. 2.2). In other words, QPEs from these CMLs are more sensitive to errors in the process of A_r estimation. Let us illustrate this problem with a brief didactic example.

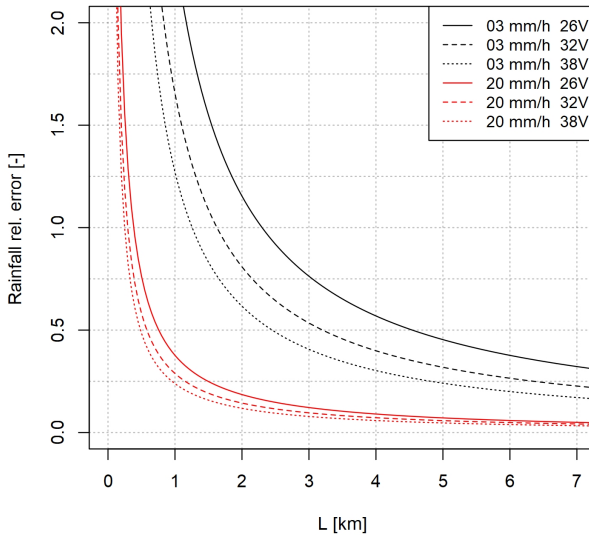


Figure 2.1: The relative error in QPEs from CMLs with vertical polarization in relation to CML path length for two rainfall intensities (3 and 20 mm/h) and three CML frequencies (26, 32, 38 GHz) as caused by an error of 1 dB in the estimate of A_r due to instrumental uncertainties.

For a 1-km-long CML working at a frequency of 32 GHz, the raindrop attenuation A_r caused by the rainfall of 20 mm/h is about 4 dB. However, for a CML with the same frequency and a path length of 4 km, A_r equals roughly 15 dB. If A_r is overestimated by 1 dB, a common value due to the instrumental uncertainties, the derived precipitation rate is overestimated by approximately 30% for the 1-km CML, and by 10% for the 4-km one (see Fig. 2.1). This becomes worse if the rainfall intensity is only 3 mm/h, because the relative errors in CML QPEs rise to 175% and 40% for the 1-km and 4-km CMLs respectively. Furthermore, for low rainfall rates, the derived rainfall is very sensitive to the CML frequency, and thus higher errors are associated with lower frequencies.

■ Wet antenna attenuation

Wet antenna attenuation (WAA) is, in contrast to raindrop-induced attenuation A_r and baseline B , independent of CML path length. Previous studies (Leijnse et al., 2008; Overeem et al., 2011) have also suggested that it is relatively insensitive to CML frequency at bands suitable for rainfall retrieval (20–40 GHz). However, antenna wetting is influenced not only by rainfall, but by other atmospheric conditions (e.g. wind, temperature, humidity or solar radiation) and also antenna hardware properties (e.g. antenna radome material or coating; van Leth et al., 2018). Due to this complexity of the antenna wetting process, reliable WAA estimation remains to be challenging (Chwala & Kunstmann, 2019).

To date, there is no unified approach to estimate WAA and reported WAA models are often based on different assumptions and result in considerably different estimates. For example, drying times of up to several hours have been reported (Schleiss et al., 2013), whereas other studies have not considered any wetting or drying dynamics at all, relating WAA only to rainfall intensity (Valtr et al., 2019; Kharadly & Ross, 2001).

It has also been suggested to estimate WAA based on water quantity and distribution (droplets, rivulets, water film) on antenna radomes (Leijnse et al., 2008; Mancini et al., 2019). Recently, it has been shown that WAA can be estimated using antenna reflectivity acting as a proxy variable for water film thickness (Moroder et al., 2019). However, applying this model is significantly limited by the unavailability of the required antenna reflectivity measurements.

Since having a globally valid WAA model only depending on known CML characteristics such as frequency does not seem possible, optimal WAA models should ideally be determined for each individual CML. This is especially true for models whose parameters depend on CML path length (e.g. Kharadly & Ross, 2001). However, optimal WAA model identification (e.g. for calibration purposes) on the level of individual CMLs is challenging, especially for real-world application with networks consisting of a high number of CMLs. As noted by (Ostrometzky et al., 2018), maintenance of dedicated equipment for the retrieval of the needed reference rainfall observations is impractical for such networks.

Due to all the above-discussed issues, application-focused studies with city or regional-scale CML networks have often not applied any WAA correction at all (Chwala et al., 2012; Smiatek et al., 2017) or have used only a simple constant offset model (Overeem et al., 2011; Roversi et al., 2020; Fencl et al., 2020). Although the latter approach may be a reasonable choice when only 15-min *TRSL* maxima and minima are available (Chwala & Kunstmann, 2019),

it can introduce considerable bias in the resulting CML QPEs (Fencl et al., 2019).

Adopting a different approach to the challenge of WAA estimation, Fencl et al. (2017) proposed continuous adjusting of A_{wa} representing WAA and α (Eq. 2.1, 2.2) to measurements from traditional rain gauges, if these are available in the vicinity of CMLs. They have shown that such adjusted high-resolution CML QPEs can, in spite of underestimating peak rainfalls, outperform the gauge data used as the adjusting reference.

Alternatively, prior calibration to reference rainfall data seems to be a reasonable way to achieve reliable WAA models. However, reference rainfall retrieval approaches employed in research studies which include intensive monitoring campaigns (e.g. Schleiss et al., 2013; van Leth et al., 2018) are impractical for high numbers of CMLs due to the costs associated with the dedicated equipment needed. Alternatively, already existing rain gauge networks or high-resolution weather radars might be used to calibrate the WAA models. However, as discussed above, such rainfall data sources are often not readily available to urban hydrologists. Moreover, the potential usefulness of CML QPEs increases with the decreasing availability of other rainfall (or other reference) data. Thus, it would come handy if WAA models could be calibrated using better available data and tools, such as low resolution rainfall measurements or stormwater discharge observations in combination with a rainfall-runoff model.

■ 2.4.2 Spatial uncertainties

Other uncertainty type arises from the spatial processing of rainfall information, e.g. algorithms used to transform path-integrated QPEs from individual CMLs to spatially distributed (typically gridded) rainfall maps (e.g. Overeem et al., 2013; Rios Gaona et al., 2018), and from the rainfall data representativeness in relation to the location/area of interest, given by the spatial relations between the CMLs and the area of interest and by the spatiotemporal rainfall variability. It has been observed that spatial (or mapping) uncertainties are relatively small compared to rainfall retrieval uncertainties (Rios Gaona et al., 2015). Nonetheless, the role of these uncertainties should not be ignored, especially if QPE retrieval uncertainties are successfully reduced.

Several more or less sophisticated methods of rainfall field reconstruction from the path-integrated CML QPEs have been introduced (e.g. Goldshtain et al., 2009; D'Amico et al., 2016; Haese et al., 2017). Nevertheless, spatial rainfall field reconstruction remains unappealing for some CML QPE hydrological applications, e.g. when using lumped or semi-distributed models and/or modelling hydrological processes in a catchment the size of which is similar to (or smaller than) the size of a rainfall grid cell.

For such tasks where areal rainfall estimates are satisfying and several CMLs are at hand, the influence of different CML topologies on the estimated areal rainfall has been investigated (Fencl et al., 2015) with a conclusions that combining QPEs from all available CMLs can very well capture the rainfall and is recommended when no prior information on CML data quality is available. However, at the same time, only a few very precise (i.e. least biased) CMLs are expected to deliver the most accurate areal rainfall data and, thus, CMLs used to derive areal rainfall should be ideally selected very carefully (Fencl et al., 2015). However, if the bias in QPEs is relatively comparable among the available CMLs, it is not clear how to identify optimal subsets of CMLs in such conditions; whether, for substance, the CML spatial relations with the area of interest can be used as the only decisive criteria.

2.5 Hydrological potential of CML QPEs

CML QPEs have a path-integrated character which makes them better suited for capturing rainfall spatial variability over a catchment than rain gauges. Moreover, unlike weather radars, they observe rainfall close to the ground. Recently, there were about four million CMLs being used worldwide within cellular networks and the number has been increasing (Ericsson, 2016). Exploiting this infrastructure for rainfall detection does not necessitate substantial additional investments. Moreover, CML data can be accessed online in high temporal resolutions and in (near) real time from network operation centers either through network monitoring systems or specifically designed server-sided applications (Chwala et al., 2016). Thanks to the dense coverage of urban areas, CMLs represent very promising rainfall sensors for urban hydrological modelling.

In fact, thanks to the intensive recent research, especially regarding the uncertainties in their retrieval, CML QPEs have proven to provide valuable rainfall information which could complement traditional observations with rain gauges and weather radars (Chwala & Kunstmann, 2019; Gosset et al., 2016; Imhoff et al., 2020; Rios Gaona et al., 2018; Uijlenhoet et al., 2018). However, despite the high potential and recent advances, only a few studies have investigated the ability of QPEs derived from real-world CML networks for quantitative hydrology, either for rural (Brauer et al., 2016; Cazzaniga et al., 2020; Smiatek et al., 2017) or urban catchments (Disch et al., 2019; Stránský et al., 2018). Therefore, many questions remain unresolved.

The studies from urban environments (Disch et al., 2019; Stránský et al., 2018) have suggested that, if available in high temporal resolutions, CML QPEs in combination with other rainfall data could be conveniently used to predict rainfall runoff. Nevertheless, CML QPEs could be particularly useful in regions where long-term rainfall monitoring networks are not available,

2. Rainfall monitoring for urban hydrology



or available only in resolutions which do not suffice for most purposes of urban hydrological modelling (Gosset et al., 2016). Yet, it is not clear how to make the best use of CML QPEs under such conditions, as their potential of a stand-alone rainfall sensors for hydrological applications is compromised by systematic errors common in the QPEs, especially those from shorter CMLs (Leijnse et al., 2008).

Chapter 3

Evaluation of rainfall data for urban hydrology

It is a common approach (e.g. Fencl et al., 2015, 2017; Rios Gaona et al., 2015; Graf et al., 2020) to evaluate and benchmark rainfall data by a direct comparison with a reference (or best-case scenario) rainfall data set. However, the limited or unknown representativeness of the reference rainfall data, compared to the true incident rainfall, represents a major uncertainty. If one was about to evaluate a data set which would better describe the ground-truth precipitation than the reference rainfall data, the potential improvement could not be discovered. Even if high-quality precipitation measurements, e.g. from a relatively dense network of rain gauges, are used as the reference, the information about precipitation included in such data can differ significantly from the true rainfall over a given area. This could be very limiting when evaluating rainfall data of unknown characteristics.

River and drainage system discharges closely reflect transformed rainfall aggregated for a whole given catchment. Especially in urban areas, stormwater runoff can be considered as a proxy variable of the catchment areal rainfall. Furthermore, stream discharges are typically measurable more reliably than the true incident precipitation over the given area. This can be especially useful in the case of convective precipitation when the true incident rainfall over a given area is often difficult to estimate using traditional reference rainfall measurements. Therefore, when evaluating the suitability of rainfall data sets for purposes of rainfall-runoff modelling, using a rainfall-runoff model and runoff observations as the reference is a common approach. This was done also in the studies of Obled et al. (1994), Segond et al. (2007), or Sikorska & Seibert (2018) which investigated natural catchments. Focusing specifically on urban rainfall-runoff modelling, Goormans & Willems (2013) and Wang et al. (2015) evaluated the suitability of weather radar data sets, and (Kleidorfer et al., 2009) studied the impact of artificially created imperfections in rainfall

data on model parameters. Nevertheless, this approach is not employed in every study with similar goals.

Ochoa-Rodriguez et al. (2015) analyzed the impact of spatial and temporal resolution of rainfall inputs on urban hydrodynamic modelling. In this study, model outputs obtained using various rainfall data sets were evaluated using, as the reference, model outputs associated with the finest resolution rainfall estimates. Nevertheless, when using this approach, similar issues as discussed above, regarding the representativeness of the reference, can arise. Furthermore, it is unclear whether the best-quality rainfall data lead to the best model performance in some circumstances, e.g. when the model used was calibrated using another rainfall data set.

Berne et al. (2004) investigated spatiotemporal rainfall-runoff dynamics in Mediterranean urban areas in relation to, among others, rainfall data integration to various temporal resolutions. The relation between the precipitation and runoff was only quantified using the lag time, i.e. “the time difference between the gravity centre of the mean rainfall over the catchment on one hand and the gravity centre of the generated hydrograph on the other hand”.

3.1 Prediction uncertainty quantification in hydrology

Additional uncertainties are introduced into the process of rainfall data evaluation when hydrological modelling is employed. It has been argued that ignoring the uncertainty, particularly related to input data, compromises (not only) hydrological modelling (Beven, 2006; Kavetski et al., 2006), or similarly, that quantification of the uncertainty associated with the models in urban stormwater modelling is a must (Dotto et al., 2012). However, quantifying the effect of all principal uncertainty sources (or, specifically, the effect of uncertainty related to rainfall data) on rainfall-runoff modelling results is a complex and challenging task. Therefore, though conceptually desirable, it is rarely practiced (Dotto et al., 2012). Researchers have often decided, instead, to put effort to maximize the reliability of modelling results, e.g. by using data measured over a long period of time (Segond et al., 2007), or by employing “verified and operational models” (Ochoa-Rodriguez et al., 2015).

Deletic et al. (2012) reviewed studies investigating uncertainty in urban hydrological modelling and identified the following key uncertainty sources:

1. Model input (measured input data and parameters) uncertainties;

2. Calibration (calibration data measuring, availability, and choices; calibration algorithms and objective functions used in the calibration process) uncertainties;
3. Model structure (conceptualisation errors, equations and numerical methods) uncertainties.

Many published urban drainage modelling studies have dealt with uncertainties associated with model parameters, often producing parameter probability distributions and estimating confidence intervals around the model's outputs (e.g. Thorndahl et al., 2008; Dotto et al., 2012). However, Deletic et al. (2012) recognized that the uncertainty sources are highly interlinked, suggesting that assessing the impact of a single source is not going to be adequate and that simultaneous propagation of key sources of uncertainties is required.

Dotto et al. (2012) observed that a common approach when trying to estimate the total uncertainty (related to parameters and all other sources) is adding a Gaussian error term to the model predictions. This approach is based on the assumption that the residuals between the measured and modelled values are normally distributed (i.e. only due to white measurement noise). However, the deviations of model outputs from observed data are usually considerably larger than random observation errors, typically due to a simplified description of the system by the deterministic model and due to input data imperfections (Reichert & Schuwirth, 2012). When ignored, such systematic deviations can lead to unrealistic (usually too narrow) uncertainty bounds of model parameters and model predictions (Reichert & Schuwirth, 2012).

Systematic deviations of model predictions from observed data, or model bias, can be addressed by increasing the complexity of the model to reduce bias or by trying to find a statistical description of the bias in model outputs. Reichert & Schuwirth (2012) adapted a statistical technique of Kennedy & O'Hagan (2001), accounting for bias in model outputs, for purposes of environmental modelling and extended it with a framework enabling for multiobjective model calibration. Sikorska & Seibert (2018) used this approach to asses the value of different precipitation data for flood prediction in an alpine catchment. Del Giudice et al. (2013) applied this technique to urban drainage modelling while proposing various formulations of the stochastic process representing the model bias (more in section 3.2). Their results showed that runoff simulations are much more reliable when bias is accounted for than when it is neglected.

While approaches based on explicit model bias consideration can improve the reliability of hydrological predictions, they only provide limited information about the causes of model bias and, therefore, do not help much to distinguish imperfections in input rainfall data from model structural errors (Del Giudice et al., 2013). A conceptually more satisfying approach is to make the input uncertain and to propagate it through the model. This can be done by using

so-called rainfall multipliers (Kavetski et al., 2006; Vrugt et al., 2008). These random variables multiply observed rainfall rates (1 multiplier per event) before feeding it into the model. They are estimated together with other model parameters and allow to quantify the rainfall-related uncertainty directly in input data. Sikorska et al. (2012) combined a stochastic error model with rainfall multipliers to separate the effect of uncertainty in the rainfall data from other errors sources. However, the rainfall multiplier approach fails when the observed precipitation has a different temporal pattern from the true one or if the true nonzero rainfall is not detected (Del Giudice et al., 2016).

To overcome the above problem, Del Giudice et al. (2016) introduced a method where the average precipitation over a given catchment is formulated as a stochastic process, parameters of which are inferred together with other model parameters during calibration. They showed that, even when starting with inaccurate precipitation data, this approach can accurately reconstruct the whole-catchment precipitation and reliably quantify the related uncertainty. However, their results suggested that even a simpler approach (e.g. Del Giudice et al., 2013) can lead to similar model parameters and prediction intervals. Therefore, if precipitation reconstructing is not of major interest, the novel approach is not appealing, given its high computational requirements.

■ 3.2 Explicit statistical consideration of model bias

Herein we describe the framework of Kennedy & O'Hagan (2001) as formulated by Reichert & Schuwirth (2012) and first used in the context of urban hydrology by Del Giudice et al. (2013). The basic principle of the method is extension of a deterministic (e.g. rainfall-runoff) model by a stochastic error model. However, a commonly used error model considering only independent and identically distributed (i.i.d.) errors is adjusted to explicitly account for the systematic model errors (bias) of the deterministic model, acknowledging the fact that simulators cannot describe the true behavior of a system (Del Giudice et al., 2013). Using this approach, the extended model can be formulated using the equation

$$Y_o(x, \theta, \psi) = y_M(x, \theta) + B(\psi) + E(\psi) \quad (3.1)$$

where variables in capitals represent random variables and those in lowercase are deterministic functions. Y_o represents the observed system output, y_M stands for the deterministic model output. To better fulfill the underlying statistical assumptions and thus obtain more reliable predictions, a transformation (details in 3.2.1) should be applied on both Y_o and y_M (Del Giudice et al., 2013). Next, B and E , respectively, stand for the bias and measurement noise in the system output. Precipitation as the external driving force is

represented by x , whereas θ and ψ respectively represent the deterministic and error model parameters.

The measurement noise of the system response E is sampled from a multivariate normal distribution with mean 0 and a diagonal covariance matrix

$$\Sigma_E = \sigma_E^2 \mathbf{1} \quad (3.2)$$

Del Giudice et al. (2013) investigated various formulations of the model bias B and presented a structured approach to select the optimal bias description for a given case study. In general, it is an autoregressive term which can be dependent on the input (rainfall) or/and output (runoff) of the system. For more details, see Del Giudice et al. (2013).

By combining the deterministic hydrological and the stochastic error models, we can quantify the probability that the observed runoffs can be explained by given predicted runoffs and error model. This can be formally expressed by a likelihood function describing the joint probability density $f(Y_o|\theta, \psi, x)$ of observed system response Y_o for given θ , ψ , and x . It can be written as

$$f(Y_o|\theta, \psi, x) = \frac{(2\pi)^{-\frac{n}{2}}}{\sqrt{\det(\Sigma(\theta, \psi, x))}} \cdot \exp\left(-\frac{1}{2}[\tilde{Y}_o - \tilde{y}_M(\theta, x)]^T \Sigma(\theta, \psi, x)^{-1} [\tilde{Y}_o - \tilde{y}_M(\theta, x)]\right) \prod_{i=1}^n \frac{dg}{dy}(Y_{o,i}, \psi), \quad (3.3)$$

where n is the number of observations (i.e. the dimension of Y_o and y_M) and $\Sigma(\theta, \psi, x)$ stands for a covariance matrix of the residuals transformed by a function $g()$. Similarly, $\tilde{y}_M = g(y_M)$.

To achieve accurate rainfall-runoff predictions and reliable quantification of their uncertainty, the extended model should be calibrated. In theory, this could be done by optimizing the likelihood function as the objective function. However, there is “a severe identifiability problem” between the deterministic model y_M and bias B “as the two components cannot be observed separately” (Reichert & Schuwirth, 2012). By implementing the Bayesian approach, i.e. combining the likelihood with prior knowledge (belief) about the extended model, we can specify that we are seeking for the smallest bias possible when calibrating the model. Although somewhat subjective choices regarding the amount of bias acceptable are required, this approach at least makes them transparent (Reichert & Schuwirth, 2012).

Performing the uncertainty analysis in the above described manner requires to follow these steps (Del Giudice et al., 2013):

1. Definition of marginal distributions of the prior joint probability distribution of the both the deterministic rainfall-runoff model parameters θ and the stochastic error model parameters ψ .

- Del Giudice et al. (2013) suggest that completely uninformative prior distributions should not be used for neither θ nor ψ parameters. Furthermore, it is “important that the prior of the bias reflects the desire to avoid model inadequacy as much as possible ... to reduce the identifiability problem between the deterministic model and the bias”.

2. Bayesian inference of the posterior parameter distribution.

- The joint probability density, a product of the prior $f(\theta, \psi)$ and the likelihood function $f(Y_o|\theta, \psi, x)$, gets conditioned on the observed discharge data, using the Bayes' theorem

$$f(\theta, \psi|Y_o, x) = \frac{f(\theta, \psi) f(Y_o|\theta, \psi, x)}{\iint f(\theta', \psi') f(Y_o|\theta', \psi', x) d\theta' d\psi'} . \quad (3.4)$$

Solving this problem analytically would include dealing with multidimensional integrals. This can be avoided by employing a numerical method such as Markov Chain Monte Carlo (MCMC) to approximate properties of the posterior distribution.

- Before the inference, a transformation $g()$ should be applied on simulation results and output data to account for the variance increasing with discharge and to reduce the heteroscedascity of residuals (Del Giudice et al., 2013). Details in 3.2.1.

3. Probabilistic predictions for the data set used for calibration

- For details on probabilistic predictions for multivariate normal distributions related to the random variables of this type, Del Giudice et al. (2013) recommend to consult Kendall et al. (1994) or Kollo & von Rosen (2006).

4. Probabilistic predictions for unseen temporal points.

- It is possible to proceed analogically as above. However, Del Giudice et al. (2013) suggest to take advantage of using bias formulated as an Ornstein–Uhlenbeck process and to “draw a realization for the entire period by iteratively drawing the realization for the next time step at time t_j from that of a previous time step at time t_{j-1} from a normal distribution”. In both cases, nevertheless, it is necessary to draw and evaluate a large sample from the posterior parameter joint distribution.

5. Verification of the statistical assumptions

- In many similar cases, it is usual to confirm the statistical assumptions of the error model by residual analysis (Reichert & Schuwirth, 2012). However, Bayesian approach implemented in this method allows us to test only the observation error E , which is the only purely frequentist term. However, since these errors are likely to constitute only a small portion of the residuals of the deterministic simulator, the informative value of this analysis might be limited.

3.2.1 Output transformation

Because of the statistical assumptions of homoscedasticity and normality of calibration residuals, a transformation $g()$ should be applied on simulation and observed output data (i.e., in our case, runoff discharges). It is a common way in hydrological modelling how to account for increasing variance with increasing discharge and thus reduce the residual heteroscedasticity. Moreover, it is expected to reduce the proportion of negative flow predictions by making error distributions asymmetric (Del Giudice et al., 2013).

According to Del Giudice et al. (2013), two most promising variance stabilization techniques for urban drainage applications are the Box–Cox (Box & Cox, 1964) and the log-sinh (Wang et al., 2012) transformation. The Box-Cox transformation has been used more often in hydrological studies than the log-sinh alternative, primarily due to the date of its first introduction. The two-parameter Box–Cox transformation can be written as

$$g(y) = \begin{cases} \log(y + \lambda_2), & \text{if } \lambda_1 = 0 \\ \frac{(y+\lambda_2)^{\lambda_1}-1}{\lambda_1}, & \text{otherwise} \end{cases} \quad (3.5)$$

and holds for $y > -\lambda_2$. The one-parameter version would need only λ_1 while keeping $\lambda_2 = 0$. Del Giudice et al. (2013) used the one-parameter version of the transformation with the parameter value $\lambda_1 = 0.35$, which had already been proven to perform satisfactorily in the past (e.g. Honti et al., 2013; Wang et al., 2012).

The log-sinh transformation was introduced for hydrological purposes only recently by Wang et al. (2012). Del Giudice et al. (2013) proposed its modification which would result in a “reparameterised form with parameters that have a more intuitive meaning”. The formula would be

$$g(y) = \beta \log\left(\sinh\left(\frac{\alpha + y}{\beta}\right)\right), \quad (3.6)$$

where α and β represent lower and upper reference outputs. This means that “ α controls how the relative error increases for low flows” and “for outputs larger than β , the absolute error gradually stops increasing” (Del Giudice et al., 2013).

3.3 Rainfall-runoff modelling performance assessment

Whether the uncertainty analysis is employed or not, there are various methods to evaluate the performance of a rainfall-runoff model. The primary output of a rainfall-runoff model is a time series of simulated discharges at a given location. Such a time series is well suited to be evaluated visually, creating a hydrograph. However, for numerical evaluation, it is preferable to summarize the performance in a single metric (or a small number of metrics). Many metrics often represent only a specific part (e.g. maximal discharge) or only a certain aspect (e.g. temporal precision, total volume discharged) of the hydrograph. If multiple rainfall-runoff events or even various catchments are to be compared, it is preferable to use standardized dimensionless criteria, e.g. the relative error of maximal discharges. Alternatively, there are metrics which take into account the whole time series and are often applied when trying to summarize the overall model performance, such as the mean squared error (*MSE*) or Nash-Sutcliffe efficiency (*NSE*). These two metrics are used very commonly in hydrological modelling although it has been shown that there are systematic problems inherent with their usage (Gupta et al., 2009; Ehret & Zehe, 2011).

When dealing with interval predictions, it is common to evaluate two aspects of the predictive performance – its precision and accuracy. The prediction precision can be quantified by the width of the determined confidence interval, referred to also as interval sharpness (e.g. Breinholt et al., 2012). The prediction accuracy can be understood as the position of observed value(s) in relation to the confidence bound(s). Time series predictions such as hydrographs can also be assessed in this manner, e.g. by calculating the prediction reliability, i.e. the share of observed data points within the predicted bounds, and the “average bandwidth” – the interval widths averaged over the entire prediction period (Del Giudice et al., 2013).

Gneiting & Raftery (2007) proposed a metric which combines the two above aspects – the interval score S_α . For a single interval prediction at a confidence level $1 - \alpha$ (determined by the prediction quantiles at levels $\frac{\alpha}{2}$ and $1 - \frac{\alpha}{2}$), the interval score is defined as

$$S_\alpha(l, u, x) = (u - l) + \frac{2}{\alpha}(l - x)\mathbb{1}\{x < l\} + \frac{2}{\alpha}(x - u)\mathbb{1}\{x > u\}, \quad (3.7)$$

where l and u stand for lower and upper interval bounds. This metric is supposed to allow for intuitive comprehension as “the forecaster is rewarded for narrow prediction intervals and incurs a penalty, the size of which depends on α , if the observation misses the interval” (Gneiting & Raftery, 2007).

For time series prediction, the idea of S_α can be extended and the mean interval scores (*MIS*) for a given period can be quantified. Bourgin et al.

..... 3.3. Rainfall-runoff modelling performance assessment

(2015) further developed the concept and, “to ease comparison between catchments and evaluate the skill of the prediction bounds”, proposed to benchmark the prediction confidence bounds by MIS for reference bounds (MIS_{ref}) obtained e.g. from long term climatological data. The mean interval skill score $MISS$ would be computed as

$$MISS = 1 - (MIS/MIS_{ref}), \quad (3.8)$$

high values of which indicate greater prediction skill, with positive scores indicating that evaluated predictions are more skillful than the reference.

Chapter 4

Material

The data used originate from an experimental urban catchment (Fig. 4.1) with an area of 1.3 km² which lies in Prague-Letňany, Czech Republic, and is drained by a separate stormwater drainage system. Approximately 35% of the catchment area is covered by impervious surfaces. The catchment is slightly inclined to the north, with the altitude gradually declining from roughly 280 to 250 m above sea level (Baltic 1957 height, EPSG:8357). The lag time between rainfall peak and runoff peak observed at the outlet from the catchment's drainage system is approximately 20 minutes.

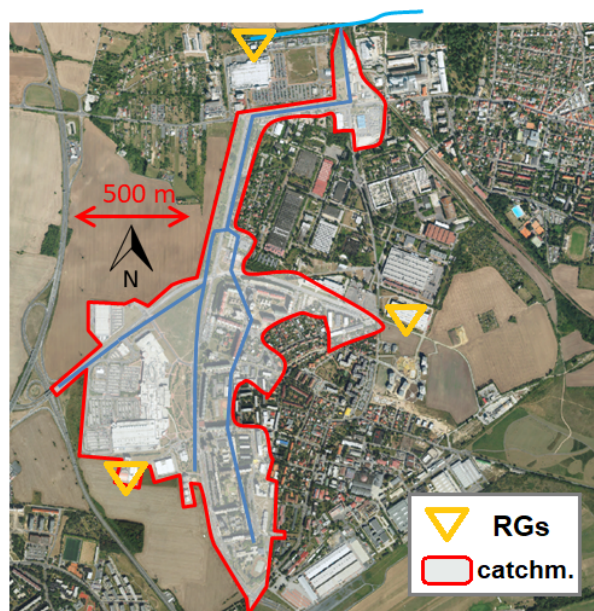


Figure 4.1: Aerial view of the urban catchment studied with the main sewers and receiving water body as well as the position of the local rain gauges (RGs).

4.1 Data retrieval and availability

We monitored 19 CMLs (Table 4.1; Fig. 4.2) and several rain gauges located in the catchment's surroundings (Figs. 4.1 and 4.2) over the period between July 2014 and October 2016, excluding the winter months (December–March) as CML signal attenuation by frozen precipitation, occurring in winter periods, is considerably different than that of liquid precipitation. Moreover, our monitoring setup is designed for periods with liquid precipitation only, as the rain gauges (see below) are not heated.

The CMLs (Mini-Link, Ericsson) broadcast at frequencies from 25 to 39 GHz, their lengths are between 611 and 5795 m, and they are operated by a major telecommunication service provider. Long CMLs extend out of the catchment for several kilometers. Signal-level data from CMLs, featuring a common quantization of 1 dB and 0.33 dB for the transmitted and received signal power, were retrieved at a 10-s resolution with a custom-made logging script (Fencl et al., 2015) and then aggregated to a 1-min resolution.

All tipping bucket rain gauges in the area (Figs. 4.1 and 4.2) were produced by the same manufacturer (MR3, Meteoservis) and feature the same characteristics: A funnel area of 500 cm², a bucket volume of 5 ml, and a single tip corresponding to 0.1 mm of rainfall. They are all dynamically calibrated (Humphrey et al., 1997) every year and the rainfall data they provide is stored at a 1-min resolution. However, the rain gauges make part of two different networks. Those located one km or more outside of the catchment (Fig. 4.2) are operated and maintained by the municipal sewer authority as a part of their long-term monitoring network with a density of one gauge per 20–25 km². These gauges are further referred to as “municipal”. In contrast, rain gauges temporarily installed at three locations around the catchment boundaries (Fig. 4.1) for research purposes are referred to as “local”.

In addition, we measured discharges at the stormwater drainage system outlet (Fig. 4.2) using an area-velocity flow meter (Triton, ADS). The flow meter was calibrated in a standard way using stream gaging and the velocity-area method employing an electromagnetic velocity probe. The temporal resolution of the discharge measurements is 2 min for wet periods and 10 min for dry periods. Observed discharge values range from approximately 2 to 2000 l/s.

During the observation period, we observed more than 100 relevant rainfall events with depths exceeding 2 mm. However, due to outages in data from the monitoring devices, it was possible to analyze data from only a considerably lower number of events. The exact number differs for each study presented due to using data from various sets of devices, the availability of the data at a given time, or differences in event definition. Details on rainfall characteristics

ID	FreqA [GHz]	FreqB [GHz]	Polarization	Length [m]
1	31.82	32.63	V	611
2	32.63	NA	H	645
3	NA	32.63	V	816
4	38.88	38.60	V	911
5	24.55	25.56	V	1022
6	37.62	37.62	V	1086
7	37.62	38.88	V	1396
8	37.62	38.88	V	1584
9	31.82	32.63	V	1858
10	24.55	25.56	H	1953
11	38.88	NA	V	1979
12	31.82	32.63	V	2611
13	24.55	25.56	V	2957
14	24.55	25.56	V	3000
15	24.55	25.56	V	3195
16	24.55	25.56	V	3432
17	25.56	24.55	V	4253
18	24.55	25.56	V	4523
19	24.55	25.56	V	5795

Table 4.1: Characteristics of the CMLs observed. FreqA and FreqB are CML frequencies for the two directions. The NA values indicate that records are not available. Polarization (Vertical/Horizontal) is the same for both directions.

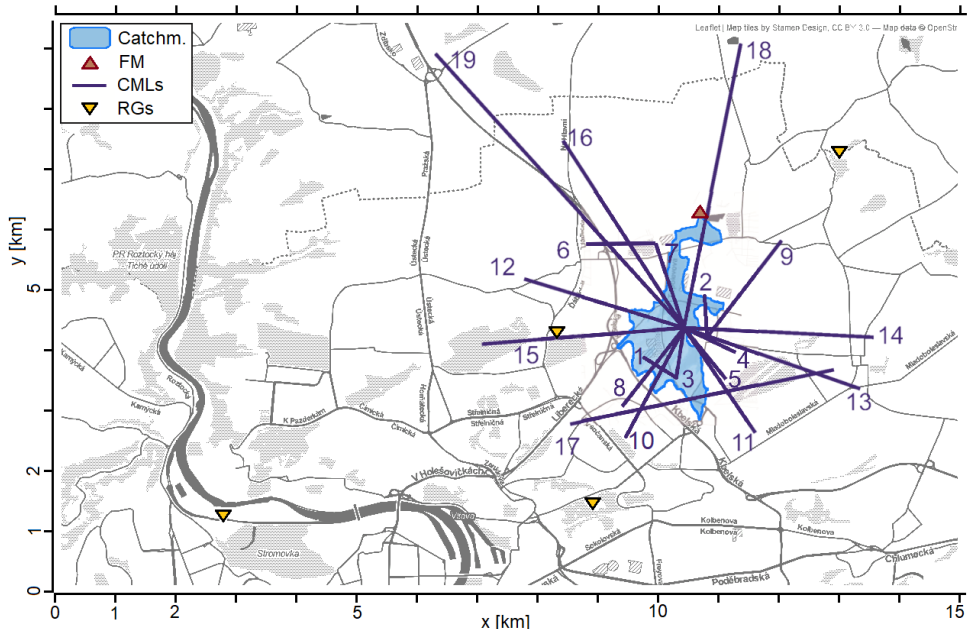


Figure 4.2: Spatial relations of the catchment, the flowmeter (FM), the CMLs (with IDs denoted), and the monitored municipal rain gauges (RGs).

for events as used in the study presented in chapter 6 (see 6.2.1) are provided in Appendix (Table A.1).

An overview of CML data availability during the monitoring period is shown in Appendix (Fig. A.1). Data from each CML were available, on average, during 80% of the events. Six CMLs had data availability higher than 95% and only two of them lower than 50%. Due to long-term outages, data from CMLs #1, #2, and #10 are analyzed only in the study presented in chapter 5, which investigates only a shorter period for which the data from these CMLs are available.

4.2 Rainfall-runoff model and its reliability

To simulate discharges at the drainage system outlet, an EPA-SWMM model is used which was constructed using detailed information about the catchment (e.g. the ratio of impervious areas for individual subcatchments) and the drainage system (e.g. pipe materials and diameters) provided by the municipal water management authority. The process of runoff generation is formulated empirically and separately for each model subcatchment (195 in total) using the respective surface-depression-storage-depth parameters. The subsequent runoff itself is modeled as one-dimensional flow expressed by Saint-Venant equations. These are numerically solved in the approximated form of a kinematic wave for surface runoff and in the full form of a dynamic wave for the following runoff in the stormwater drainage network. The model was calibrated using an independent data set, i.e. measurements obtained from the three local rain gauges (Fig. 4.1) before the above specified observation period (Pastorek, 2014).

In the cases of all rainfall data sets studied, except for the local rain gauges, the rainfall model input is always implemented as areal rainfall in the model, meaning that rainfall intensity in a given time step has a constant value over all model subcatchments. For the local rain gauges, the catchment is divided into three Thiessen polygons, corresponding to the local gauges at three locations. This means that every subcatchment is assigned the same rainfall intensity as measured at the closest local rain gauge.

The reliability of model predictions was tested using rainfall data from the three local rain gauges, i.e. the same devices that were used for the model calibration. This verification was performed for 56 rainfall-runoff events (see section 6.2.1) from the observed period between July 2014 and October 2016. Hydrographs for all analyzed events are provided in the Supplementary Data appended to the study of Pastorek et al. (2019b). Results of this verification are summarized in Fig. 4.3. These results suggest that the model predicts very realistic rainfall runoff. First, on average 78% of simulated discharges

4.2. Rainfall-runoff model and its reliability

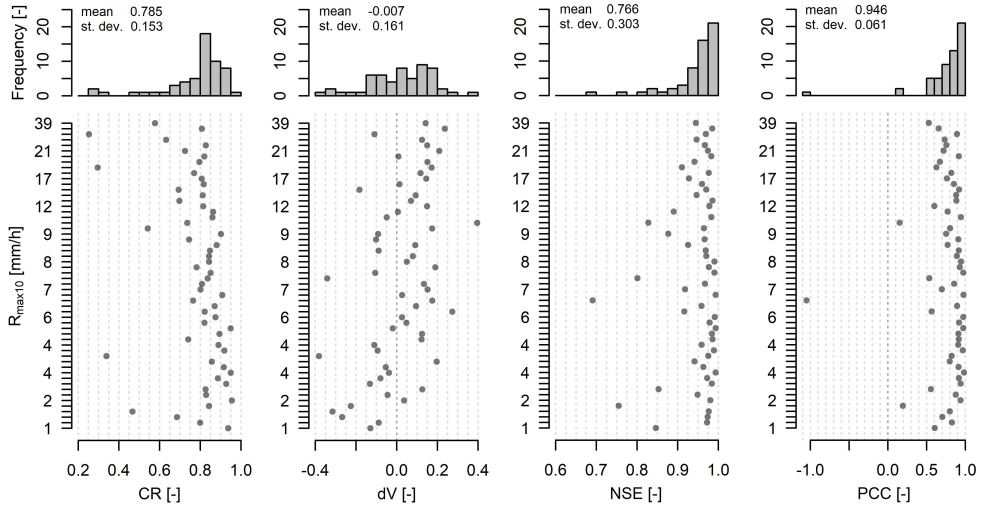


Figure 4.3: Results of the rainfall-runoff model verification. Top: Histograms of the statistics for all evaluated events. Bottom: Scatter plots showing the statistics for single events with respect to the maximal 10-minute rainfall intensity ($R_{max,10}$) observed by the local rain gauges during these events.

fall within the 95% confidence bands of observed runoff defined by 2.5% and 97.5% quantiles of observation errors (see section 6.2.4), i.e. the mean containing ratio $CR [-]$ is 0.78, and its st. dev. is 0.15. Second, the relative error in volume on average is only -0.7%, and modelled discharge shows a 0.95 Pearson's correlation coefficient in relation to the observed values. The Nash–Sutcliffe efficiency is also high (mean 0.77 and st. dev. 0.3). The model performs less satisfactorily in terms of predicting peak flows during heavy rainfalls, they are often substantially overestimated (on average by 40%). This is probably related to errors associated with the rainfall measurement or strong assumptions regarding rainfall spatial variability over the catchment area. For some of the heaviest rainfalls, peak flows are overestimated by more than 100%, which is probably also due to the model structural deficiencies, e.g. unmodelled overland flows during extreme events. In summary, the rainfall-runoff model performs very well except for extreme events.

Chapter 5

On the value of CML QPEs for urban rainfall-runoff modelling: The pilot study

Rainfall-runoff modelling in urban catchments requires reliable rainfall data with high temporal and spatial resolution. Such data are often not available and, thus, unmeasured spatial rainfall variability is an important source of uncertainty in urban rainfall-runoff modelling. Recently, commercial microwave links (CMLs) have been introduced as a new source of rainfall data with the necessary resolution. We compare rainfall data from CMLs with more conventional observations from rain gauges on the basis of rainfall-runoff modelling of a small urbanized catchment, performed with the investigated rainfall data sets and evaluated against observed runoffs. We employ a method based on Bayesian inference to calibrate our rainfall-runoff model and to estimate the uncertainty of modelling outputs. Results of the performed analyses show that CML rainfall data, when a suitable adjustment is applied (e.g. using information from nearby rain gauges), allow for better detection of dynamics of precipitation and subsequent runoff than data from point rain gauges alone, especially in the case of heavy rainfalls which are highly variable in space and time. Thus, CMLs seem to represent a relevant rainfall data source, which can conveniently complement existing rainfall monitoring networks.

The bulk of this chapter was originally published in:

Pastorek, J., Fencl, M., Stránský, D., Rieckermann, J., & Bareš, V. 2017. **Reliability of microwave link rainfall data for urban runoff modelling**. In *Proceedings of the 14th IWA/IAHR International Conference on Urban Drainage* (pp. 1340–1343). Prague, Czech Republic.

Pastorek, J., Fencl, M., Rieckermann, J., Sýkora, P., Stránský, D., Dohnal, M., & Bareš, V. 2018. **Posouzení srážkových dat z mikrovlnných spojů v městském povodí pomocí analýzy nejistot hydrologického modelu**. [The Evaluation of CML Rainfall Data in Urban Catchment by Means of Hydrologic Model Uncertainty]. *SOVAK: Časopis oboru vodovodů a kanalizací*, 27, 16–22.

5.1 Introduction

Reliable rainfall data are crucial when performing urban rainfall-runoff modelling. Nevertheless, high spatial variability of rainfall during convective events negatively affects the representativeness of point precipitation measurements from rain gauges. This could be avoided by employing commercial microwave links (CMLs), which allow for indirect path-averaged precipitation detection and are typically very dense in urban areas. However, to date, only a few studies have investigated the ability of quantitative precipitation estimates (QPEs) from CMLs for quantitative hydrology.

Smiatek et al. (2017) investigated the potential of QPEs from CMLs for streamflow prediction in an orographically complex mountainous region. In urban settings, Fencl et al. (2013) assessed the potential of CMLs to capture spatiotemporal rainfall dynamics and thus improve urban rainfall-runoff modelling, however, using only virtual rainfall fields. In a similar analysis, Fencl et al. (2015) evaluated QPEs derived from real-world CML data, however, without using these for hydrological modelling. Thus, to the best of our knowledge, no research has been presented yet in relevant literature where real-world CML QPEs would be applied for urban rainfall-runoff modelling.

In this study, we target the above research gap and analyze whether QPEs obtained from CMLs can be regarded as a viable alternative for rainfall data in the field of urban rainfall-runoff modelling. As CML QPEs are often highly biased, what limits their usability for practical purposes, we analyze CML QPEs derived using both a standard approach and a recently proposed (Fencl et al., 2017) method for adjusting the QPEs to existing rain gauges.

The CML QPEs, as well as traditional data from rain gauges, are propagated through a calibrated rainfall-runoff model and evaluated against observed discharges. Since additional uncertainties are introduced into the process of rainfall data evaluation by employing the rainfall-runoff modelling, we use a thorough statistical method which allows for reliable quantification of the runoff prediction uncertainty associated with various rainfall observation layouts.

5.2 Methods

The defined problem is addressed using rainfall and runoff data collected in a small urban catchment in Prague-Letňany, Czech Republic (details in chapter 4) during three months (August – October) of 2014. Precipitation

time series from six rainfall observation layouts are propagated through a rainfall-runoff model (chapter 4.2) and evaluated against observed runoffs. In order to quantify the associated uncertainties, the hydrological model is operated by means of prediction uncertainty quantification as first used in a similar context by Del Giudice et al. (2013) and introduced in chapter 3.2.

5.2.1 Rainfall observation layouts

We investigate rainfall data observed during 15 rainfall-runoff events from the summer season of 2014 using the six following observation layouts:

1. Measurements from three local rain gauges

Rainfall data from three local rain gauges installed for research purposes (Fig. 4.1) around the catchment of interest. This data set represents rainfall information observed on site which, however, in the context of the Czech Republic, is available only for short term experimental purposes. In this study, this data set is considered as the best-case-scenario reference.

2. Measurements from a single local rain gauge

Rainfall data at a 1-min resolution from the local rain gauge located at the south-west catchment boundary (Fig. 4.1). This data set represents rainfall information observed on site which could be available more commonly than the data above, however typically also only for a limited period of time, e.g. in order to evaluate the effect of (re)construction works in the catchment.

3. Measurements from three municipal rain gauges

Rainfall data from the three municipal rain gauges closest to the catchment (Fig. 4.2). Due to their 1-min resolution, for which correlations are low for the given distances (Villarini et al., 2008), only a single time series, constructed as the mean of the instantaneous R [mm/h] values of the three gauges, is evaluated. This data set represents rainfall data standardly available in long-term perspectives in urbanized areas of the Czech Republic.

4. QPEs from four CMLs adjusted by the local rain gauge,

Data from the single local rain gauge specified above, aggregated to 15-min time steps, is used to adjust (Fencl et al., 2017) CML QPEs with a 1-min resolution. In particular, wet

antenna attenuation (A_{wa} from Eq. 2.2) and α (Eq. 2.1) are adjusted, while keeping $\beta = 1$. Only short CMLs (path length < 1500 m) located close to the catchment center are used (#1, #2, #5, #7; Fig. 4.2; #3 and #4 are excluded due to outages and erratic behavior, respectively). Only a single time series, constructed as the mean of the instantaneous R [mm/h] values of the four CMLs, is evaluated. This rainfall data set showcases application of CML QPEs when traditional rainfall information is available directly in the catchment area, however, not in a satisfying spatial resolution.

5. QPEs from four CMLs adjusted by the municipal rain gauges

The instantaneous mean of the QPEs from the same four CMLs as above, adjusted in the same way, however, using the mean of the data from the three municipal rain gauges (specified above). This rainfall data set showcases application of CML QPEs in situations when rainfall is not measured directly in the catchment, but there are gauges in the distance of 2–3 km, which, however, provide data in lower temporal resolutions (e.g. 15, 30, or 60 min).

6. Unadjusted QPEs from all CMLs available (Fig. 4.2).

The instantaneous mean of QPEs derived, using a standard approach, from all 19 CMLs available in the area in a given time. A_{wa} is estimated as a constant offset with the value of 2.5 dB, which was determined by comparing the specific raindrop attenuation γ [dB/km] of short and long CMLs. The rainfall intensity R [mm/h] is calculated with parameter values α and β chosen in accordance with ITU Radiocommunication Sector (2005). This data set represents a situation when traditional rainfall information is not available in the catchment's surroundings.

In the cases of all CML data, prior to applying the correction for A_{wa} , baseline B [dB] (Eq. 2.2) is separated in the same manner as in Fencl et al. (2017).

5.2.2 Rainfall-runoff modelling and uncertainty analysis

Rainfall time series retrieved using all the five observation layouts are propagated through a rainfall-runoff model (4.2) and evaluated against discharges observed at the outlet from the local stormwater drainage system. When using rainfall data from the three local rain gauges, the rainfall input is implemented in the model using three Thiessen polygons. This means that

the rainfall intensity above a given model subcatchment is assumed to be the same as measured at the closest gauge. In all other cases, rainfall input is implemented as areal rainfall, meaning that rainfall intensity in a given time step has a constant value over all subcatchments of the model.

In order to acknowledge uncertainties of the rainfall-runoff model predictions, we employ uncertainty analysis framework of Kennedy & O'Hagan (2001) as formulated by Reichert & Schuwirth (2012) and first used in a context similar to ours by Del Giudice et al. (2013). The basic principle of the method (details in section 3.2) is the extension (Eq. 3.1) of a deterministic (i.e., in our case, rainfall-runoff) model by a stochastic error model which explicitly accounts for systematic model errors, i.e. bias.

Del Giudice et al. (2013) investigated various formulations of the model bias and various transformation functions. Based on their recommendations and our previous analyses (Pastorek, 2016), as transformation $g()$, we use the Box-Cox transformation (Box & Cox, 1964) with parameters $\lambda_1 = 0.45$ and $\lambda_2 = 1$. Moreover, we formulate the bias $B(\psi)$ as an autoregressive stationary random process with a long-term equilibrium value of zero and a constant variance. It is a mean-reverting Ornstein–Uhlenbeck process (Uhlenbeck & Ornstein, 1930), “the discretisation of which would be a first-order autoregressive process with Gaussian independent and identically distributed noise” (Del Giudice et al., 2013). It can be expressed using the following differential equation:

$$dB(t) = -\frac{B(t)}{\tau} dt + \sqrt{\frac{2}{\tau}} \sigma_B dW(t), \quad (5.1)$$

where τ represents the correlation time, σ_B the asymptotic standard deviation of the random fluctuations around the equilibrium, and $dW(t)$ a Wiener process, i.e. standard Brownian motion.

By varying the input rainfall data while keeping the rainfall-runoff model structure unchanged, we are able to trace the associated changes in the prediction uncertainty back to the respective rainfall data. However, to achieve accurate rainfall-runoff predictions and reliable quantification of their uncertainty, the extended model should be calibrated first. Although the deterministic rainfall-runoff model has been calibrated in the past, we optimize its parameters also here, together with the stochastic error model parameters, as we aim to maximize both the discharge prediction accuracy and precision.

Prior distribution definition and model calibration

Since the extended model has to be calibrated in a Bayesian framework, prior probability distribution of the model parameters which are to be calibrated must be first defined. Del Giudice et al. (2013) suggest that completely uninformative prior distributions should not be used for parameters of neither

the deterministic rainfall-runoff model (θ) nor the stochastic error model (ψ). Furthermore, it is “important that the prior of the bias reflects the desire to avoid model inadequacy as much as possible”. Considering the chosen bias model, σ_B is unlikely to be higher than the variability of observed discharge, τ should represent the characteristic correlation length of the residuals, and σ_E should mirror the measurement noise of the system output Del Giudice et al. (2013).

In accordance with Del Giudice et al. (2013) (see 3.2), we do not use completely uninformative prior parameter distributions. In contrast, the priors are chosen based on knowledge of the urban catchment and consultations with experts who have already used the method. For all the parameters, marginals of the prior joint distribution are defined (Table 5.1) as truncated normal distributions with four defining parameters - mean (μ), standard deviation (σ), minimum, and maximum. It should be noted that ψ parameters σ_B and σ_E are defined in a transformed space via a transformation $g()$. When θ parameters are concerned, they represent multiplicative (scaling) values of the actual model parameters. This means that when a given parameter, e.g. imp , is set to 1.1, the respective imp values for all 195 subcatchments are multiplied by 1.1.

parameter	abbrev.	μ	σ	min.	max.
Percentage of impervious areas [%]	imp	1	1	0.8	1.2
Width of overland flow path [m]	wid	1	1	0.3	1.7
Manning’s N for impervious areas	N_{im}	1	1	0.3	1.7
Surface depression storage for impervious areas [mm]	S_{im}	1	1	0.3	1.7
Percentage of impervious areas with no depression storage [%]	$pc0$	1	1	0.3	1.7
Manning’s N for drainage pipes	N_{co}	1	1	0.3	1.7
Correlation time [h]	τ	0.5	0.25	0.01	3
Asymptotic stand. dev. of independent errors [$g(1/s)$]	σ_E	$g(0.5)$	$g(0.25)$	0.01	1.5
Asymptotic stand. dev. of the random fluctuations around the equilibrium [$g(1/s)$]	σ_B	$g(50)$	$g(25)$	0	10 000 000

Table 5.1: Summary of the prior marginal distributions.

Data from five out of the 15 available rainfall-runoff events are used to calibrate the extended model. The calibration itself is performed in two steps. First, we use the generalized simulated annealing function of the GenSA package (Xiang et al., 2013), which was designed to “search for global minimum of a very complex non-linear objective function with a very large number of optima”. Second, we use a numerical Monte Carlo Markov Chain

sampler as implemented by Scheidegger (2012) according to the proposal of Vihola (2012). This function first tunes the covariance matrix of the jump distribution to achieve a desired acceptance rate. Next, a non-adaptive Metropolis sampling is employed to draw from the posterior distribution.

5.2.3 Performance assessment

After performing the extended model calibration, data from the ten remaining rainfall-runoff events are used to analyze the model predictions. To evaluate the rainfall-runoff predictions visually, we produce hydrographs for each of the ten events and rainfall data from each of the five observation layouts. We do not evaluate the prediction performance by examining separately the uncertainty intervals for the deterministic rainfall-runoff model output. This is in accordance with Del Giudice et al. (2013), who see this approach as “not conclusive because the field observations are not realisations of the deterministic model but of the model plus the errors”. Instead, we only evaluate the total uncertainty intervals associated with the extended model, i.e. the deterministic and the stochastic model together.

We also employ common summary hydrological metrics such as the Nash-Sutcliffe efficiency NSE [-], the total discharged volume during a whole given event, or the discharged volume during peak flow period. In particular, we compute relative errors of the total discharged volume dV [-] and of the volume during peak flow dV_{peak} [-] for every single prediction of the extended model. When calculating dV_{peak} , the time step with the maximal discharge observed is identified first and the volume discharged during eight minutes around the time step (four minutes before and four after) is computed afterwards. The difference between the modelled time with the maximal discharge and the observed one dt_{Qmax} [h] is another metric we quantify for every model prediction.

The uncertainty in the metrics NSE , dV , dV_{peak} , and dt_{Qmax} is evaluated by calculating the median and other quantiles for the whole set of predictions associated with a given rainfall observation layout, which are then graphically presented in boxplots. This is in accordance with Fencl et al. (2013) who also used the relative error of the total discharged volume and interpreted its mean \bar{dV} as the volume prediction bias and its standard deviation $sd(dV)$ as the prediction uncertainty. Moreover, the discharge prediction reliability associated with a given observation layout is quantified as the fraction of discharge observations falling into the predicted 90% confidence intervals.

To better interpret the results, we classify the rainfall events as either light or heavy, based on the maximal 10-minute precipitation rate.

5.3 Results

First, we present hydrographs showing observed and modelled discharges for a heavy and a light rainfall event which characterize well typical features of the overall results. Next, a summary of the results for all 10 events used, as well as only those classified as heavy (maximal 10-min rainfall intensity $R_{max,10} > 12 \text{ mm/h}$), and those classified as light ($R_{max,10} \leq 12 \text{ mm/h}$), is presented in boxplots, with a special attention on the heavy rainfalls.

Hydrographs of a chosen light rainfall event (Fig. 5.1 top) show that the prediction performance during such an event is very similar for five out of the six evaluated rainfall observation layouts. The runoff dynamics as well as volumes are captured very well in all cases and errors occur in the same part of the hydrographs - the rising limbs. In contrast, results for the unadjusted CML QPEs present different characteristics. There is a tendency to notably underestimate the discharges. The runoff dynamics feature similar trends as before, however, not as precisely. Interestingly, many observations are out of the prediction bounds, meaning that the prediction reliability is low for this rainfall observation layout.

Hydrographs of a chosen heavy rainfall event (Fig. 5.1 bottom) present a slightly different picture than the light rainfalls above. The worst runoff prediction was obtained using rainfall data from three municipal rain gauges. In particular, the peak flows were considerably underestimated in this case. Rainfall data from all other observation layouts, including unadjusted CML QPEs, reproduced well the peaks as well as all other hydrograph features.

Summary results presented in Fig. 5.2 confirm the previously mentioned tendencies. First of all, unadjusted CML QPEs feature remarkably different results than other five observation layouts which quite resemble each other. The unadjusted QPEs considerably underestimate the runoff volumes for light rainfalls, circa by 75% in median. However, for heavy rainfall events, the bias is at the same level as in other cases. This is also reflected in the associated *NSE* values, which are around -0.5 in median for light and around 0.7 for heavy rainfalls. A certain level of bias is present as well in result for the five other observation layouts, roughly between -10% and -20% in median. Interestingly, in the cases of both the single local rain gauge and the three municipal gauges, CML QPEs adjusted using the gauge data feature smaller bias than the gauge data used alone. This also affects the associated *NSE* values, which are higher for the adjusted CML QPEs than for the rain gauge data, especially when the heavy rainfalls are considered.

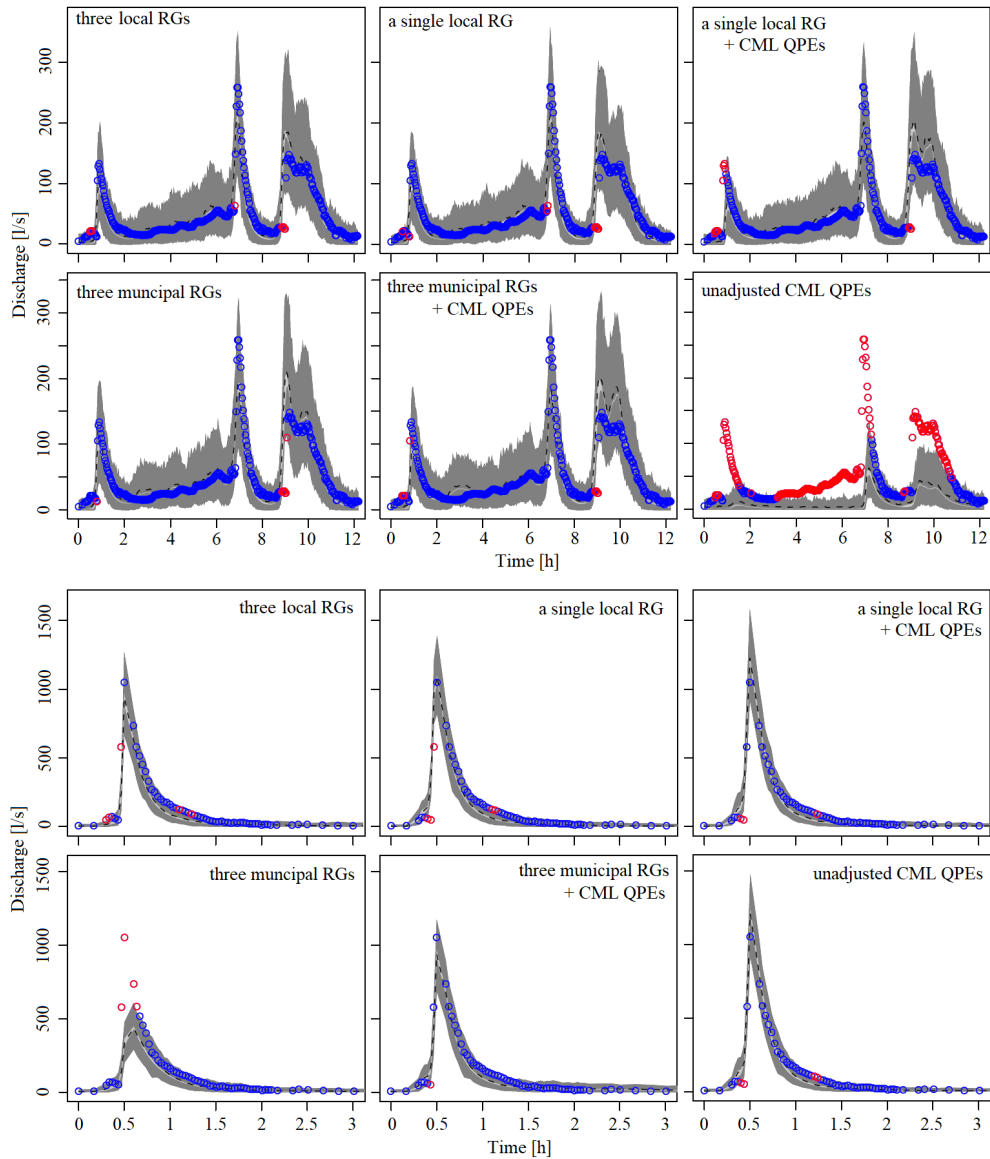


Figure 5.1: Hydrographs associated with a light rainfall observed on 11th August 2014 with a start at 02:24 am (top) and a heavy rainfall observed on 29th August 2014 with a start at 02:56 pm (bottom). Predicted discharges at a confidence level of 90% are shown as grey bands. The dashed line represents median prediction for a given timestep. Observed discharges are shown as circles (blue if within the prediction bounds, red if outside).

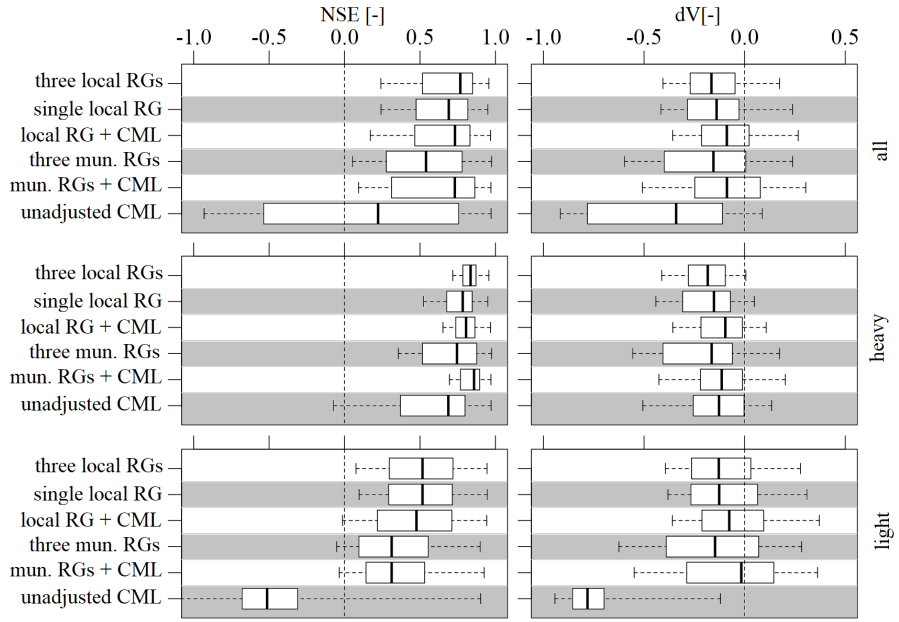


Figure 5.2: Boxplots showing prediction performance summaries in terms of NSE (left) and dV (right) for all 10 events (top), heavy rainfalls (center), and light rainfalls (bottom). Boxplot whiskers extent from the 10th to 100th percentile for NSE and from the 5th to 95th percentile for dV .

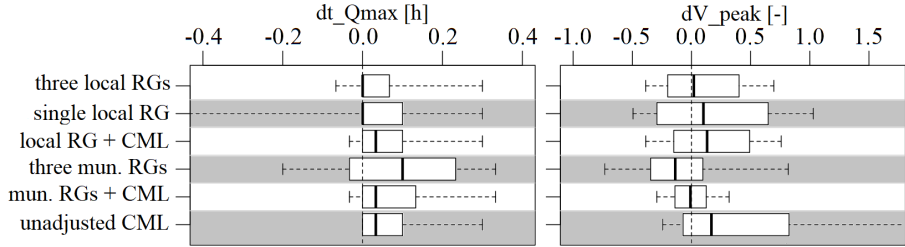


Figure 5.3: Boxplots showing prediction performance summaries in terms of $dt_{Q_{max}}$ (left) and dV_{peak} (right) for heavy rainfalls. Boxplot whiskers extent from the 5th to 95th percentile.

Heavy rainfall events are analyzed in more detail in terms of their peak flows in Fig. 5.3. This shows that unadjusted CML QPEs most overestimate the peak discharges. However, adjusting CML QPEs to rain gauge data reduces the variance in dV_{peak} values, even when compared to the rain gauge data themselves. In fact, most accurate and precise peak flows are obtained using the QPEs adjusted to the three municipal rain gauges. When timing of the discharge maximum is considered, the worst results in terms of precision are obtained using the single local rain gauge, and in terms of accuracy using the

three municipal gauges. CML QPEs, both adjusted and unadjusted, perform very similarly as the best-case-scenario three local rain gauges.

5.4 Discussion

The main findings of the study are that CML QPEs derived using a standard approach, which are often biased, lead to biased rainfall-runoff predictions, especially their underestimation during light rainfall events. However, for heavy rainfalls, which are often associated with convective events, the bias is notably lower, and runoff temporal dynamic are captured similarly well as when using high-resolution local rain gauge data. Moreover, compared to traditional rain gauge data (a single local rain gauge or three municipal gauges) used alone, adjusting CML QPEs to these gauge data has lead to an improvement in the reproduction of peak discharges and the overall modelling performance in terms of *NSE* for heavy rainfalls, for which CMLs play out the advantage of excellent spatial coverage.

These findings suggests that CML QPEs can be regarded as a viable additional rainfall data source for the field of urban rainfall-runoff modelling, especially for the monitoring of heavy rainfalls when the availability of traditional rain gauge data is limited. This is in agreement with Smiatek et al. (2017) who investigated the potential of CML QPEs for streamflow prediction in an orographically complex mountainous region. They found that, during an extreme flooding period with many local heavy rainfall events, a considerable improvement in hydrograph reproduction can be achieved when CML QPEs are employed. Our findings are also in agreement with those of Fencl et al. (2017), who found that adjusting CML QPEs to rain gauge data reduces the bias in the QPEs, which can then outperform each of the rainfall data types used individually.

Nevertheless, the relevance of our findings should be subject to further research using more extensive data sets ideally from multiple locations, since our data set only covers three consecutive months in the area of a single urban catchment. Next, it should be stressed out that the observation layouts of unadjusted CML QPEs consists of data from all 19 CMLs available in the area in that time. However, due to high computational demands, the CML QPEs adjusting to rain gauge data has been done only for four rather short CMLs which were assumed to correspond well to the catchment topology. Therefore, a similar analysis should be performed where data from CMLs of more variable path lengths and other relevant characteristics (e.g. frequency) would be evaluated, and the potential role of these characteristics on the results would be studied.

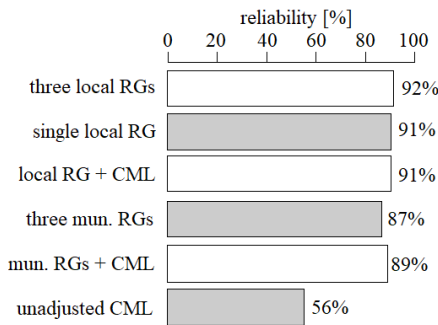


Figure 5.4: Discharge prediction reliability for all 10 events.

Next, the bias in simulated runoffs when using the unadjusted CML QPEs, especially pronounced during light rainfall events, has not been adequately compensated for by extending the prediction intervals (see e.g. Fig. 5.1 top) which has also lead to low overall prediction reliability as presented in Fig 5.4. For all other observational layouts, the prediction reliability at the declared 90%-confidence level is very close to 90%, however, it is only 56% for the unadjusted CML QPEs. This behavior, which could be explained by an inappropriately calibrated stochastic error model, does not compromise the main findings regarding rainfall data from this observational layouts Nevertheless, it should be analyzed what factors (e.g. the definition of the parameter prior distributions, or the choice of meta-parameters necessary for the calibration process) have caused this effect so that similar erratic behavior could be avoided in future analyses.

It should also be noted that, during the extended model calibration, the internal structure of the deterministic rainfall-runoff model stays unchanged for a given θ parameter, which is used only as a scaling factor affecting all sub-parts of the model in the same way (see 5.2.2). This could be avoided by employing additional stochastic parameters which would introduce random changes into the internal proportions of the θ parameters and might, in theory, improve the model structure and thus reduce the associated uncertainties. However, we have chosen not to implement this, for the sake of modelling simplicity (lower number of parameters) and results interpretability.

■ 5.5 Conclusions

This study has presented the first analysis of using QPEs from real-world CMLs for rainfall-runoff modelling in a small urban catchment. This has included a comparison of the modelling performance with traditional rain gauge data and a robust statistical analysis of the model prediction uncertainty.

Our results have shown that stormwater discharges modelled using CML QPEs derived using a standard approach are often considerably biased, especially during light rainfall events. On the other hand, these QPEs can very well reproduce the runoff temporal dynamics. Moreover, adjusting the CML QPEs to traditional rain gauge data in sub-optimal resolutions has lead to an improvement in the reproduction of peak discharges and the overall modelling performance in terms of *NSE* for heavy rainfalls, compared to using the rain gauge data alone. Such adjusted CML QPEs can even lead to the same rainfall-runoff modelling performance as high-resolution rain gauge data during heavy precipitation events.

The above findings suggest that CML QPEs can be regarded as a viable additional rainfall data source for the field of urban rainfall-runoff modelling, especially for monitoring of heavy rainfalls, if local rain gauge data in high spatial resolution are not available in a given catchment. In such cases, adjusting CML QPEs to gauges from a low-density network, e.g. operated by national meteorological service or similar institutions, could provide rainfall information of adequate quality, especially when heavy rainfalls, crucial for design and operation of urban drainage systems, are considered.

Using CML QPEs in situations when other rainfall data are not available, i.e. when adjusting is not an option, would be complicated by the systematic errors in these data. However, more advanced pre-processing of CML QPEs could in theory reduce these errors in the future.

Future studies should also assess the validity of our findings using more extensive data sets which would cover longer time periods and ideally various experimental areas with CMLs of various relevant characteristics (path length, frequency), and could thus evaluate the potential role of these various factors for the CML QPE suitability for urban rainfall-runoff modelling.

Chapter 6

The effect of link characteristics and their position on runoff simulations

This study addresses the ability of individual commercial microwave links (CMLs) to provide relevant quantitative precipitation estimates (QPEs) for urban rainfall-runoff simulations and specifically investigates the influence of CML characteristics and position on the predicted runoff. QPEs from real world CMLs are used as inputs for urban rainfall-runoff predictions and subsequent modelling performance is assessed by comparing simulated runoffs with measured stormwater discharges. The results show that model performance is related to both the sensitivity of CML to rainfall and CML position. The bias propagated into the runoff predictions is inversely proportional to CML path length. The effect of CML position is especially pronounced during heavy rainfalls, when QPEs from shorter CMLs, located within or close to catchment boundaries, better reproduce runoff dynamics than QPEs from longer CMLs extending far beyond the catchment boundaries. Interestingly, QPEs averaged from all available CMLs best reproduce the runoff temporal dynamics. Adjusting CML QPEs to three rain gauges located 2–3 km outside of the catchment substantially reduces the bias in CML QPEs. Unfortunately, this compromises the ability of the CML QPEs to reproduce runoff dynamics during heavy rainfalls.

The bulk of this chapter was originally published in:

Pastorek, J., Fencl, M., Rieckermann, J., & Bares, V. 2019. **Commercial microwave links for urban drainage modelling: The effect of link characteristics and their position on runoff simulations.** *Journal of Environmental Management*, 251, 109522. <https://doi.org/10.1016/j.jenvman.2019.109522>.

6.1 Introduction

Inaccuracies in quantitative precipitation estimates (QPEs) from commercial microwave links (CMLs) are very much dependent on CML's sensitivity to inaccurate estimation of raindrop-induced attenuation A_r [dB] which is largely determined (see 2.4.1) by its characteristics such as transmission frequency and path length (Leijnse et al., 2008).

Path lengths of CMLs typically range from a few hundred meters up to a few kilometers. Longer CMLs are less prone to bias in CML QPEs caused by inaccurate A_r estimation due to, e.g., imprecise correction for wet antenna attenuation (WAA). However, their path lengths often do not correspond well to relatively small scales of urban (sub)catchments and, thus, they cannot capture rainfall spatial variability at corresponding scales. On the other hand, shorter path lengths, fitting the typical urban catchment scale well, make CMLs more prone to bias. Nonetheless, shorter CMLs typically operate at higher frequencies which are associated with a lower liability to bias.

Unfortunately, very little is known about the combined effect of the CML characteristics and their spatial representativeness on efficient use of CML QPEs for hydrological applications such as rainfall-runoff modeling. This study addresses the above knowledge gap and investigates in how far CML instrumental parameters and network topology influence the performance of CMLs as rainfall sensors for hydrological modelling. This complex problem is addressed in three steps:

1. The sensitivity of QPEs to the CML path length and transmission frequency is analyzed.
2. The CML spatial representativeness related to their path length, position, and the spatial structure of the rainfall event are investigated.
3. As, in theory, CML QPEs should outperform point measurements from rain gauges during extreme or heavy rainfall, we analyze the performance of CML QPEs in such conditions in greater detail.

In our view, main innovations of the study include also the following:

1. It is among the very first which investigate the potential of CML QPEs for urban rainfall-runoff modelling at catchment scales;
2. It employs a unique real-world data set which was collected over three consecutive summer seasons and which contains comprehensive, high-resolution data from a dense network of 19 CMLs; and
3. It provides specific recommendations on how to select CMLs suitable for urban rainfall-runoff modelling.

6.2 Methods

QPEs from real-world CMLs (4.1) are used as inputs in a calibrated urban rainfall-runoff model (4.2). The model performance is evaluated for CML QPEs from various observation layouts by comparing the simulated runoffs with those observed at the stormwater drainage system outlet. Next, we perform an exploratory data analysis on CML attributes to better understand their influence on volumes and temporal dynamics of the simulated runoff.

6.2.1 Data availability

Due to outages in data from the monitoring devices, it was possible to perform and evaluate rainfall-runoff simulations for 71 events from the monitoring period (4.1). For each of the events, there were data available from between 9 and 17 CMLs (47%–89%). To improve the robustness of the statistical evaluation, we have excluded from the analysis 12 rainfall events with less than two thirds of the CMLs available. Also, we excluded three extreme rainfall events for which runoff predictions were unsatisfactory, i.e. maximal discharges were overestimated by more than 100% when modelled using high-quality rainfall data from the three local rain gauges (Fig. 4.1). Similarly, three CMLs (#1, #2, #10), which experienced long outages during the experimental period, are not analyzed in the study. In summary, after rigorous quality control, the analysis is performed for 16 CMLs and 56 events. Details on the rainfall event characteristics are provided in Appendix (Table A.1).

6.2.2 From signal levels to QPEs

Although we deliberately chose a pragmatic approach to derive CML QPEs, several steps are necessary to estimate precipitation-induced attenuation for a given CML and to derive the associated precipitation rates:

1. The difference between the transmitted and received signal level $TRSL$ [dB] is calculated for each of two CML channels.
2. A quality check is performed to identify erratic CML behavior which has to be filtered out. The following behavior is regarded as erratic:
 - Sudden peaks where, within two time steps, $TRSL$ increases and then decreases (or vice versa) by more than 5 dB,
 - Longer periods (days) with no signal fluctuation, and

- Periods with random noise larger than 2 dB.
- 3. TRSL data are aggregated to regular 1-min time series by averaging values within 1-min intervals.
- 4. TRSL time series from the two CML channels are averaged.
- 5. Baseline attenuation B is estimated with a low-pass filter parameter $m = 0.00145$ (Fenicia et al., 2012) and separated from TRSL (Eq. 2.1).

After the baseline separation, we proceed by applying WAA correction (A_{wa} from Eq. 2.2) and calculating the rainfall intensity R [mm/h] (Eq. 2.1) in two different ways:

- WAA A_{wa} is modelled as a constant offset with values suggested by Overeem et al. (2011). Parameters α and β are chosen in accordance with ITU Radiocommunication Sector (2005).
- The mean of the instantaneous R values of the three municipal rain gauges closest to the catchment (Fig. 4.2), aggregated to 15-min time steps, is used for adjusting A_{wa} and α , while keeping $\beta = 1$, as proposed by Fencl et al. (2017).

6.2.3 Observation layouts and their evaluation

Rainfall data from 18 different observation layouts are used as precipitation inputs into the rainfall-runoff model. The rainfall model input is in all cases implemented as areal rainfall in the model meaning that rainfall intensity in a given time step has a constant value over all subcatchments of the model.

Firstly, we employ QPEs derived from only a single CML at a time, using each of the 16 CMLs consecutively. Next, we construct a time series calculated as the arithmetic mean of all available CML QPEs (not weighted) for every time step. These 17 observational layouts based on the CML data are used for both methods of deriving CML QPEs (see the end of section 6.2.2). Additionally, to compare CML QPEs with a traditional way of rainfall monitoring, the mean of the three rain gauges from the municipal network is used as the model input. These are the same rain gauges as those used for CML adjusting, but the original 1-min resolution is used in this case.

The rainfall-runoff simulations are not performed continuously for the whole observation period, but only for individual rainfall-runoff events. The model performance is evaluated, for the 18 studied observation layouts, both CML QPE deriving methods, and each of the 56 events, by comparing the simulated runoffs and observed stormwater discharges. Performance metrics are

Nash–Sutcliffe efficiency NSE [-], the Pearson correlation coefficient PCC [-], and the relative error of the total runoff volume dV [-].

The model performance for the rainfall observation layouts is analyzed also with respect to rainfall intensities of evaluated events. For these purposes, we classify the events into “light”, “moderate” and “heavy” (Table 6.1). Runoff simulations for heavy rainfalls are investigated in more detail to demonstrate the ability of CMLs for capturing heavy rainfalls, which are often characterized by high spatial variability and thus difficult to measure reliably with point rain gauge observations. However, we expect that location and spatial scale of CMLs might play a larger role than their instrumental errors when used for modelling runoff generated by heavy (spatially variable) rainfalls.

	Light	Moderate	Heavy
Defining $R_{max,10}$ [mm/h]	$x \leq 5$	$5 < x < 12$	$12 \leq x$
Number of events	20	20	16

Table 6.1: Categorization of rainfall events. The defining maximal 10-min rainfall intensity $R_{max,10}$ as measured by the three local rain gauges temporarily installed around the catchment. For detailed info, see Appendix (Table A.1).

6.2.4 Data uncertainty

To interpret correctly the study results, it is crucial to estimate expected errors of both CML QPEs and discharge measurements. The errors in CML QPEs are addressed in section 2.4.1. The uncertainty of the measured discharges at the outlet of the catchment are estimated following the suggestions of Muste et al. (2012). The discharge is computed from pipe radius R [m], measured flow depth h [m], and measured cross sectional velocity V [m/s], which are assumed to have uncorrelated errors. The following values of input variables are propagated: $R = 0.75$ m with a standard uncertainty (at a 68% level of confidence) $u(R) = 0.0015$ m. The discharge uncertainty is estimated only for periods with stormwater runoff, therefore, we assume that the standard uncertainty of measured flow depth h is $u(h) = 0.015$ m. The standard uncertainty of the flow velocity V in the cross section is estimated as $u(V) = 0.05V$. Finally, the expanded uncertainty (at a 95% level of confidence) of measured discharge $U(Q)$ is estimated for all discharge measurements. The expanded uncertainty $U(Q)$ varies for different flow depths, e.g. for 10% pipe filling, $U(Q) = \pm 0.0282$ m³/s, what is equivalent to $\pm 31.0\%$ of the total value $Q = 0.091$ m³/s. For 50% pipe filling, the uncertainty $U(Q) = \pm 0.245$ m³/s, corresponding to ($\pm 11.0\%$) of the discharge $Q = 2.17$ m³/s.

6.3 Results

Firstly, typical features of simulated discharge are illustrated on a hydrograph of one of the 56 events. Secondly, the performance of the rainfall-runoff model is investigated in relation to the CML lengths and frequencies. Afterwards, the model performance is evaluated separately for heavy rainfalls to understand the effect of CML lengths and positions during spatially more variable rainfalls. Finally, runoff simulations for CML QPEs adjusted to rain gauges are presented.

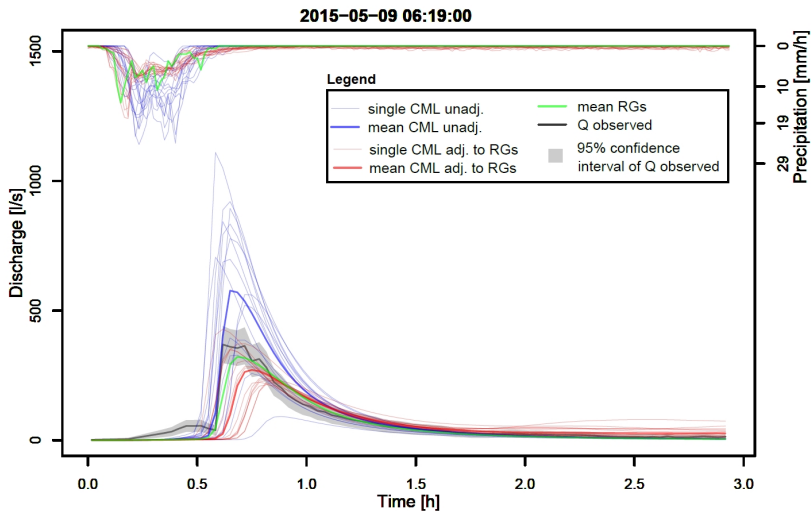


Figure 6.1: Modelled and observed discharges for a selected rainfall-runoff event and all examined rainfall observation layouts: QPEs from individual CMLs both unadjusted (“single CML unadj.”) and adjusted to rain gauges (“single CML adj. to RGs”); The mean of both unadjusted and adjusted QPEs from all available CMLs (“mean CML unadj.” and “mean CML adj. to RGs”); The mean of the three municipal rain gauges (“mean RGs”).

6.3.1 Characteristic features of simulated hydrographs

A hydrograph which illustrates well typical features of the rainfall-runoff process is shown in Fig. 6.1. Firstly, one can see that discharge simulations using unadjusted CML QPEs (in blue) can be highly biased, however, this bias varies substantially for various individual CMLs (dV between -0.709 and 0.823). In contrast, the correlation with the observed runoff is relatively high (PCC 0.878 in mean) and much more stable among various CMLs (0.15 in st. dev.). Secondly, the efficiency of adjusting CML QPEs to rain gauge observations (in red) is highly conditional on the rain gauge data. The adjustment reduces the bias in simulated discharges (dV between -0.280 and

0.066), but it does not always outperform simulations based on the mean of the rain gauges (dV -0.152).

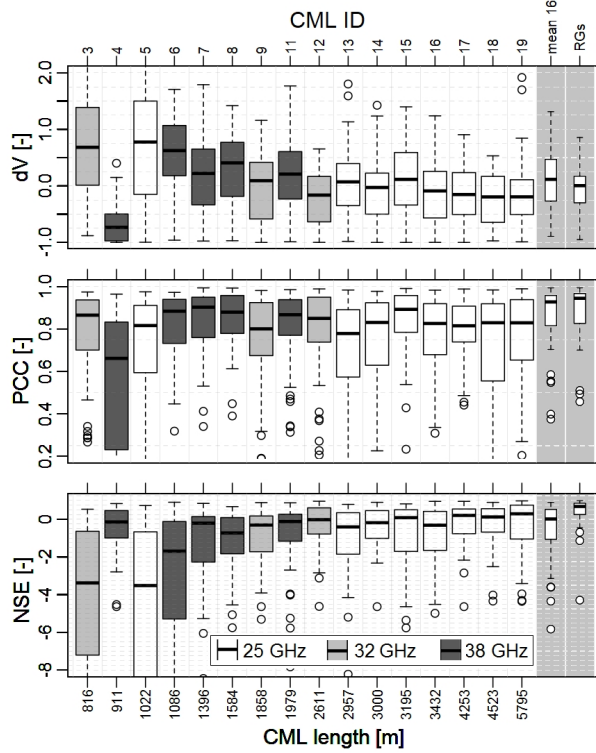


Figure 6.2: Boxplots of performance metrics (see 6.2.3) obtained using unadjusted CML QPEs, summarized for all available rainfall-runoff events. "Mean 16" stands for the mean of all QPEs from all 16 individual CMLs, "RGs" stands for the mean of the three municipal rain gauges. Boxes represent the interquartile range, whiskers extend to the most extreme data point which is no more than 1.5 times the interquartile range from the box, and circles represent outliers.

6.3.2 Performance in relation to CML lengths and frequencies

Fig. 6.2 shows boxplots of the model performance when using unadjusted CML QPEs for all 56 rainfall-runoff events, where each boxplot belongs to one observation layout. The layouts are sorted by the CML path length. Predicted discharges are on average highly biased and the large whiskers indicate substantial inter-event variability outside the upper and lower quartiles for all metrics. The largest dV values tend to be associated with unadjusted QPEs from short CMLs (the exception of CML #4 is discussed below). Similarly, the inter-event variability in dV is largest for simulations with short unadjusted CMLs. Such positive bias linked to the high sensitivity of short CMLs to wet antenna attenuation has been observed in the past (e.g. Fencl et al., 2019).

CML #4 is a distinctive exception to the observations formulated above. Although it is very short, unadjusted QPEs from this CML lead to substantially underestimated runoff volumes. Additional analyses identified malfunction in one of the two channels of this CML causing unusually low values of observed attenuation. Since we use the mean of the observed attenuation of the two channels to estimate rainfall intensity, the intensities derived from this CML, and consequently the simulated runoffs, are systematically underestimated.

The model performance in terms of *PCC* (Fig. 6.2, middle), which is insensitive to linear bias, does not show a clear dependence on CML path lengths. Better-than-average values are obtained using QPEs from 38 GHz CMLs. This is probably because these CMLs cover the catchment relatively well while being more sensitive to rainfall than lower frequency CMLs. Interestingly, the best performing CML QPEs, with *PCC* values similar to the rain gauges, are those derived from the mean of all available CMLs. *NSE* values (Fig. 6.2, bottom) are generally unsatisfactory, due to the high bias in the unadjusted CML QPEs. As expected, *NSE* values are better for longer CMLs and for the mean of QPEs from all 16 CMLs.

Using the given CML network topology, the relation between the CML frequency and its performance cannot be studied completely independently of the CML path length. Nevertheless, results of CMLs #9 and #11 or #12 and #13, which have similar lengths but different frequencies, indicate that higher frequencies (which are more sensitive to raindrop attenuation) tend to provide better results, especially in terms of better correlations.

In general, when evaluating discharge simulations using volume-related performance metrics (*dV* and *NSE*), instrumental errors seem to dominate over errors related to CML spatial representativeness. The longest least biased CMLs distinctively outperform shorter CMLs. The short CMLs are within or close to the catchment boundaries, and their lengths correspond better to the catchment scale (Fig. 4.2), but they are more prone to bias due to wet antenna attenuation (see 2.4.1). On the other hand, correlations are slightly better for shorter 38 GHz CMLs than for longer 26 GHz CMLs. However, the spatial representativeness of CMLs in relation to the catchment area might be more pronounced during heavy rainfalls, which are typically highly spatially variable and during which we can expect CMLs to be relatively less prone to instrumental errors (see 2.4.1). This is investigated in greater detail in the following subsection.

6.3.3 Performance during heavy rainfalls

Fig. 6.3 summarizes the rainfall-runoff modelling performance for heavy rainfalls. General tendencies for volume-related statistics are similar as when summarizing for all available events. It can be seen that there is still a

considerable dependency between the CML path length and the bias in simulated discharges (dV , Fig. 6.3, top), which also affects the performance in terms of NSE (Fig. 6.3, bottom). Interestingly, the temporal dynamics (PCC , Fig. 6.3, middle) are now best reproduced (median PCC 0.94, st. dev. 0.04) by the mean of all CML QPEs. This suggests that such averaged data contain valuable information about the rainfall spatiotemporal dynamics above the catchment. For the individual CML QPEs, the highest PCC values are reached by QPEs from relatively short 38 GHz CMLs (#6, #7, #8) located in the western part of the catchment. This demonstrates that even biased CML QPEs can very well reproduce runoff dynamics if the CMLs cover the catchment area well. Nevertheless, the bias in the QPEs from short CMLs considerably limits their performance in terms of volume-related performance metrics, which are important for applications such as modelling of water balance or designing large retention tanks. Elimination of the bias in CML QPEs by adjusting to rain gauges is presented in the next section.

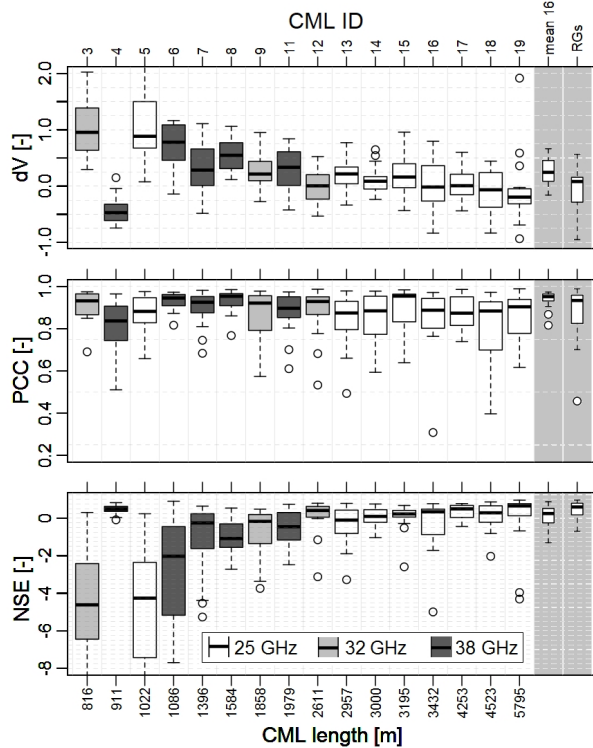


Figure 6.3: Boxplots of performance metrics obtained using unadjusted CML QPEs, summarized only for heavy rainfalls. "Mean 16" stands for the mean of all QPEs from all 16 individual CMLs, "RGs" stands for the mean of the three municipal rain gauges. Boxes represent the interquartile range, whiskers extend to the most extreme data point which is no more than 1.5 times the interquartile range from the box, and circles represent outliers.

6.3.4 Discharge simulations from adjusted CML QPEs

Although the adjustment of CML QPEs to rain gauges greatly reduces the bias (median dV between 0.01 and 0.12; Fig. 6.4), it does not outperform the rain gauge data (median dV 0.01). There are no clear trends associated with CML path length, neither in terms of the dV median nor the dV inter-event variability (st. dev. between 0.37 and 0.61). Similarly, for all CML QPEs, correlations of simulated and observed discharges are in similar ranges as for the rain gauges used alone (PCC medians around 0.9, st. dev. around 0.27). For six of the individual CMLs (including short ones) and for the mean of all CMLs, the adjusted QPEs lead to slightly less variable NSE values than the rain gauges (st. dev. between 0.6 and 0.73). However, no CML QPEs lead to decisively higher median NSE values.

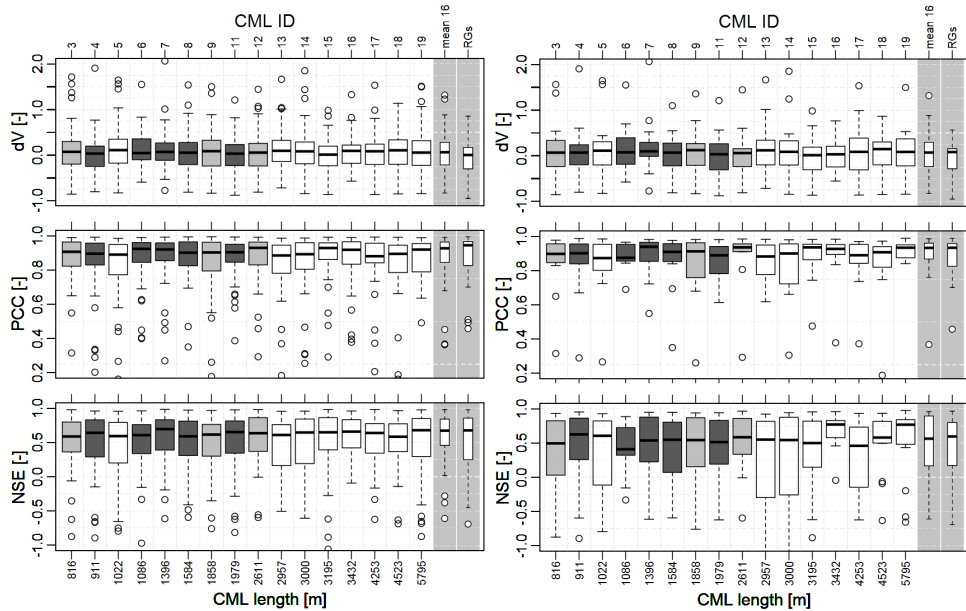


Figure 6.4: Boxplots of performance metrics obtained using the adjusted CML QPEs, summarized for all available rainfall events (left) and only for heavy rainfalls (right). “Mean 16” stands for the mean of all QPEs from all 16 individual CMLs, “RGs” stands for the mean of the three municipal rain gauges. Boxes represent the interquartile range, whiskers extend to the most extreme data point which is no more than 1.5 times the interquartile range from the box, and circles represent outliers.

Adjusting CML QPEs to rain gauge data effectively minimizes the bias in the CML QPEs, though it is considerably constrained by the reliability of the rain gauge data. This is especially critical during heavy rainfalls when observations from rain gauges located 2–3 km from the catchment often do not represent rainfall intensities directly in the catchment. In these cases, adjusted CML QPEs tend to be unreliable and can even worsen CML performance,

especially in terms of their ability to capture temporal dynamics of rainfall and subsequent runoff. This is demonstrated in Fig. 6.5, where discharge simulations based on *i*) only rain gauges, *ii*) the mean of all unadjusted CML QPEs, and *iii*) the mean of all adjusted CML QPEs are evaluated in terms of *PCC* and compared with each other. For heavy rainfall events, the unadjusted CML QPEs clearly outperform the rain gauge data (Fig. 6.5, left). Adjusting CML QPEs to rain gauges improves the *PCC* performance for light and moderate rainfall events, but it also worsens the results for heavy (and a few moderate) rainfall events (Fig. 6.5, right). When comparing the adjusted CML QPEs and the rain gauge data (Fig. 6.5, middle), there is no clear difference between the respective *PCC* values.

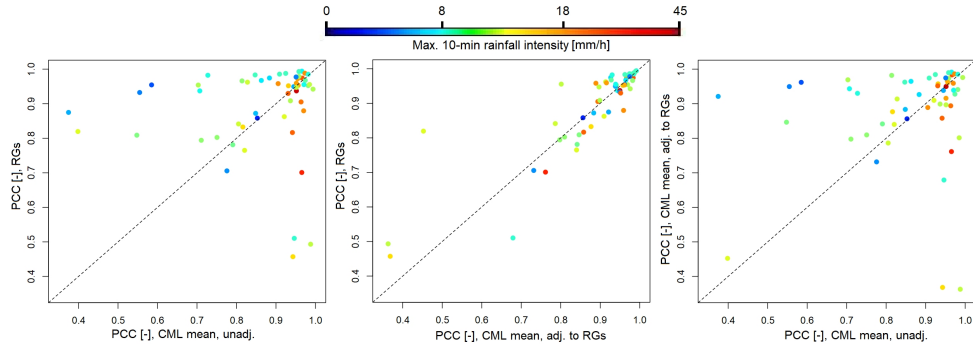


Figure 6.5: Scatterplots of PCC with color-coded max. 10-min rainfall intensities ($R_{max,10}$) of individual events. Left: The mean of unadjusted CML QPEs (x axis) vs. rain gauges (y axis). Middle: The mean of adjusted CML QPEs (x axis) vs. rain gauges (y axis). Right: The mean of unadjusted (x axis) and the mean of adjusted CML QPEs (y axis).

6.4 Discussion

Our experimental results on using QPEs from CMLs for urban rainfall-runoff predictions suggest that CMLs can indeed provide valuable rainfall data. However, if CML QPEs are not adjusted to rain gauges, the large bias in CML QPEs leads to unsatisfactory performance, especially for short CMLs. Nevertheless, the results strongly depend on the reliability of the rainfall-runoff model and discharge observations, the pre-processing method applied

to obtain CML QPEs, and the quality and availability of the CML data. Therefore, to better interpret our results, it is necessary to discuss:

- the combined effect of uncertainty in measured discharges and the rainfall-runoff model on overall performance of CML-based discharge simulations,
- CML preprocessing with a special focus on eliminating the bias in CML QPEs, and
- the effect of the quality and availability of CML QPEs on the representativeness of the results and their transferability to different catchments.

The rainfall-runoff model was validated using independent rainfall observations from three rain gauges located within or close to the catchment boundaries (Fig. 4.1, left) for all events analyzed in this study. This enables us to directly quantify the reliability of the model (see section 4.2). The validation shows that the model reproduces runoff very well in terms of both discharge volumes (dV) and temporal dynamics (PCC , partly NSE). The relative error in dV is small for most of the evaluated events (mean -0.007, st. dev. 0.153). These values are more than a magnitude lower than those obtained using unadjusted QPEs from short CML, and about two times lower in comparison to those of the best performing CML. Therefore, the bias in CML-based discharge simulations can be attributed mostly to the uncertainty (the bias) in CML QPEs and not to the combined uncertainty of observed discharges and the rainfall-runoff model.

The validation also shows that the simulated discharges are highly correlated with the observed ones (mean 0.95, st. dev. 0.06). The mean PCC for CML-based discharge simulations is between 0.49 and 0.86, with st. dev. between 0.15 and 0.43. Thus, the deficit in reproducing runoff dynamics can also be attributed predominantly to uncertainties in CML QPEs. The only exception are discharge simulations for heavy rainfalls obtained from the mean of all unadjusted CML QPEs (Fig. 6.3, boxplot ‘mean 16’), for which PCC values are comparable (mean 0.94, st. dev. 0.04) to the excellent runoff predictions using the local rain gauges (mean 0.96, st. dev. 0.02). In summary, the validation of the rainfall-runoff model demonstrates that the combined uncertainty related to measured discharges and the rainfall-runoff model introduces only very little variability and, most importantly, no systematic errors into the performance assessment.

Results of this study show that bias in unadjusted CML QPEs negatively affects their usefulness for rainfall-runoff modelling, especially in terms of volume-related statistics. Most importantly, unadjusted QPEs were increasingly overestimated as CML path length decreased since shorter CMLs are relatively more sensitive to errors in A_r estimation (2.4.1) due to, e.g. inaccurate WAA correction (Eq. 2.2). In our pragmatic rainfall retrieval approach,

WAA A_{wa} was considered constant and its value was taken from literature (Overeem et al., 2011). It can be expected that calibrating the WAA model using independent rainfall data, or stormwater runoff measurements which reflect transformed rainfall aggregated for a whole catchment well (Pastorek et al., 2019a), would result in less biased QPEs, on average. However, the large inter-event variability indicates that the simple wet antenna correction with a constant threshold is not satisfactory, and more precise WAA models (e.g. with WAA A_{wa} proportional to rainfall intensity) are necessary to obtain unbiased CML QPEs.

Adjusting CML QPEs to measurements from traditional rain gauges (Fencl et al., 2017) successfully minimizes the bias. However, using adjusted CML QPEs does not outperform predictions based on rain gauge data. Moreover, the adjustment considerably worsens the ability of CML QPEs to reproduce runoff dynamics during heavy rainfalls, except for QPEs from long individual CMLs with end nodes located further from the catchment than rain gauges. This is because the adjustment method strongly depends on the reliability of rain gauge observations which are often too far from each other to accurately observe small-scale rainfall variability. Thus, although the adjusting is conceptually promising for eliminating the bias, it requires further development. One important advantage of the adjustment suggested by Fencl et al. (2017) is that, thanks to the high temporal resolution of CML QPEs, it performs well also for rain gauge data with hourly resolution. Thus, this method can be recommended for disaggregating rainfall data in catchments where rain gauge data are available only in temporal resolutions suboptimal for urban drainage modelling.

We show that runoffs simulated using QPEs from (relatively short) CMLs located within or close to the catchment boundaries are, in spite of being biased, very well correlated with the observed runoffs. Moreover, in this respect they outperform runoffs simulated using the relatively unbiased QPEs from long CMLs, primarily during heavy rainfalls. This is probably because heavy rainfalls are often characterized by high spatial variability, and the paths of the long CMLs extend far beyond the catchment. Thus, these long CMLs cannot accurately capture areal rainfall over the catchment. For larger catchments, even relatively long CMLs might not extend out of the catchment, and thus they could be better suited to provide representative rainfall information. However, larger catchments might also require spatially distributed rainfall information, and assuming uniform rainfall, as in our study, might provide unsatisfying results. On the other hand, our results show that averaging unadjusted QPEs from all available CMLs best reproduces runoff dynamics, probably because it best captures the temporal variability of areal rainfall over the catchment, even though the averaging concerns a substantially larger area. This is in accordance with the findings of Ochoa-Rodriguez et al. (2015), who identified temporal variability of rainfall as the most sensitive attribute for urban rainfall-runoff simulations. Therefore,

it can be expected that CML QPEs will be suitable for modelling runoff dynamics also in other urban catchments where CML coverage corresponds to the spatial extent of typical rainfalls.

6.5 Conclusions

This study has evaluated the suitability of quantitative precipitation estimates (QPEs) from commercial microwave links (CMLs) for urban rainfall-runoff modelling. Using a unique data set from three summer seasons collected in a small (1.3 km^2) urban catchment in Prague-Letňany, runoff observed in the catchment was compared to runoff predicted using rainfall data from different observational layouts, in particular QPEs derived from various individual CMLs. We used a hydrodynamic model which accurately describes the rainfall-runoff process, although it underestimates flows for extreme events. The results have demonstrated that CML QPEs can be conveniently used for rainfall-runoff modeling. However, the CML data pre-processing, characteristics of the individual CMLs, such as frequency or path length, and their position influence the quality of the retrieved QPEs. The main conclusions are as follows:

- The sensitivity of CMLs to rainfall, which is given by their frequency, polarization, and length, is the most influential factor affecting the accuracy of CML QPEs, especially their bias, i.e. systematic under- or overestimation. This bias is greatest for the shortest CMLs, however, it is also variable among events. Thus, the ability of such biased CML QPEs to provide reliable flow estimates is predominantly low.
- As expected, the position of CMLs within the small urban catchment affects their ability to capture rainfall-runoff dynamics, such as the onset of a runoff event, timing of the hydrograph rising limb, runoff peak, and recession limb. The effect of CML position is especially pronounced for heavy rainfalls, when shorter CMLs with paths within or close to the catchment boundaries reproduce runoff dynamics better than longer CMLs extending far beyond the catchment.
- The best performance in terms of capturing runoff dynamics is obtained when rainfall observations of all CMLs are averaged. Notably promising results are obtained during heavy rainfall events, probably because areal rainfall from all the CMLs captures the temporal rainfall variability especially well, and runoff dynamics in small urban catchments are often more sensitive to temporal than spatial variations. Therefore, averaging of CML QPEs can be especially recommended for applications where the temporal structure of runoff and timing of peak flows is

more important than volume-related statistics, e.g. alarms during sewer construction/maintenance works.

- Adjusting the CML QPEs to data from rain gauges substantially reduces their bias while minimizing the difference among CMLs of various characteristics. Unfortunately, the adjustment also considerably worsens the ability of CML QPEs to reproduce runoff dynamics during heavy rainfalls, except for QPEs from long individual CMLs. On the other hand, the adjustment can be recommended for disaggregating rainfall data in catchments where traditional rainfall data are available only in temporal resolutions suboptimal for urban drainage modelling.
- Our experimental results demonstrate that CMLs cannot replace observation networks designed for long-term continuous hydrological monitoring. Many events had to be excluded from the analysis because of the limited CML data availability due to removal or replacement of CML units, communication outages, or hardware malfunctions, to name just a few challenges. Nevertheless, CMLs can very well complement the traditional networks and provide valuable data for operational hydrology. We expect that this is especially the case for sparsely gauged or completely ungauged regions.

Reducing systematic errors in CML QPEs remains a major challenge compromising their applications in water management tasks where runoff volume is essential, e.g. water balance modelling or designing retention capacity of drainage systems. CML QPE preprocessing methods tailored to different water management tasks, catchments, and CML networks could solve this problem. Therefore, it is necessary to better understand the interactions between the CML QPE observation errors and catchment runoff characteristics. Although modelling studies with virtual drop size distribution fields (Fencl et al., 2013) can be useful to investigate topological issues, more monitoring campaigns and experimental case studies are necessary to understand error-generating processes related to CML hardware, such as antenna wetting.

Chapter 7

Practical Approaches to Wet-Antenna Correction

This study analyzes how, when deriving quantitative precipitation estimates (QPEs) from commercial microwave links (CMLs), wet antenna attenuation (WAA) can be corrected without dedicated rainfall monitoring. For a set of 16 CMLs, the performance of six empirical WAA models is studied, both when calibrated to rainfall observations from a permanent municipal rain gauge network and when using model parameters from the literature. The transferability of WAA model parameters among CMLs of various characteristics is also addressed. The results show that high-quality quantitative precipitation estimates with a bias below 5% and RMSE of 1 mm/h in the median could be retrieved, even from sub-kilometer CMLs where WAA is relatively large compared to raindrop attenuation. Models in which WAA is proportional to rainfall intensity provide better WAA estimates than constant and time-dependent models. It is also shown that the parameters of models deriving WAA explicitly from rainfall intensity are independent of CML frequency and path length and, thus, transferable to other locations with CMLs of similar antenna properties.

The bulk of this chapter was originally published in:

Pastorek, J., Fencl, M., Rieckermann, J., & Bareš, V. 2022. **Precipitation Estimates from Commercial Microwave Links: Practical Approaches to Wet-Antenna Correction.** *IEEE Transactions on Geoscience and Remote Sensing* 60, 1–9.
<https://doi.org/10.1109/TGRS.2021.3110004>.

7.1 Introduction

The complexity of the antenna (radome) wetting process, namely its dependence on antenna hardware properties (e.g. coating; van Leth et al., 2018) and on atmospheric conditions other than precipitation, is a major challenge to reliable estimation of wet antenna attenuation (WAA). It also negatively affects the transferability of WAA models among different commercial microwave links (CMLs) and, thus, optimal WAA models should ideally be determined for each individual CML. This is especially true for models whose parameters depend on CML path length (e.g. Kharadly & Ross, 2001). However, optimal WAA model identification (e.g. for calibration purposes) on the level of individual CMLs is challenging for real-world application with networks consisting of a high number of CMLs. As noted by Ostrometzky et al. (2018), maintenance of dedicated equipment for the retrieval of the needed reference rainfall observations is impractical for such networks. Consequently, application-focused studies with city or regional-scale CML networks have often not applied any WAA correction at all (Chwala et al., 2012; Smiatek et al., 2017) or have used only a simple constant offset model (Pastorek et al., 2019b; Overeem et al., 2011; Roversi et al., 2020; Fencl et al., 2020). Although the latter approach may be a reasonable choice when observations of the difference between the transmitted and received signal levels $TRSL$ [dB] are available only as 15-min maxima and minima (Chwala & Kunstmann, 2019), it can introduce considerable bias in resulting CML quantitative precipitation estimates (QPEs) (Pastorek et al., 2019b; Fencl et al., 2019). To avoid such errors, Graf et al. (2020) recently tested a time-dependent (Schleiss et al., 2013) and a semi-empirical WAA model assuming a homogeneous water film on antenna radomes which depends on rain rate through a power law (Leijnse et al., 2008). However, in the case of both WAA models, only a single set of fixed parameters for all of around 4000 CMLs from their extensive dataset was used and this did not address the suitability of the WAA model parameters for individual CMLs.

This study analyzes, for the first time, six empirical WAA models, including a newly proposed one, based on considerably different assumptions and tests their performance in detail. In contrast to previous studies, often limited by a low number of CMLs investigated (Schleiss et al., 2013; Leijnse et al., 2008; van Leth et al., 2018), short time series of a few months (Leijnse et al., 2008; Overeem et al., 2011; Roversi et al., 2020) or 15-min CML data sampling intervals (Overeem et al., 2011; Rios Gaona et al., 2018), a rich dataset of more than two years of data retrieved from 16 CMLs with a sub-minute sampling rate is used. Motivated by the vision of reducing the costs of future studies with high numbers of CMLs, we also address the previously recognized need (Ostrometzky et al., 2018; Graf et al., 2020) to minimize the amount of auxiliary data necessary for WAA estimation without compromising the quality of retrieved QPEs and, thus, we introduce three

conceptual innovations not previously presented in relevant literature. Firstly, we show how the investigated empirical WAA models can be calibrated while notably minimizing the requirements on the reference rainfall data necessary, i.e. using only a rain gauge network with a spatial resolution of one gauge per $20-25 \text{ km}^2$ and a temporal resolution of 15 minutes. Secondly, we analyze the variability in WAA model parameters optimized for different CMLs, thus indirectly assessing parameter uncertainties, and investigate which of the studied models can provide reliable WAA estimates without being calibrated for each individual CML. This includes a reformulation of a previously reported WAA model (Valtr et al., 2019). Thirdly, we suggest a procedure enabling the application of rainfall-dependent WAA models without any auxiliary rainfall observations, i.e. using only CML data.

7.2 Methods

Attenuation data from 16 CMLs collected over a 3-year period (see section 4.1) are processed (section 7.2.1) and corrected for WAA using six empirical WAA models (sections 7.2.2 and 7.2.3). The resulting CML QPEs are evaluated against the rain gauge data from the municipal network (section 7.2.4).

7.2.1 From signal levels to QPEs

CML data processing steps before baseline separation, including a quality check and aggregation to a 1-min resolution, are done in the same way as described in section 6.2.2. Baseline attenuation B [dB] is assumed to equal $TRSL$ [dB] (Eq. 2.2) during dry periods. During wet periods, B is estimated by linearly interpolating from the dry periods. Data available from both CMLs and rain gauges for the wet period identification are used. First, we identify wet timesteps for the CML data (mean $TRSL$ of all CMLs) using a climatological threshold (Schleiss & Berne, 2010) defined as the 90th percentile of the rolling standard deviation of a 60-minute window. For the rain gauge data, timesteps are identified as wet when gauge tipping is observed at one or more gauges. Subsequently, wet periods are defined for both sensor types by setting the start of a wet period to one minute before the first observed wet timestep and the end to 60 minutes after the last one to ensure that baseline interpolation is not affected by wet antennas. Afterwards, the wet periods defined by the two sensor types are merged by taking the earliest starts and the latest ends. These are then used for the baseline separation using the linear baseline model.

From the above defined wet periods, only hydrologically relevant rainfall events (total rainfall depth $H > 2 \text{ mm}$) are selected for further processing.

After eliminating events with substantial data gaps, 53 events (360 hours) are available.

After the baseline separation, WAA A_{wa} [dB] is estimated (details in the next section) and subtracted to obtain raindrop attenuation A_r [dB] (Eq. 2.2). Then, A_r is divided by the CML path length and thus transformed into specific raindrop attenuation γ [dB/km] from which rainfall intensity R [mm/h] is calculated using Eq. 2.1, with parameters α and β according to ITU Radiocommunication Sector (2005). These parameter values are in very good agreement with values derived directly from drop size distribution observations (Chwala & Kunstmann, 2019; Valtr et al., 2019), however, they may not be optimal for other rain type regions (Rios Gaona et al., 2018).

7.2.2 Empirical WAA models

We evaluate a scenario without correcting for WAA (Zero) and six empirical models for WAA correction (overview in Table 7.1). For all models, it is assumed that WAA is estimated for two antennas, i.e. at both CML ends. The simplest approach is to model WAA A_{wa} as a constant offset (O; Overeem et al., 2011). In a more complex method, we model A_{wa} as time-dependent, exponentially increasing towards an upper limit during wet periods, and decreasing exponentially afterwards (S; Schleiss et al., 2013).

Next, we evaluate models where A_{wa} depends on R . Valtr et al. (2019) proposed a model (V) where the dependence on R is explicit through a power law

$$A_{wa} = 2k'R^{\alpha'} \quad (7.1)$$

where k' and α' are the power law parameters. We also analyze a model (KR) suggested by Kharadly & Ross (2001) deriving A_{wa} from observed attenuation after baseline separation A [dB] (see Eq. 2.2), i.e. depending on R implicitly. However, as A is dependent on CML path length, optimal parameters of the KR model would differ for two CMLs with the same hardware but with different path lengths. To eliminate this feature, we propose a model (KR-alt) in which A_{wa} is bounded by an upper limit, as in Kharadly & Ross (2001), but derived from R explicitly through a power law

$$A_{wa} = C(1 - \exp(-dR^z)) \quad (7.2)$$

where C [dB] represents the maximal A_{wa} possible, and d and z are power law parameters. Nevertheless, as optimal C and d values are not independent and can compensate for each other (similar to the KR model, see Fig. 7.4), we reduce the number of parameters to two by setting $d = 0.1$.

WAA models with parameters independent of CML path length can also be formulated when A_{wa} is derived explicitly from γ , not only R . However, it is

unclear which of the two alternatives would provide WAA model parameters independent of CML frequency. Unlike γ , R is independent of CML frequency. The results from Leijnse et al. (2008) suggest that A_{wa} is also considerably less sensitive to CML frequency than A_r or γ . Therefore, parameters of the models deriving A_{wa} from R explicitly are probably more transferrable among frequencies. To confirm this hypothesis, we reformulate the model of Valtr et al. (2019) (V-alt), and replace R with γ so that:

$$A_{wa} = 2p\gamma^q \quad (7.3)$$

where p and q are the power law parameters.

As neither R nor γ can be observed directly using CMLs, the V, V-alt, and KR-alt model equations must be rearranged to include only one unknown variable, A_{wa} , which can thus be quantified from A (details in the next section). The rearranged equations are then solved numerically.

WAA model	Parameter values from the literature	Abbrev.
Zero WAA (no WAA correction)	—	Zero
Constant non-zero offset	$A_{wa} = 1.585$ dB the mean of the optimal values identified in Overeem et al. (2011)	O
Dynamic (time-dependent) (Schleiss et al., 2013)	$W = 2.3$ dB $\tau = 15$ min from Schleiss et al. (2013)	S
Depending on A explicitly with an upper limit (Kharadly & Ross, 2001)	$C = 8$ dB $d = 0.125$ from Kharadly & Ross (2001); for 27 GHz	KR
Depending on R explicitly with an upper limit	—	KR-alt
Power-law relation to R (Valtr et al., 2019)	$k' = 0.68$ $\alpha' = 0.34$ from Valtr et al. (2019)	V
Power-law relation to γ (reformulated V)	—	V-alt

Table 7.1: Overview of the investigated WAA models and their parameters.

7.2.3 Practical details on WWA model equations

Herein we show how WAA models dependent on rainfall intensity can be used during the CML data processing routine without the need for auxiliary rainfall observations. In particular, we formulate single-unknown equation forms of the models which relate WAA A_{wa} [dB] explicitly to the rainfall intensity R [mm/h] and to the specific raindrop attenuation γ [dB/km]. Using these rearranged equations, A_{wa} can be quantified directly from the observed attenuation after baseline separation A [dB], e.g. by solving the equations numerically. The relation between V and V-alt models is also provided.

■ V model

The original equation of V model (Eq. 7.1; Valtr et al., 2019), where k' and α' are the WAA model's power law parameters, requires independent observation of the rainfall intensity R [mm/h] as its input. However, it holds that:

$$R = \alpha\gamma^\beta \quad (7.4)$$

where α and β are the power law parameters with values depending on the CML frequency and polarization. Moreover, if L [km] is the CML path length, then

$$\gamma = (A - A_{wa})/L. \quad (7.5)$$

Therefore, using Eq. 7.4 and 7.5, the original Eq. 7.1 can be rearranged into the following single-unknown form which can be used to quantify A_{wa} from A :

$$A_{wa} = 2k'(\alpha((A - A_{wa})/L)^\beta)^{\alpha'}. \quad (7.6)$$

■ V-alt model

Starting from its original equation in which A_{wa} is explicitly dependent on R (Eq. 7.1), V model can be reformulated using Eq. 7.4 in the following manner:

$$A_{wa} = 2k'R^{\alpha'} = 2k'(\alpha\gamma^\beta)^{\alpha'} = 2k'\alpha^{\alpha'}\gamma^{\beta\alpha'}. \quad (7.7)$$

If ($p = k'\alpha^{\alpha'}$ and $q = \beta\alpha'$), then the V-alt model (Eq. 7.3) represents a reformulation of the V model in which A_{wa} is explicitly dependent on γ .

Similarly as the original V model, also the V-alt model (Eq. 7.3) can be rearranged using Eq. 7.5 into a single-unknown form which can be used to quantify A_{wa} from A :

$$A_{wa} = 2p((A - A_{wa})/L)^q. \quad (7.8)$$

■ KR-alt model

The following original KR model (Kharadly & Ross, 2001), where C [dB] and d are the model parameters, relates A_{wa} explicitly to A :

$$A_{wa} = C(1 - \exp(-dA)). \quad (7.9)$$

However, as A is affected by CML path length, optimal parameters of the KR model would differ for two CMLs with the same hardware but different path lengths. To eliminate this feature, we have proposed a WAA model (Eq.

7.2; KR-alt) in which A_{wa} is, similar to Eq. 7.9, bounded by an upper limit, but derived from R explicitly through a power law.

Analogically to the V model (Eq. 7.1), also the KR-alt model (Eq. 7.2) can be rearranged, by applying Eq. 7.4 and 7.5, into a single-unknown form which can be used to quantify A_{wa} from A :

$$A_{wa} = C(1 - \exp(-d(\alpha((A - A_{wa})/L)^\beta)^z)). \quad (7.10)$$

7.2.4 Calibration and performance of WAA models

The WAA models studied are evaluated when using parameter values taken from the literature, if available, and when calibrated to rainfall data from the three municipal rain gauges. Moreover, for each WAA model, calibration is done in three scenarios:

- separately for each of the 16 CMLs;
- separately for each frequency band; and
- for all CMLs at once.

In total, data from 53 rainfall events (360 hours) are available for WAA model calibration and evaluation. From these, we randomly select 25 events (281 hours) for the calibration. Model parameters are optimized by comparing the CML QPEs with the mean R of the three municipal rain gauges. Both data sets are aggregated from a 1-min to a 15-min resolution to reduce observation noise. The root mean square error (*RMSE*) is used as the objective function and optimized with simulated annealing, an optimization method designed for complicated non-linear functions with many local minima (Xiang et al., 2013). For calibration scenarios using multiple CMLs at once, the mean RMSE of the CMLs is optimized.

Once the optimal WAA model parameters are identified, they are used to derive CML QPEs for the remaining 28 events (349 hours) not used for calibration. The CML QPEs are aggregated from the 1-min to the 15-min resolution and evaluated by direct comparison with the rain gauge data (the mean of the three gauges in the 15-min resolution). The QPEs are evaluated individually for each CML using a time series consisting of all 28 events, the performance for individual events is not quantified. Performance metrics employed are:

- the relative error of the rainfall depth dH [%] reflecting the bias;
- the root mean square error $RMSE$ [mm/h]; and
- the Spearman rank correlation coefficient SCC [-] which quantifies the strength of a monotonic relationship between two variables and is independent of both linear and non-linear bias.

■ 7.3 Results

Firstly, the performance of the estimated CML QPEs summarized for all CMLs is presented (7.3.1). Secondly, the QPEs are investigated in closer detail on the level of individual CMLs (7.3.2). Parameter values used for the WAA model evaluation are also presented (7.3.3).

■ 7.3.1 Summary for all CMLs

The results summarized in Fig. 7.1 show that, when calibrated individually for each CML, models in which A_{wa} is proportional to R (KR, V, KR-alt, V-alt) can lead to CML QPEs with a bias lower than 5% in the median (up to 10% for most CMLs) and with $RMSE$ between 0.8 and 1.2 mm/h. Models explicitly relating A_{wa} to R (V and KR-alt) attain similarly good values (median bias less than 5%, standard deviation 18%) not only when calibrated individually for each CML, but also when calibrated for groups of CMLs with the same frequency and for all CMLs at the same time. Similarly, $RMSE$ obtained using these two models is almost the same, between 0.8 and 1.2 mm/h, for all three calibration approaches. A very similar performance is reached using the V-alt model, which relates A_{wa} to γ , when calibrating separately for each of the three frequency bands. However, when calibrating the V-alt model for all CMLs at once, the standard deviation of dH increases to 25% and $RMSE$ values reach up to 1.4 mm/h for some CMLs. Calibrating models O and S leads to markedly underestimated dH values for most CMLs (around 40% in median) for all three calibration approaches. This also affects the respective $RMSE$ values which are around 1.4 mm/h in the median for

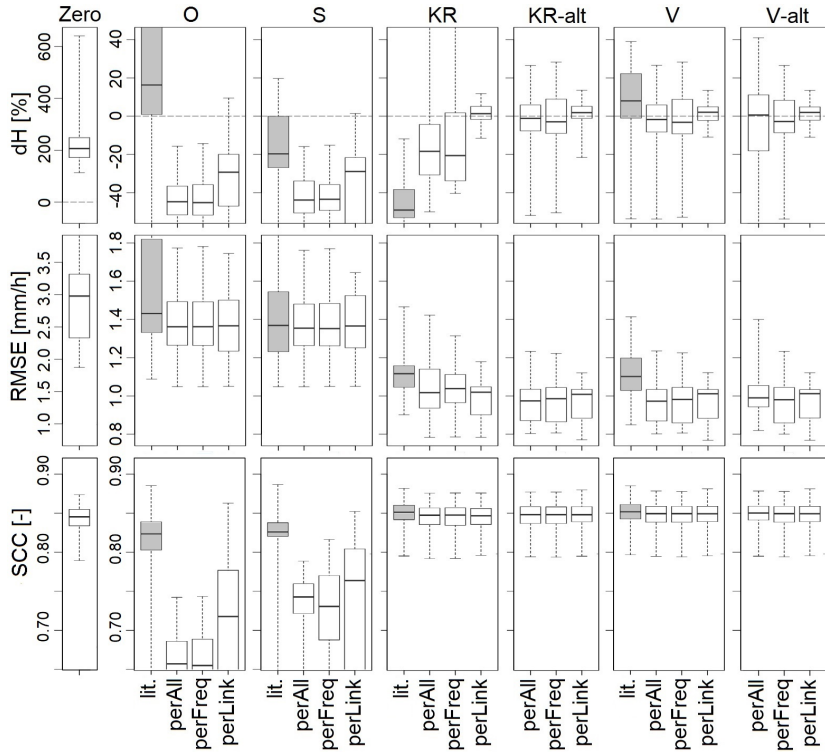


Figure 7.1: Boxplots showing variation in the performance of the QPEs from the 16 individual CMLs quantified by the performance metrics dH (top), $RMSE$ (middle), and SCC (bottom). CML QPEs have been derived without WAA correction (Zero) and using the six WAA models. Sub-boxplots show the effect of WAA model calibration (lit. – parameter values from literature, perAll – calibrated for all CMLs at once, perFreq – calibrated separately for CMLs operating at the three various frequency bands, perLink – calibrated separately for each CML). Note the different ranges of the y-axes for the Zero model.

all calibration approaches. Interestingly, using the S model with parameter values from the literature leads to a lower bias for most CMLs (dH -20% in the median). However, the $RMSE$ is virtually the same as for the calibrated model, with only a slightly larger variance. For other WAA models, the literature values perform, in general, worse than those optimized during the calibration, both in terms of dH and $RMSE$. As expected, without the WAA correction, CML QPEs are considerably overestimated (median dH ca. 200%, $RMSE$ ca. 3 mm/h).

The correlation in terms of SCC (Fig. 7.1 bottom) reaches very similar values (about 0.85 in median) for all WAA models in which A_{wa} is proportional to R (KR, V, KR-alt, V-alt), regardless of whether/how they are calibrated. Only negligibly lower values are reached when not using any WAA model at all (scenario Zero). For most CMLs, SCC values between 0.8 and 0.85 are associated with the O and S models with parameter values from the

literature. Calibrating these two models has led not only to a considerable underestimation of rainfall, but also to relatively low *SCC* values (medians between 0.65 and 0.76).

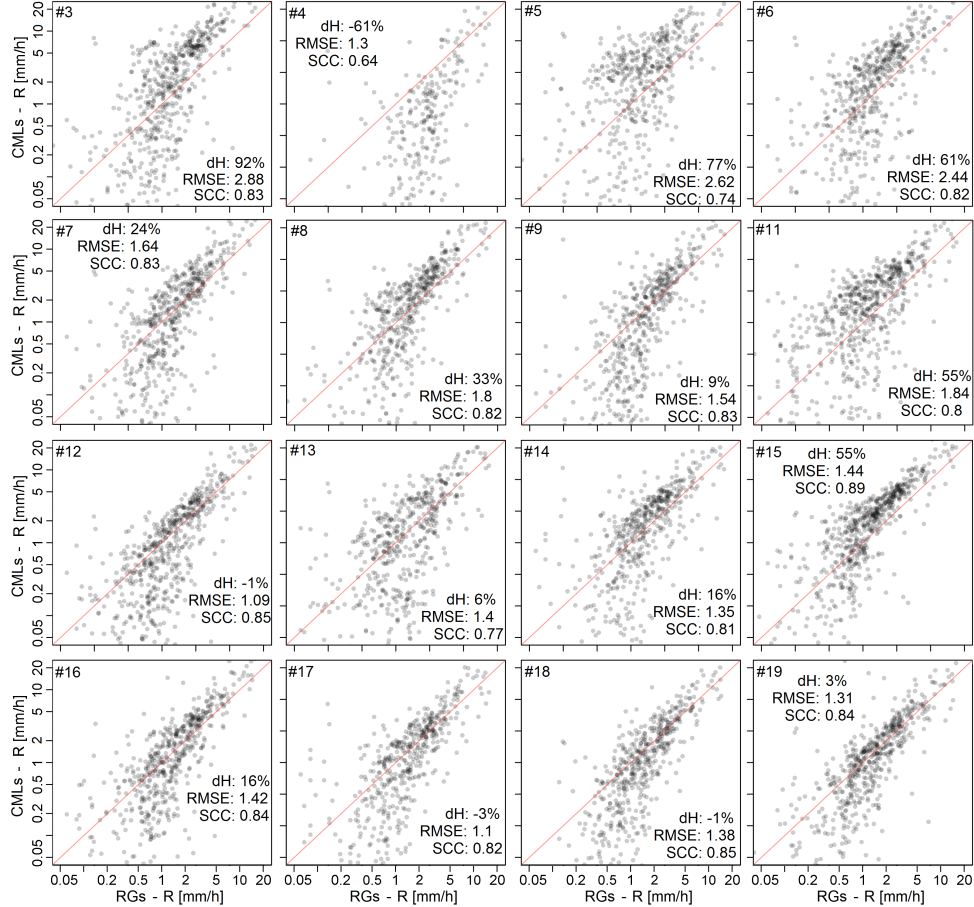


Figure 7.2: Scatter plots comparing rain gauge data (RGs) with CML QPEs for the O model with parameters from the literature. Note that the axes are in logarithmic scales. The presented 15-minute data from the 28 rainfall events used for the evaluation represent 349 hours of observations. In 835 out of the 1,401 time steps, rain gauge data contain non-zero records. Most points with RG rainfall intensity below 0.3 mm/h are out of the plotting range, as the respective CML QPEs are below 0.05 mm/h.

7.3.2 Individual CMLs

In addition, we analyze the estimated QPEs on the level of individual CMLs for two WAA modelling scenarios. First, CML QPEs derived using the commonly used O model with parameter values from literature are compared with the rain gauge data (Fig. 7.2). Next, representing the better performing WAA models from above, the same is done for the V model with parameters

optimized for all CMLs at once (Fig. 7.3). The V model leads to a distinct improvement over the O model. The V model reduces the bias for low and high R and thus removes the dependence of errors in CML QPEs on R . Therefore, the performance metrics dH and $RMSE$ are improved for most CMLs, however, the change of SCC is practically negligible. The reduction of errors is most significant for the shortest CMLs, as the relative contribution of A_{wa} to A decreases with the increasing path length.

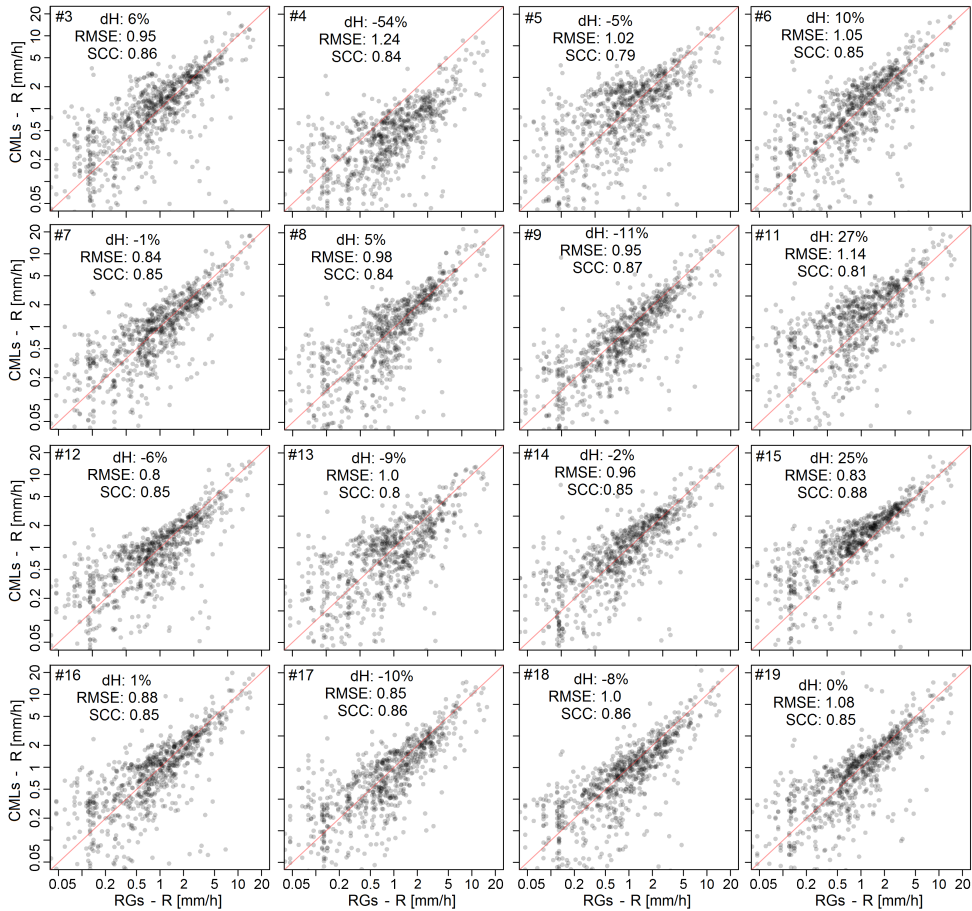


Figure 7.3: Scatter plots comparing rain gauge data (RGs) with CML QPEs for the V model with the same parameters used for all the CMLs (obtained by optimizing for all CMLs at once). Note that the axes are in logarithmic scales. The presented 15-minute data from the 28 rainfall events used for the evaluation represent 349 hours of observations. In 835 out of the 1,401 time steps, rain gauge data contain non-zero records.

7.3.3 WAA model parameters

We also present parameter values used for the WAA model evaluation, both optimized during calibration and taken from the literature (Fig. 7.4). Op-

timized parameter values of the V and KR-alt models are similarly located in their parameter spaces. Moreover, optimal parameter values for the three various frequency bands are, for these two models, located very close to the optimal values obtained when calibrating for all CMLs at once. This stands in contrast to the V-alt method for which a dependence between the frequency band and the optimal parameter values can be seen. For the KR model, the clear dependence of the two model parameters is most striking. For the S model, optimal values of the W parameter are similar to the parameter values of the O model. However, there is no clear relation to the CML frequency for either of these two WAA models. Parameter values taken from the literature are, in all four cases, located relatively close to the optimized parameters.

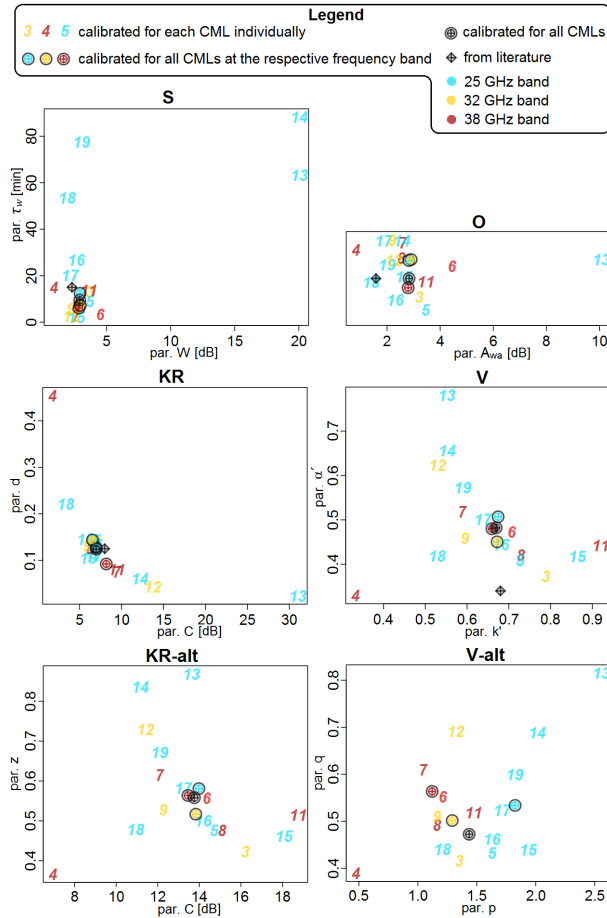


Figure 7.4: WAA model parameter values used for WAA model evaluation, both optimized during calibration and taken from literature (if available). The numbers indicate CML IDs and the colors indicate frequency.

7.4 Discussion

The best results, in terms of dH and RMSE, are, in general, achieved for the models in which WAA A_{wa} is proportional to rainfall intensity R (KR, V, KR-alt, V-alt). For these models, QPEs of the same high quality can be obtained when calibrating for each CML separately. However, the V model and the newly proposed KR-alt model, which both relate A_{wa} to R explicitly, perform very well, even when using the same parameter set for all CMLs. As the KR model relates A_{wa} to A , which is dependent on CML path length, it performs markedly worse when using the same parameter set for more CMLs. The V-alt model performs very well when using the same parameters for CMLs operating at one frequency band and moderately worse when using the same parameter set for all frequency bands. This is in agreement with the calibrated model parameter values (Fig. 7.4) and supports the hypothesis that the parameters of models deriving A_{wa} from R explicitly (V, KR-alt) are more transferrable among CMLs of various frequencies than the parameters of models deriving A_{wa} explicitly from (V-alt).

The results of calibrating the O and S models resemble each other in terms of estimated rainfalls (Fig. 7.1), optimal model parameters (Fig. 7.4), and WAA levels (Fig. 7.5). The rainfall underestimation (i.e. WAA overestimation) associated with the O and S models is likely caused by different optimal parameter values for $RMSE$, used as the calibration objective function, and dH due to the systematic errors in rainfall estimates when modelling WAA A_{wa} as completely or almost constant.

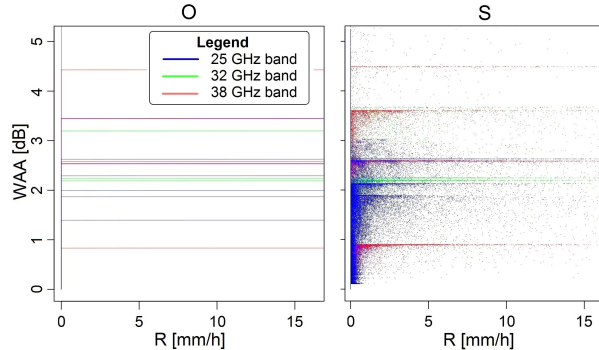


Figure 7.5: WAA levels obtained using the O and S WAA models when calibrated separately for each CML in relation to the respective CML QPEs. The vertical line in the left panel at $R = 0 \text{ mm/h}$ is caused by the nature of the O model. If observed attenuation after baseline separation A is lower than a given parameter value of the O model, WAA is considered equal to A , i.e. there is no rainfall observed.

In total, our results show that unbiased CML QPEs could be retrieved without the need for extensive additional rainfall monitoring when empirical models for

WAA estimation are calibrated to rainfall data from the permanent municipal rain gauge network. Models in which WAA is dependent on rainfall intensity provide the best WAA estimates. Moreover, models explicitly relating WAA to rainfall intensity can provide optimal results even when using the same set of parameter values for CMLs of different characteristics.

The presented results confirm the importance of appropriately correcting for WAA when deriving QPEs from CMLs which is in agreement with previous research (Chwala & Kunstmann, 2019). In particular, the results imply that modelling WAA as constant (O model) is not satisfying when TRSL data in 1-min resolution are available. This is in accordance with Pastorek et al. (2019b); Fencl et al. (2019) and contradicting Ostrometzky et al. (2018), however, it should be noted that the latter study focused on WAA estimation for purposes of CML network design and investigated E-band CMLs. Nonetheless, our findings do not dispute the statement that this approach may be a reasonable choice if only 15-min TRSL maxima and minima are available (Chwala & Kunstmann, 2019).

It is shown that the most accurate rainfall estimates are associated with models relating WAA to rainfall intensity, which is in agreement with the WAA estimation approaches presented in Valtr et al. (2019); Kharadly & Ross (2001); Leijnse et al. (2008); Fencl et al. (2019). On the other hand, having provided a comparison of the performance of different WAA models, Schleiss et al. (2013) came to different conclusions. Although their results correspond to ours in terms of *RMSE*, not only for the scenario without WAA correction (Zero; 3.15 mm/h), but also for the WAA models O (1.34 mm/h) and KR (0.91 mm/h), they observed the best performance for the time-dependent S model (0.72 mm/h). It should be noted that they used data from only a single CML and that the parameter values differed from those used in our study because the models were calibrated to local rainfall data from five disdrometers along the CML path. Since, in our case, the S model has only performed (and generally behaved) very similarly as the constant O model, it seems that, in accordance with van Leth et al. (2018), wetting dynamics play a much smaller role for the antennas used in this study than for those analyzed by Schleiss et al. (2013). Recently, similar behavior was observed by Graf et al. (2020) who found that a semi-empirical WAA model assuming a homogeneous water film on antenna radomes dependent on rain rate through a power law (Leijnse et al., 2008) led to more precise CML QPEs than the S model. As their analysis was based on a large country-wide dataset of around 4000 CMLs, it can be concluded that CML antennas for which WAA is not affected by the wetting dynamics are rather usual.

However, the relevance of our findings for other CML networks should be subject to further research. Firstly, it is likely that the capacity of rainfall data from rain gauge networks for calibrating WAA models will depend on gauge network density as the correlation among the gauges decreases

with increasing distance. Aggregating the data to coarser resolutions for the calibration might improve the results as it would improve the correlation (Villarini et al., 2008). Nevertheless, if the sensors are too far from each other, it might be more appropriate to use long-term (e.g. monthly) precipitation heights.

Secondly, the reference areal rainfall used to evaluate the performance of the WAA models has been derived from the same three rain gauges that had been previously used to calibrate the WAA models. However, the rain gauge network density of one gauge per $20 - 25 \text{ km}^2$ might not be sufficient to reliably represent areal rainfall for events with high spatial variability, e.g. storms with small convective cells. Therefore, out of the 28 individual rainfall events used for the WAA model evaluation, we have identified 11 events with the highest variability among the rain gauges and repeated our analysis using only the data from the remaining 17 events. Differences between the results for the 17 events and for all 28 events together are subtle. The estimated rainfall heights are slightly higher when evaluating all 28 events together than when using the 17 less variable events only. However, differences in terms of RMSE and SCC are minimal, and mutual relations of the individual WAA models and calibration scenarios are not affected.

Due to the use of only three rain gauges, we are also not able to precisely estimate rainfall starts and ends specifically for each CML. Therefore, the process of wet period identification has been designed to avoid classifying wet timesteps as dry, rather than vice versa. This approach makes wet periods longer, however, as the baseline is relatively stable (Schleiss et al., 2013), the order of errors in the estimated baseline levels is well below 1 dB.

Next, all CMLs used in this study are from the same product family of the same manufacturer (Ericsson, Mini-Link) and have aged similarly due to exposure to similar climatic conditions. However, different behavior might be observed for CML antenna hardware of different producers, exposed to different climates for different time periods, or for other specific conditions (e.g. non-zero antenna elevation angles), and thus, the results of this study might not be directly applicable in such circumstances.

Lastly, it should be noted that the V model was originally derived (Valtr et al., 2019) by using one of our 16 CMLs and data from one of the three summer seasons that we have investigated herein.

7.5 Conclusions

We have shown in this study that virtually unbiased QPEs could be retrieved from CMLs without the need for dedicated rainfall monitoring campaigns.

CML QPEs with a bias lower than 5% and $RMSE$ of 1 mm/h in the median have been obtained when the empirical models for WAA estimation have been calibrated to rainfall data from the permanent municipal rain gauge network with a spatial resolution of one gauge per $20 - 25 \text{ km}^2$. It has been shown that such high-quality QPEs can even be derived from short, sub-kilometer CMLs where WAA is relatively large compared to raindrop attenuation. Models relating WAA to rainfall intensity, implicitly or explicitly, have led to the best results. For the latter, parameter sets have been found to be suitable for CMLs of various path lengths operating at various frequency bands, which could thus be transferred to other locations with CMLs of similar antenna hardware characteristics. Moreover, it has been demonstrated how these WAA models can be successfully applied without any auxiliary rainfall observations, i.e. using CML data only.

This study has confirmed both the potential of CMLs as a source of high-quality rainfall data and the importance of appropriate WAA correction when deriving the QPEs. The presented advances in minimizing the requirements on auxiliary data necessary, both during the calibration of WAA models and during their implementation in the CML data processing routine, represent a legitimate step towards the retrieval of reliable QPEs from large CML networks in conditions where rainfall data are scarce. However, since the potential usefulness of CML QPEs increases with the decreasing availability of other rainfall (or other reference) data, further studies are needed, ideally with extensive datasets containing different CML hardware, to advance our capacity to correct for WAA in the data-scarce conditions. This would also be greatly beneficial for the application of CML QPEs in quantitative hydrological tasks such as urban rainfall-runoff predictions.

Chapter 8

On the value of CML QPEs for urban rainfall-runoff modelling: The final study

blabla bla bla

The bulk of this chapter ...:

Pastorek, J., Fencl, M., & Bareš, V. **Blabla**. Submitted to *blabla*.

8.1 Introduction

Quantitative precipitation estimates (QPEs) retrieved from commercial microwave links (CMLs) have been found to provide valuable rainfall information which could complement traditional observations with rain gauges and weather radars (Chwala & Kunstmänn, 2019; Gosset et al., 2016; Imhoff et al., 2020; Rios Gaona et al., 2018; Uijlenhoet et al., 2018). However, despite the high potential and recent advances, only a few studies have investigated the ability of QPEs derived from real-world CML networks for quantitative hydrology, either for rural (Brauer et al., 2016; Cazzaniga et al., 2020; Smiatek et al., 2017) or urban catchments (Disch et al., 2019; Pastorek et al., 2019b; Stránský et al., 2018). Therefore, many questions regarding their hydrological applications remain unanswered.

It has been shown that using CML QPEs can lead to very well predicted temporal dynamics of runoff from a small urban catchment. However, systematic errors in QPEs, common especially for short (ca. < 2 km) CMLs, make them unsuitable for practical applications where volume is of high importance (Pastorek et al., 2019b, Chapter 6). This is unfortunate because such QPEs could be particularly useful for urban hydrology as they often represent well the typical scales of small urban catchments. Moreover, shorter CMLs are

better suited to capture small-scale rainfall spatial variability which is of high importance for urban hydrology. It remains to be investigated to what extent the recent advances in CML QPE retrieval can improve the value of QPEs from such CMLs for urban rainfall-runoff modelling.

It has also been concluded that CML QPEs, if available in high temporal resolutions, could be conveniently used for urban hydrological modelling in combination with other rainfall data, e.g. to disaggregate cumulative rainfall measurements from point rain gauges (Disch et al., 2019; Stránský et al., 2018). Nevertheless, CML QPEs could be particularly useful in regions where long-term rainfall monitoring networks are not available, or available only in resolutions which do not suffice for most purposes of urban hydrological modelling (Gosset et al., 2016). Yet, it is not clear how to make the best use of CML QPEs under such conditions.

It has been argued that ignoring the uncertainty, particularly related to input data, compromises (not only) hydrological modelling (Beven, 2006; Kavetski et al., 2006), or similarly, that quantification of the uncertainty associated with the models in urban stormwater modelling is a must (Dotto et al., 2012). However, extensive quantification of the uncertainties related to applying CML QPEs in urban hydrology, and a comparison with traditional rainfall data uncertainty, has not been presented yet in relevant literature.

We address the above mentioned knowledge gaps and assess the value of CML QPEs for rainfall-runoff modelling in a small (1.3 km^2) urban catchment. The rainfall-runoff modelling performance associated with the CML QPEs is evaluated by quantifying the uncertainties in the rainfall-runoff modelling outputs. We do this while trying to reduce the systematic errors in the CML QPEs with the help of three various reference data sets. We believe that an equivalent of at least one of these datasets could be available to most urban hydrology professionals. These datasets include:

- 60-min data from three rain gauges located 2–3 km outside of the catchment;
- 60-min data from a single rain gauge located in a 8-km distance from the catchment;
- Stormwater discharge observations in combination with a rainfall-runoff model.

8.2 Methods

The study is performed using rainfall and runoff data collected during 46 rainfall-runoff events (670 hours) observed over a three-year period in an urban

catchment with the area of 1.3 km^2 (section 8.2.1). QPEs are derived from CMLs using recent state-of-the-art approaches which could be implemented with the data available (section 8.2.2). We seek to reduce the bias in CML QPEs by calibrating the wet-antenna attenuation (WAA) estimation model to the three reference datasets available, using data from 23 randomly selected events (section 8.2.3). The remaining 23 events are used in the validation stage (section 8.2.5), in which rainfall data retrieved using all observation layouts of interest (section 8.2.4) are propagated through a rainfall-runoff model and the model outputs are evaluated against observed discharges. The model performance is analyzed using a robust prediction uncertainty quantification method.

8.2.1 Data acquisition

The dataset used in this study was collected in a small (1.3 km^2) urban catchment drained by a stormwater sewer system and located in the Letňany neighborhood of Prague, Czech Republic (details in chapter 4). Most importantly, we collected signal-level data from 16 CMLs located within the catchment and its surroundings (Fig. 4.2). These data were retrieved at a 10-s resolution. The CMLs (Mini-Link, Ericsson) belong to a major telecom operator, broadcast at 25–39 GHz frequencies and feature path lengths between 816 and 5795 m. Next, we use rain gauge data from a permanent monitoring network operated by the municipal sewer authority with the density of 1 gauge per $20\text{--}25 \text{ km}^2$ (Fig. 4.2). These gauges are referred to as “municipal”. Moreover, we observed rainfall using additional rain gauges temporarily installed at three locations around the catchment with the intention of increasing the rain gauge network density in the area (Fig. 4.1). These gauges are referred to as “local”. All the rain gauges are tipping-bucket rain gauges (MR3, Meteoservis) and their observations were recorded at a 1-min resolution. When the rain gauge data are used as the reference for WAA model optimization, their resolution is aggregated to 60 min for the sake of this study. In addition, using an area-velocity flowmeter (Triton, ADS), we measured discharges at the stormwater drainage system outlet (Fig. 4.2). The temporal resolution of the discharge measurements is 2 min for wet periods and 10 min for dry periods.

From the three-year observation period, we select data from hydrologically relevant rainfall events (rainfall height $H > 2 \text{ mm}$) and only use these in the presented study. After eliminating events with substantial data gaps, 46 rainfall-runoff events (670 hours) are available, from which we randomly select 23 (340 hours) to be used for the WAA model calibration (section 8.2.3). The remaining 23 events (330 hours) are used in the validation stage (section 8.2.5).

8.2.2 Deriving CML QPEs

Rainfall retrieval from commercial microwave links follows the general concept presented in chapter 2.3. Up to the baseline separation, the first steps of processing the observed *TRSL* [dB] data, including a quality check and aggregation to a 1-min resolution, are done in the same way as in 6.2.2. Baseline is estimated as a moving median with a centered window having the length of 1 week applied on *TRSL* time series averaged over 60-min intervals (Fencl et al., 2020). To estimate WAA, we use the model proposed by (Valtr et al., 2019, see Eq. 7.1). Values of the model parameters k' and α' are obtained by calibration to the individual reference data sets available (details in section 8.2.3).

After subtracting baseline B [dB] and WAA A_{wa} [dB] from the observed $TRSL$ (Eq. 2.2), raindrop-induced attenuation A_r [dB] is used to compute rainfall intensity R [mm/h] (Eq. 2.1) with parameters α and β according to ITU Radiocommunication Sector (2005), similarly as in chapter 7.2.1.

8.2.3 WAA model calibration

Reference data sets used to calibrate the WAA estimation models include the following:

- 60-min data from the three closest municipal rain gauges located 2–3 km outside of the catchment (Fig. 4.2). A single time series, constructed as the mean of the instantaneous R [mm/h] values of the three gauges, is used.
 - 60-min data from a municipal rain gauge located at the Prague central waste water treatment plant (WWTP) in an 8-km distance to the south-west from the catchment (Fig. 4.2).
 - Stormwater discharges observed at the catchment's drainage system outlet (Fig. 4.2) at a 2-min resolution for wet periods and a 10-min resolution for dry ones.

The WAA model is calibrated successively for each individual reference dataset available. The optimization is performed separately for each single CML.

When using rain gauge data as the reference, the WAA model parameters are optimized by comparing QPEs with the gauge data as described in 7.2.4, however, with CML QPEs aggregated to 60-min resolution to match the gauge data resolution. The root mean square error is used as the objective function.

When employing the discharge measurements, we repeatedly propagate the CML QPEs in the original 1-min resolution through a deterministic rainfall-runoff model (details in chapter 4.2) and optimize the WAA model parameters by comparing the modelled and observed discharges. Now, the Nash–Sutcliffe efficiency is the objective function. In the case of both calibration approaches, the objective functions evaluate the QPEs as whole time series consisting of all 23 events, i.e. not considering the performance for individual events.

8.2.4 Rainfall observation layouts

Using data from the 23 rainfall-runoff events not employed in the calibration stage, several rainfall observation layouts are evaluated. Most importantly, we asses three sets of CML QPEs derived using the calibrated WAA models, corresponding to the three reference datasets used for WAA calibration (section 8.2.3). It has been concluded that only a few very precise CMLs are expected to deliver the most accurate areal QPEs (Fencl et al., 2015) and that the position of CMLs within a small urban catchment affects their ability to capture rainfall-runoff dynamics (Pastorek et al., 2019b, chapter 6). Therefore, for all three CML QPE observation layouts, we evaluate the mean QPEs of only those CMLs the paths of which best cover the catchment of interest, i.e. CMLs #3, #7, #8, #12, and #15 (Fig. 4.2). The potential of other CML subsets is discussed in chapter 8.4.

Next, to provide a comparison with capabilities of traditional rain gauge observations, we also asses data from the rain gauges used for the WAA model calibration. In particular, we evaluate 60-min records from the single gauge at an 8-km distance and data from the three gauges at 2–3 km distances (Fig. 4.2) in the original resolution of 1 min. The former layout represents a observations potentially available in data-scarce conditions, whereas the latter corresponds to the best data usually available in long-term in the context of Czech Republic. Additionally, we evaluate as well the performance of 1-min observations from the three local rain gauges representing the best-case-scenario regarding the availability of traditional rainfall data (Fig. 4.1).

8.2.5 Rainfall data validation by rainfall-runoff modelling

Rainfall data retrieved using the above observation layouts are propagated through a rainfall-runoff model, and the model outputs are evaluated against observed discharges. We decide to quantify uncertainties of the rainfall-runoff model predictions and employ the Bayesian uncertainty analysis framework of Kennedy & O'Hagan (2001) as formulated by Reichert & Schuwirth (2012) and first used in a context similar to ours by Del Giudice et al. (2013). More recently, this approach has been successfully applied by Sikorska & Seibert

(2018) to analyze the value of different precipitation data for flood prediction in an alpine catchment. The basic principle of the method is to extend the deterministic rainfall-runoff model by a stochastic error model which explicitly accounts for systematic model errors, i.e. bias. More information on the principles or particular details of this uncertainty quantification method can be found in chapter 3.2.

The deterministic rainfall-runoff model was built in the EPA-SWMM software. It was calibrated in the past and has shown to perform well, except for extreme rainfalls. A detailed description of the rainfall-runoff model and an analysis of its performance can be found in chapter 4.2. We use the model to simulate discharges at the outlet of the local stormwater drainage system. Except for data from the local rain gauges, rainfall input is implemented in the model as areal rainfall, meaning that rainfall intensity in a given time step has a constant value over all model subcatchments. For the local rain gauges, the catchment is divided into three Thiessen polygons, corresponding to the local gauges at three locations (Fig 4.1).

To maximize the accuracy of rainfall-runoff predictions and the reliability of the associated uncertainty quantification, the whole extended model should be calibrated. Nevertheless, we only optimize the stochastic error model parameters in this study, since the deterministic rainfall-runoff model has been calibrated in the past and has shown to perform well (chapter 4.2). As the model is to be calibrated in a Bayesian framework, prior probability distribution of the model parameters must be first defined (Table 8.1). The part of the error model representing the random noise only has a single parameter - the asymptotic stand. dev. of the random errors σ_E [l/s]. The part of the stochastic model representing the bias is formulated in this study as an autoregressive stationary random process with a long-term equilibrium value of zero and a constant variance (Del Giudice et al., 2013). Two parameters associated with the bias model are calibrated – the asymptotic stand. dev. of the random fluctuations around the equilibrium σ_B [l/s] and the associated correlation time τ [h]. To better fulfill underlying statistical assumptions, discharge data are transformed using a transformation function $g()$, which is the Box-Cox transformation (Box & Cox, 1964) with parameters $\lambda_1 = 0.45$ and $\lambda_2 = 1$. Therefore, error model parameters σ_E and σ_B (Table 8.1) are also employed in the transformed space with units [$g(1/s)$].

parameter	μ	σ	min.	max.
σ_E [l/s]	2	2	0.01	100
σ_B [l/s]	0.001	25	0	1000
τ [h]	0.5	0.25	0.01	3

Table 8.1: Marginal prior distribution of the error model parameters defined as truncated normal distributions with four defining parameters - mean μ , standard deviation σ , minimum, and maximum.

When calibrating the stochastic error model, data from the same 23 events as when optimizing the WAA estimation model are employed. The calibration by means of Bayesian inference (details in chapter 3.2) is performed in two steps (similarly to chapter 5.2.2). First, we use a generalized simulated annealing function which was designed to “search for a global minimum of a very complex non-linear objective function with a very large number of optima” (Xiang et al., 2013). Second, we use a numerical Monte Carlo Markov Chain sampler which “achieves often a high efficiency by tuning the proposal distributions to a user defined acceptance rate” as implemented by Scheidegger (2012) according to the proposal of Vihola (2012).

To validate the rainfall-runoff modelling performance associated with a given rainfall observation layout, we use data from the 23 events not employed in the calibration stage. We produce hydrographs of each event showing median predictions and 90% confidence intervals. For the median prediction, as well as for every single stochastic model prediction associated with a given event, we quantify the normalized Nash–Sutcliffe efficiency $NNSE$ [-] summarizing the overall performance, the relative error of the total runoff volume dV [-], the Spearman rank correlation coefficient SCC which quantifies the strength of a monotonic relationship between two variables and is independent of both linear and nonlinear bias, and dQ_{max} [-] which is the relative error of the sum of discharges during eight minutes around the observed maximal discharge (four minutes before and four after). The uncertainty of the performance metrics is analyzed by visualizing the most favorable 90% intervals within their distributions. Next, the discharge prediction reliability is quantified for each event as the fraction of discharge observations falling into the 90% confidence intervals. We also use a metric which takes into account both the prediction accuracy and precision - normalized mean interval skill score $NMISS$ [-]. It is based on the interval score (Gneiting & Raftery, 2007; Breinholt et al., 2012) which rewards the forecaster for narrow prediction intervals and, depending on a predefined confidence level, penalizes the forecaster if the observation misses the prediction interval (Eq. 3.7). This concept has been extended into mean interval skill score $MISS$ [-] (Bourgin et al., 2015; Bock et al., 2018) which benchmarks the prediction confidence bounds by reference bounds obtained, e.g., from long-term climatological data (Eq. 3.8). We apply this approach and determine $MISS$ for each event, however, we benchmark the 90% confidence bounds by the 90% range of the runoff observations for the given event. To confine its values to the interval of $[-1, 1]$, we transform $MISS$ into $NMISS$ using the equation

$$NMISS = 1/(2 - MISS), \quad (8.1)$$

8.3 Results

... We pay special attention to events with high rainfall spatial variability, as they are often associated with both a low representativeness of traditional rain gauge observations and with high rainfall intensities which are of special interest for many urban hydrology tasks, e.g. evaluation of urban stormwater systems.

8.3.1 Retrieved rainfall

60-min data from the single RG at the WWTP differ from the 1-min data from closer RGs (see Fig. 8.1)

CML QPEs calibrated to the data from the RG at the WWTP also differ other CML QPE layouts, which are very similar (!)

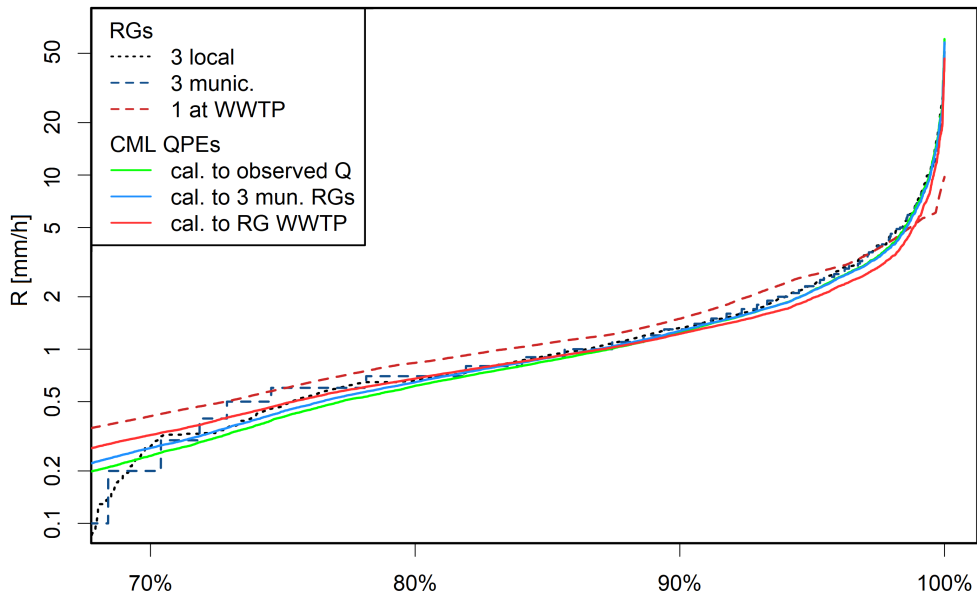


Figure 8.1: Rainfall retrieved over the 23 validation events (330 hours) ordered by the rainfall intensity R [mm/h], only showing the highest 30%. Note that the y-axis is in a log scale. All observation layouts evaluated are shown: the mean of the 1-min records from the three local rain gauges (3 local), the mean of the 1-min records from the three municipal gauges at 2–3 km distances (3 munic.), 60-min records from the single gauge at an 8-km distance (1 at WWTP), CML QPEs derived using the WAA model calibrated to observed discharges (cal. to observed Q), to data from the three municipal gagues (cal. to 3 mun. RGs), and to data from the single gauge at an 8-km distance (cal. to RG WWTP).

8.3.2 Scatter

Q modelled using CML QPEs are better (at least in volumes) than those for the municipal RGs (see Fig. 8.2)

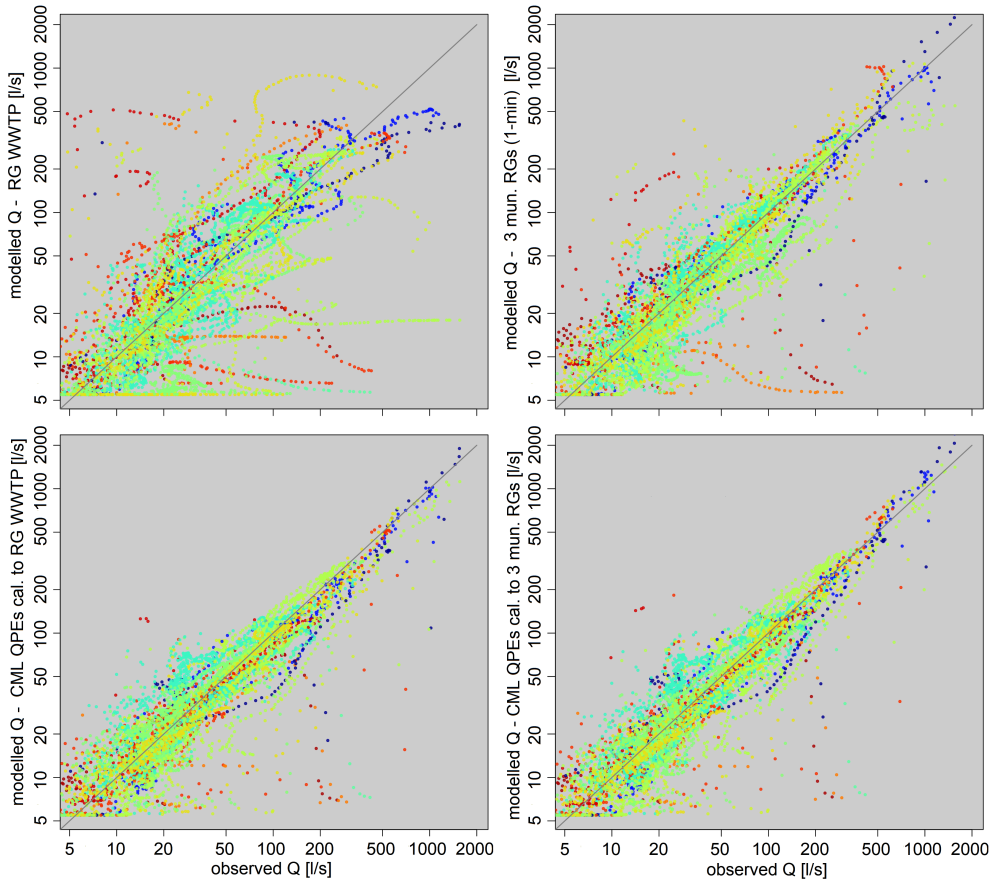


Figure 8.2: Scatterplots comparing observed and modelled discharge Q [l/s] at the level of individual data points (time steps) for four rainfall observation layouts: 60-min records from the single rain gauge at an 8-km distance, i.e. at the central WWTP (top left), 1-min records from the three municipal gauges at distances of 2–3 km (top right), CML QPEs retrieved with WAA model calibrated to the 60-min records from the gauge at the WWTP (bottom left), and CML QPEs retrieved with WAA model calibrated to the 60-min records from the three municipal gauges (bottom right). Each of the 23 events is displayed in a different colour which represents the rainfall spatial variability during the given event (blue – low variability, red – high variability). Note that the axes are in logarithmic scales.

8.3.3 Hydrographs

CML QPEs can be better than the munic. RGs also in terms of timing

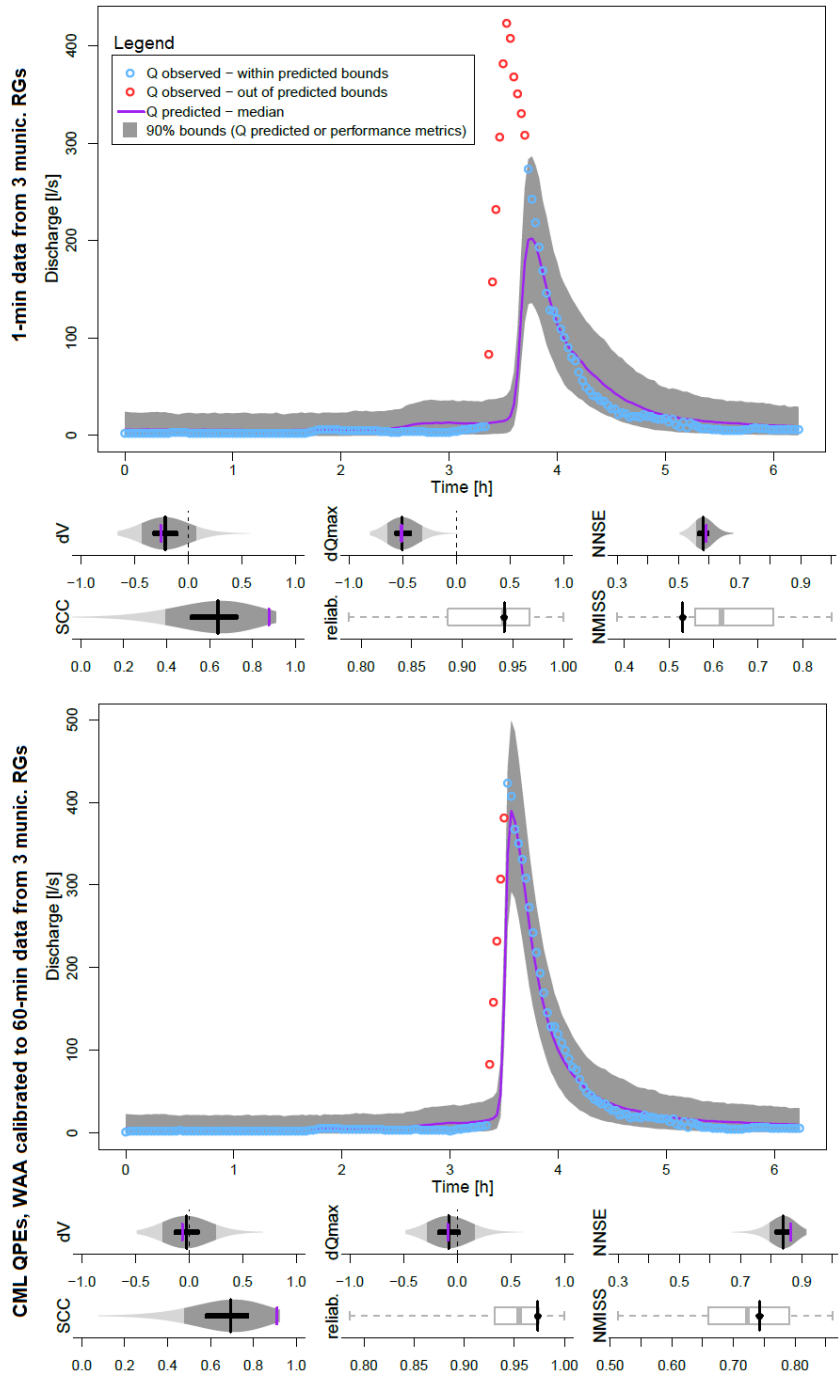


Figure 8.3: Hydrographs showing 90% prediction bounds for a chosen rainfall-runoff event (2016-08-29, 02:28) obtained using 1-min data from the three municipal rain gauges (top) and CML QPEs retrieved with the WAA model calibrated using 60-min data from the same gauges (bottom). The violin-plots show the metrics (dV , dQ_{max} , $NNSE$, SCC) which can be evaluated for each individual model prediction within the uncertainty ensemble. The other two metrics (reliability, $NMISS$) show the only value associated with the given event (in black) whereas the background boxplots (in light gray) show the variability among all 23 events.

■ 8.3.4 Summary

The above tendencies are confirmed in the summary results (Fig. 8.4)

CML QPEs calibrated to observed Q are as good as those calibrated to munic. RGs - better than munic. RGs themselves, almost as good as local RGs

For spatially most variable events (Fig. 8.5), CML QPEs calibrated to observed Q lead to least biased Q

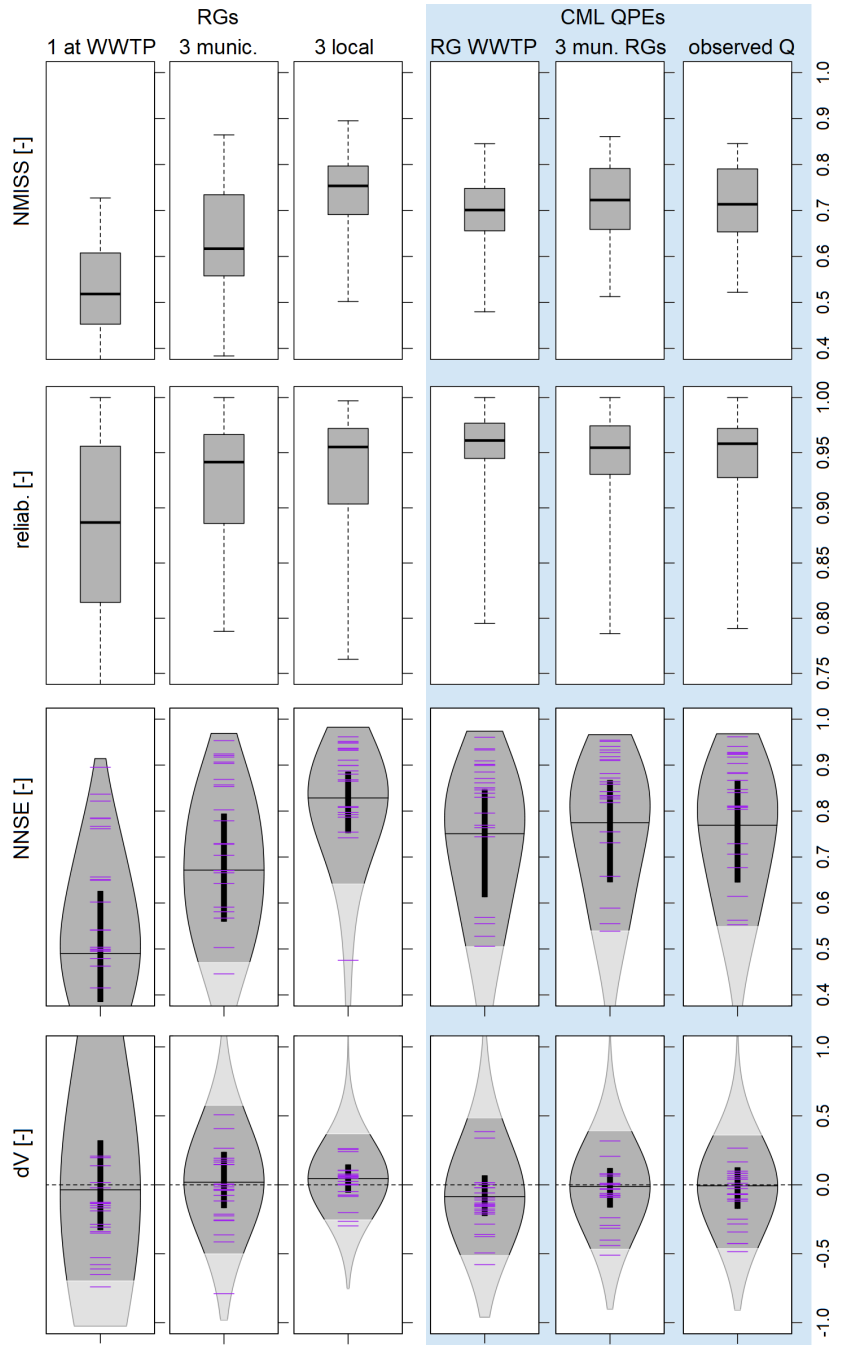


Figure 8.4: The output uncertainty of the rainfall-runoff modelling associated with all six rainfall observation layouts evaluated, summarized for all 23 events. The violin-plots show the metrics (dV , $NNSE$) which were evaluated for each individual model prediction within the uncertainty ensemble. The purple lines reflect the median predictions for each event. Areas in darker gray highlight the best 90% of the predictions. The boxplots feature metrics ($NMISS$, $reliab.$) which can be calculated only for the band prediction as a whole and thus only visualize the variability among 23 values associated with the individual events.

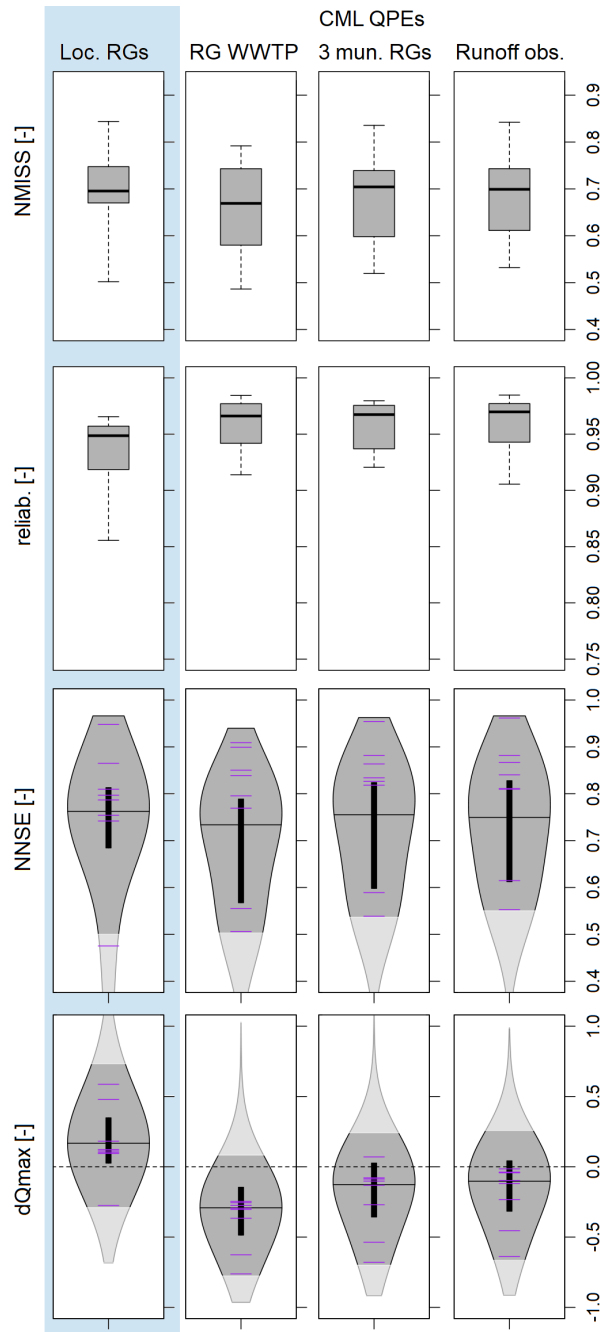


Figure 8.5: The output uncertainty of the rainfall-runoff modelling associated with the 1-min records from the three local rain gauges (left) and with all three CML QPE observation layouts, summarized for eight events with the highest rainfall spatial variability. The violin-plots show the metrics (dQ_{max} , $NNSE$) which were evaluated for each individual model prediction within the uncertainty ensemble. The purple lines reflect the median predictions for each event. Areas in darker gray highlight the best 90% of the predictions. The boxplots feature metrics (reliability, $NMISS$) which can be calculated only for the band prediction as a whole and thus only visualize the variability among eight values associated with the individual events.

8.4 Discussion

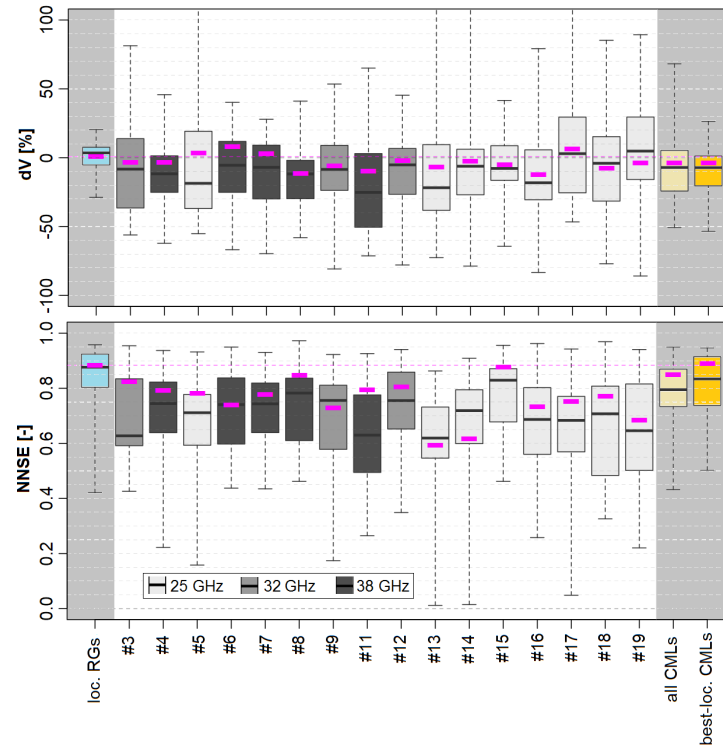


Figure 8.6: Deterministic rainfall-runoff modelling performance in terms of dV (top) and $NNSE$ (bottom) obtained using 1-min records from local rain gauges (loc. RGs), QPEs from individual CMLs (#3, ..., #19), mean QPEs from all CMLs available (all CMLs), and mean QPEs from those CMLs the paths of which best cover the catchment of interest (best-loc. CMLs; see chapter 8.2.4). All CML QPEs were retrieved using the WAA model calibrated to the 60-min data from the three municipal rain gauges. Each boxplot reflects the variability among all 23 events used for the validation. The pink bars show the performance calculated for the time series consisting of the 23 events as a whole. The CMLs are ordered according to the increasing path length, their frequencies are colour-coded.

Chapter 9

Conclusions

Lorep ipsum ?

Chapter 5 Both the CML QPEs and traditional rainfall data are used for rainfall-runoff modelling in a small urban catchment, the performance of which is evaluated against observed discharge measurements. The study's results suggest that CMLs could represent a relevant rainfall data source, especially for monitoring of heavy rainfalls, if local rain gauge data in high spatial resolution are not available in a given catchment.

9.1 bla

9.1.1 bla

the position of CMLs in respect to the small urban catchment affects their ability to capture rainfall-runoff dynamics, such as the onset of a runoff event, timing of the hydrograph rising limb, runoff peak, and recession limb;

CMLs with short paths, which typically correspond well to (sub-)catchment scales are often considerably biased, what compromises their usability for urban hydrology



Appendix

Both the CML QPEs and traditional rainfall data are used for rainfall-runoff modelling in a small urban catchment, the performance of which is evaluated against observed discharge measurements. The study's results suggest that CMLs could represent a relevant rainfall data source, especially for monitoring of heavy rainfalls, if local rain gauge data in high spatial resolution are not available in a given catchment.

Appendix

start (id)	end	duration [min]	height [mm]	R _{max} [mm/h]	R _{max,10} [mm/h]
2014-09-19 15:41	2014-09-20 00:45	544	5.7	33.9	24.3
2014-09-20 14:46	2014-09-20 17:19	153	2	10.8	7.3
2014-09-21 19:16	2014-09-22 02:27	431	7.5	9.5	6.3
2014-10-13 22:55	2014-10-14 10:15	680	18.1	19.1	17.4
2014-10-15 16:36	2014-10-16 11:25	1129	8.2	24.5	10.1
2014-10-16 17:02	2014-10-16 19:31	149	2.1	35.3	12.5
2014-10-21 21:58	2014-10-22 02:51	293	6.2	12.9	8
2014-10-22 10:36	2014-10-23 08:31	1315	11.6	5.9	3.9
2015-04-27 18:41	2015-04-28 00:21	340	8.9	30.8	18.3
2015-04-28 07:35	2015-04-28 17:11	576	8.9	10.7	7.3
2015-05-03 20:36	2015-05-04 01:15	279	2.4	5	2.4
2015-05-05 21:07	2015-05-06 12:09	902	6.9	6	3.2
2015-05-09 06:19	2015-05-09 09:15	176	2.5	10.3	8.6
2015-05-29 22:06	2015-05-30 02:47	281	10.4	54.4	39.3
2015-06-08 19:54	2015-06-09 13:11	1037	29.2	34.5	21
2015-06-13 13:50	2015-06-13 20:31	401	3.8	14.8	7.2
2015-06-23 00:22	2015-06-23 05:51	329	4.1	5.1	3.6
2015-07-07 02:12	2015-07-08 03:45	1533	6.8	35.1	18
2015-07-25 04:23	2015-07-25 17:20	777	4.5	9.8	6
2015-07-27 13:51	2015-07-27 18:01	250	5.6	43.7	28.2
2015-07-29 14:48	2015-07-29 20:23	335	3.2	16.4	8.2
2015-08-17 06:08	2015-08-19 14:28	3380	49.9	22.8	13.5
2015-09-01 16:45	2015-09-02 04:11	686	4.1	6	4.7
2015-09-07 11:03	2015-09-07 15:55	292	2.2	14	6.7
2015-09-09 12:05	2015-09-09 17:05	300	2.5	22.9	13
2015-10-07 00:55	2015-10-07 07:59	424	7.8	10.1	7.8
2015-10-07 10:15	2015-10-07 16:31	376	5	9	6.9
2015-10-07 17:17	2015-10-08 16:33	1396	10.5	4	2.3
2015-10-14 01:20	2015-10-14 18:39	1039	10.3	5.9	4.8
2015-10-14 20:48	2015-10-15 13:21	993	8.1	4.8	3.1
2015-11-15 04:02	2015-11-15 15:51	709	2.7	3.4	2
2015-11-19 16:36	2015-11-20 06:41	845	15.1	23	18.6
2015-11-20 10:48	2015-11-21 01:31	883	4.7	5.1	1.7
2015-11-30 03:28	2015-12-01 02:29	1381	11	23.8	14
2015-12-01 04:41	2015-12-01 12:11	450	3.1	7.7	4.2
2015-12-09 14:49	2015-12-09 20:35	346	2.1	3.4	1.8
2016-05-03 18:25	2016-05-04 19:36	1511	5.4	3	1.3
2016-05-24 13:53	2016-05-25 03:07	794	13.9	31.6	22.4
2016-05-31 04:41	2016-05-31 09:25	284	6.2	18.1	9.3
2016-06-02 13:19	2016-06-02 21:41	502	5.1	18	9.8
2016-06-02 23:03	2016-06-03 10:41	698	6.4	6	4.3
2016-06-12 15:47	2016-06-12 21:59	372	15.7	49.9	38.7
2016-06-16 19:20	2016-06-17 01:33	373	4.2	10.8	5.6
2016-06-17 04:36	2016-06-17 13:24	528	6.5	35.8	15.6
2016-06-25 13:54	2016-06-26 02:07	733	4.7	23	9.6

Table continues on the next page.

Table starts on the previous page.

start (id)	end	duration [min]	height [mm]	R _{max} [mm/h]	R _{max,10} [mm/h]
2016-07-01 01:55	2016-07-01 06:01	246	15.5	51.9	43.2
2016-07-12 04:46	2016-07-12 10:00	314	3.1	5.1	3.9
2016-07-13 12:45	2016-07-14 17:45	1740	18.2	14.5	10.2
2016-08-10 13:46	2016-08-10 17:03	197	3.1	8	7.2
2016-08-29 11:38	2016-08-29 19:31	473	7.4	21.6	16.7
2016-09-05 13:38	2016-09-05 17:45	247	2.4	18.7	8.7
2016-09-16 15:52	2016-09-17 12:03	1211	45.3	62.3	33.8
2016-10-02 11:35	2016-10-02 23:38	723	4.2	5.1	2.5
2016-10-03 08:56	2016-10-03 22:03	787	15.8	36.2	23
2016-10-03 23:59	2016-10-04 11:05	666	10.7	6.9	4.8
2016-10-11 13:37	2016-10-12 00:03	626	2.3	6.9	4.5
2016-10-12 01:05	2016-10-12 10:41	576	2.3	2.6	0.9
2016-10-19 05:59	2016-10-19 12:17	378	5.1	15.8	8.8
2016-10-25 02:45	2016-10-25 08:51	366	4.5	6.1	4.8

Table A.1: Rainfall

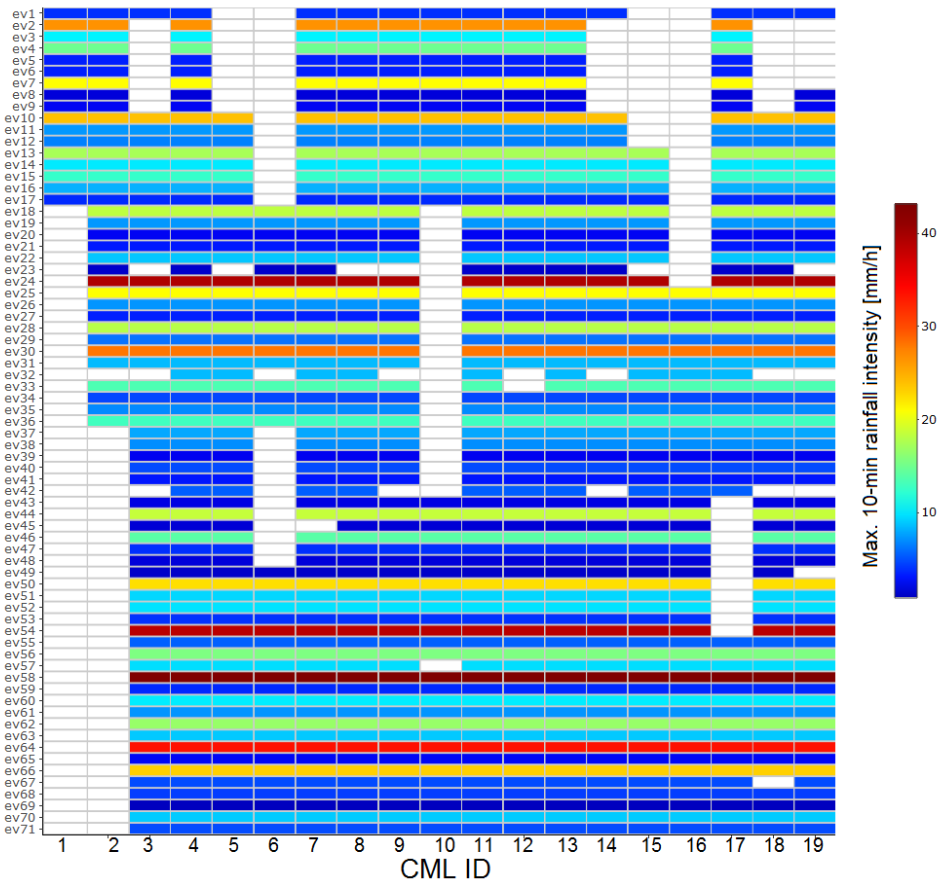


Figure A.1: Rainfall



Bibliography

- Ahm, M. & Rasmussen, M. R. (2017). Weather Radar Adjustment Using Runoff from Urban Surfaces. *Journal of Hydrologic Engineering*, 22(5).
- Anagnostou, E. N., Krajewski, W. F., & Smith, J. (1999). Uncertainty Quantification of Mean-Areal Radar-Rainfall Estimates. *Journal of Atmospheric and Oceanic Technology*, 16(2), 206–215.
- Atlas, D. & Ulbrich, C. W. (1977). Path- and Area-Integrated Rainfall Measurement by Microwave Attenuation in the 1–3 cm Band. *Journal of Applied Meteorology*, 16(12), 1322–1331.
- Bárdossy, A. & Pegram, G. (2017). Combination of radar and daily precipitation data to estimate meaningful sub-daily point precipitation extremes. *Journal of Hydrology*, 544, 397–406.
- Berne, A., Delrieu, G., Creutin, J.-D., & Obled, C. (2004). Temporal and spatial resolution of rainfall measurements required for urban hydrology. *Journal of Hydrology*, 299(3-4), 166–179.
- Berne, A. & Krajewski, W. (2013). Radar for hydrology: Unfulfilled promise or unrecognized potential? *Advances in Water Resources*, 51, 357–366.
- Beven, K. (2006). On undermining the science? *Hydrological processes*, 20, 3141–3146.
- Bock, A. R., Farmer, W. H., & Hay, L. E. (2018). Quantifying uncertainty in simulated streamflow and runoff from a continental-scale monthly water balance model. *Advances in Water Resources*, 122, 166–175.
- Borup, M., Grum, M., Linde, J. J., & Mikkelsen, P. S. (2016). Dynamic gauge adjustment of high-resolution X-band radar data for convective rain storms: Model-based evaluation against measured combined sewer overflow. *Journal of Hydrology*, 539, 687–699.
- Bourgin, F., Andréassian, V., Perrin, C., & Oudin, L. (2015). Transferring global uncertainty estimates from gauged to ungauged catchments. *Hydrology and Earth System Sciences*, 19(5), 2535–2546.

Bibliography

- Box, G. E. & Cox, D. R. (1964). An analysis of transformations. *Journal of the Royal Statistical Society. Series B (Methodological)*, (pp. 211–252).
- Brauer, C. C., Overeem, A., Leijnse, H., & Uijlenhoet, R. (2016). The effect of differences between rainfall measurement techniques on groundwater and discharge simulations in a lowland catchment: Rainfall Measurement Techniques for Hydrological Simulations. *Hydrological Processes*, 30(21), 3885–3900.
- Breinholt, A., Møller, J. K., Madsen, H., & Mikkelsen, P. S. (2012). A formal statistical approach to representing uncertainty in rainfall–runoff modelling with focus on residual analysis and probabilistic output evaluation – Distinguishing simulation and prediction. *Journal of Hydrology*, 472–473, 36–52.
- Cazzaniga, G., De Michele, C., Deidda, C., D'Amico, M., Ghezzi, A., Nebuloni, R., & Sileo, A. (2020). Calculating the hydrological response of a mountain catchment using conventional and unconventional (CML) rainfall observations: The case study of Mallero catchment. In *EGU General Assembly 2020* (pp. EGU2020–16368).
- Chen, H. & Chandrasekar, V. (2015). The quantitative precipitation estimation system for Dallas–Fort Worth (DFW) urban remote sensing network. *Journal of Hydrology*, 531, 259–271.
- Chwala, C., Gmeiner, A., Qiu, W., Hipp, S., Nienaber, D., Siart, U., Eibert, T., Pohl, M., Seltmann, J., Fritz, J., & Kunstmann, H. (2012). Precipitation observation using microwave backhaul links in the alpine and pre-alpine region of Southern Germany. *Hydrology and Earth System Sciences*, 16(8), 2647–2661.
- Chwala, C., Keis, F., & Kunstmann, H. (2016). Real-time data acquisition of commercial microwave link networks for hydrometeorological applications. *Atmospheric Measurement Techniques*, 9(3), 991–999.
- Chwala, C. & Kunstmann, H. (2019). Commercial microwave link networks for rainfall observation: Assessment of the current status and future challenges. *Wiley Interdisciplinary Reviews: Water*, 6(2), e1337.
- Cristiano, E., ten Veldhuis, M.-C., & van de Giesen, N. (2017). Spatial and temporal variability of rainfall and their effects on hydrological response in urban areas – a review. *Hydrology and Earth System Sciences*, 21(7), 3859–3878.
- D'Amico, M., Manzoni, A., & Solazzi, G. L. (2016). Use of Operational Microwave Link Measurements for the Tomographic Reconstruction of 2-D Maps of Accumulated Rainfall. *IEEE Geoscience and Remote Sensing Letters*, 13(12), 1827–1831.
- de Vos, L., Leijnse, H., Overeem, A., & Uijlenhoet, R. (2017). The potential of urban rainfall monitoring with crowdsourced automatic weather stations in Amsterdam. *Hydrology and Earth System Sciences*, 21(2), 765–777.
- Del Giudice, D., Albert, C., Rieckermann, J., & Reichert, P. (2016). Describing the catchment-averaged precipitation as a stochastic process improves parameter and input estimation. *Water Resources Research*, 52(4), 3162–3186.
- Del Giudice, D., Honti, M., Scheidegger, A., Albert, C., Reichert, P., & Rieckermann, J. (2013). Improving uncertainty estimation in urban hydrological modeling by statistically describing bias. *Hydrology and Earth System Sciences*, 17, 4209–4225.

- Deletic, A., Dotto, C., McCarthy, D., Kleidorfer, M., Freni, G., Mannina, G., Uhl, M., Henrichs, M., Fletcher, T., Rauch, W., Bertrand-Krajewski, J., & Tait, S. (2012). Assessing uncertainties in urban drainage models. *Physics and Chemistry of the Earth, Parts A/B/C*, 42–44, 3–10.
- Disch, A., Scheidegger, A., Wani, O. F., & Rieckermann, J. (2019). Impact of different sources of precipitation data on urban rainfall-runoff predictions: A comparison of rain gauges, commercial microwave links and radar. *Rainfall monitoring, modelling and forecasting in urban environments. UrbanRain18: 11th International Workshop on Precipitation in Urban Areas. Conference Proceedings*.
- Dotto, C. B., Mannina, G., Kleidorfer, M., Vezzaro, L., Henrichs, M., McCarthy, D. T., Freni, G., Rauch, W., & Deletic, A. (2012). Comparison of different uncertainty techniques in urban stormwater quantity and quality modelling. *Water research*, 46, 2545–2558.
- Ehret, U. & Zehe, E. (2011). Series distance – an intuitive metric to quantify hydrograph similarity in terms of occurrence, amplitude and timing of hydrological events. *Hydrology and Earth System Sciences*, 15(3), 877–896.
- Einfalt, T., Arnbjergnielsen, K., Golz, C., Jensen, N., Quirmbach, M., Vaes, G., & Vieux, B. (2004). Towards a roadmap for use of radar rainfall data in urban drainage. *Journal of Hydrology*, 299(3-4), 186–202.
- Ericsson (2016). Ericsson Microwave Outlook. Trends and needs in the microwave industry. <https://www.ericsson.com/assets/local/microwave-outlook/documents/ericsson-microwave-outlook-report-2016.pdf>.
- Fencl, M., Dohnal, M., Rieckermann, J., & Bareš, V. (2017). Gauge-adjusted rainfall estimates from commercial microwave links. *Hydrology and Earth System Sciences*, 21(1), 617–634.
- Fencl, M., Dohnal, M., Valtr, P., Grabner, M., & Bareš, V. (2020). Atmospheric observations with E-band microwave links – challenges and opportunities. *Atmospheric Measurement Techniques*, 13(12), 6559–6578.
- Fencl, M., Rieckermann, J., Schleiss, M., Stránský, D., & Bareš, V. (2013). Assessing the potential of using telecommunication microwave links in urban drainage modelling. *Water Science & Technology*, 68.
- Fencl, M., Rieckermann, J., Sýkora, P., Stránský, D., & Bareš, V. (2015). Commercial microwave links instead of rain gauges: Fiction or reality? *Water Science and Technology*, 71(1), 31–37.
- Fencl, M., Valtr, P., Kvičera, M., & Bareš, V. (2019). Quantifying Wet Antenna Attenuation in 38-GHz Commercial Microwave Links of Cellular Backhaul. *IEEE Geoscience and Remote Sensing Letters*, 16(4), 514–518.
- Fenia, F., Pfister, L., Kavetski, D., Matgen, P., Iffly, J.-F., Hoffmann, L., & Uijlenhoet, R. (2012). Microwave links for rainfall estimation in an urban environment: Insights from an experimental setup in Luxembourg-City. *Journal of Hydrology*, 464–465, 69–78.
- Gharesifard, M., Wehn, U., & van der Zaag, P. (2017). Towards benchmarking citizen observatories: Features and functioning of online amateur weather networks. *Journal of Environmental Management*, 193, 381–393.

Bibliography

- Gires, A., Giangola-Murzyn, A., Abbes, J.-B., Tchiguirinskaia, I., Schertzer, D., & Lovejoy, S. (2015). Impacts of small scale rainfall variability in urban areas: A case study with 1D and 1D/2D hydrological models in a multifractal framework. *Urban Water Journal*, 12(8), 607–617.
- Gneiting, T. & Raftery, A. E. (2007). Strictly proper scoring rules, prediction, and estimation. *Journal of the American Statistical Association*, 102, 359–378.
- Goldshtein, O., Messer, H., & Zinevich, A. (2009). Rain Rate Estimation Using Measurements From Commercial Telecommunications Links. *IEEE Transactions on Signal Processing*, 57(4), 1616–1625.
- Goormans, T. & Willems, P. (2013). Using Local Weather Radar Data for Sewer System Modeling: Case Study in Flanders, Belgium. *Journal of Hydrologic Engineering*, 18(2), 269–278.
- Gosset, M., Kunstmann, H., Zougmore, F., Cazenave, F., Leijnse, H., Uijlenhoet, R., Chwala, C., Keis, F., Doumounia, A., Boubacar, B., Kacou, M., Alpert, P., Messer, H., Rieckermann, J., & Hoedjes, J. (2016). Improving Rainfall Measurement in Gauge Poor Regions Thanks to Mobile Telecommunication Networks. *Bulletin of the American Meteorological Society*, 97(3), ES49–ES51.
- Graf, M., Chwala, C., Polz, J., & Kunstmann, H. (2020). Rainfall estimation from a German-wide commercial microwave link network: Optimized processing and validation for 1 year of data. *Hydrology and Earth System Sciences*, 24(6), 2931–2950.
- Gupta, H. V., Kling, H., Yilmaz, K. K., & Martinez, G. F. (2009). Decomposition of the mean squared error and NSE performance criteria: Implications for improving hydrological modelling. *Journal of Hydrology*, 377(1-2), 80–91.
- Haese, B., Hörning, S., Chwala, C., Bárdossy, A., Schalge, B., & Kunstmann, H. (2017). Stochastic Reconstruction and Interpolation of Precipitation Fields Using Combined Information of Commercial Microwave Links and Rain Gauges. *Water Resources Research*, 53(12), 10740–10756.
- Harrison, D. L., Scovell, R. W., & Kitchen, M. (2009). High-resolution precipitation estimates for hydrological uses. *Proceedings of the Institution of Civil Engineers - Water Management*, 162(2), 125–135.
- Heistermann, M., Jacobi, S., & Pfaff, T. (2013). Technical Note: An open source library for processing weather radar data (wradlib). *Hydrology and Earth System Sciences*, 17(2), 863–871.
- Honti, M., Stamm, C., & Reichert, P. (2013). Integrated uncertainty assessment of discharge predictions with a statistical error model. *Water Resources Research*, 49, 4866–4884.
- Humphrey, M. D., Istok, J. D., Lee, J. Y., Hevesi, J. A., & Flint, A. L. (1997). A New Method for Automated Dynamic Calibration of Tipping-Bucket Rain Gauges. *Journal of Atmospheric and Oceanic Technology*, 14(6), 1513–1519.
- Ichiba, A., Gires, A., Tchiguirinskaia, I., Schertzer, D., Bompard, P., & Ten Veldhuis, M.-C. (2018). Scale effect challenges in urban hydrology highlighted with a distributed hydrological model. *Hydrology and Earth System Sciences*, 22(1), 331–350.

- Imhoff, R. O., Overeem, A., Brauer, C. C., Leijnse, H., Weerts, A. H., & Uijlenhoet, R. (2020). Rainfall Nowcasting Using Commercial Microwave Links. *Geophysical Research Letters*, 47(19).
- ITU Radiocommunication Sector (2005). Recommendation 838-3: Specific attenuation model for rain for use in prediction methods.
- Kavetski, D., Kuczera, G., & Franks, S. W. (2006). Bayesian analysis of input uncertainty in hydrological modeling: 1. Theory: INPUT UNCERTAINTY IN HYDROLOGY, 1. *Water Resources Research*, 42(3).
- Kendall, M., Stuart, A., & Ord, J. (1994). *The Advanced Theory of Statistics: Distribution Theory (Vol. 1)*. Arnold, London.
- Kennedy, M. C. & O'Hagan, A. (2001). Bayesian calibration of computer models. *Journal of the Royal Statistical Society: Series B (Statistical Methodology)*, 63, 425–464.
- Kharadly, M. M. Z. & Ross, R. (2001). Effect of wet antenna attenuation on propagation data statistics. *IEEE Transactions on Antennas and Propagation*, 49(8), 1183–1191.
- Kidd, C. & Huffman, G. (2011). Global precipitation measurement: Global precipitation measurement. *Meteorological Applications*, 18(3), 334–353.
- Kleidorfer, M., Deletic, A., Fletcher, T. D., & Rauch, W. (2009). Impact of input data uncertainties on urban stormwater model parameters. *Water Science and Technology*, 60(6), 1545–1554.
- Kollo, T. & von Rosen, D. (2006). *Advanced Multivariate Statistics with Matrices*, volume 579. Springer Science & Business Media.
- Leijnse, H., Uijlenhoet, R., & Berne, A. (2010). Errors and Uncertainties in Microwave Link Rainfall Estimation Explored Using Drop Size Measurements and High-Resolution Radar Data. *Journal of Hydrometeorology*, 11(6), 1330–1344.
- Leijnse, H., Uijlenhoet, R., & Stricker, J. N. M. (2007). Rainfall measurement using radio links from cellular communication networks: RAPID COMMUNICATION. *Water Resources Research*, 43(3).
- Leijnse, H., Uijlenhoet, R., & Stricker, J. N. M. (2008). Microwave link rainfall estimation: Effects of link length and frequency, temporal sampling, power resolution, and wet antenna attenuation. *Advances in Water Resources*, 31(11), 1481–1493.
- Lorenz, C. & Kunstmann, H. (2012). The Hydrological Cycle in Three State-of-the-Art Reanalyses: Intercomparison and Performance Analysis. *Journal of Hydrometeorology*, 13(5), 1397–1420.
- Mancini, A., Lebron, R. M., & Salazar, J. L. (2019). The Impact of a Wet S-Band Radome on Dual-Polarized Phased-Array Radar System Performance. *IEEE Transactions on Antennas and Propagation*, 67(1), 207–220.
- McKee, J. L. & Binns, A. D. (2016). A review of gauge–radar merging methods for quantitative precipitation estimation in hydrology. *Canadian Water Resources Journal / Revue canadienne des ressources hydriques*, 41(1-2), 186–203.

Bibliography

- Messer, H., Zinevich, A., & Alpert, P. (2006). Environmental monitoring by wireless communication networks. *Science*, 312, 713–713.
- Montesarchio, V., Lombardo, F., & Napolitano, F. (2009). Rainfall thresholds and flood warning: An operative case study. *Natural Hazards and Earth System Sciences*, 9(1), 135–144.
- Moroder, C., Siart, U., Chwala, C., & Kunstmänn, H. (2019). Modeling of Wet Antenna Attenuation for Precipitation Estimation From Microwave Links. *IEEE Geoscience and Remote Sensing Letters*, (pp. 1–5).
- Muste, M., Lee, K., & Bertrand-Krajewski, J.-L. (2012). Standardized uncertainty analysis for hydrometry: A review of relevant approaches and implementation examples. *Hydrological Sciences Journal*, 57(4), 643–667.
- Nešpor, V. & Sevruk, B. (1999). Estimation of Wind-Induced Error of Rainfall Gauge Measurements Using a Numerical Simulation. *Journal of Atmospheric and Oceanic Technology*, 16(4), 450–464.
- Notaro, V., Fontanazza, C. M., Freni, G., & Puleo, V. (2013). Impact of rainfall data resolution in time and space on the urban flooding evaluation. *Water Science and Technology*, 68(9), 1984–1993.
- Obled, C., Wendling, J., & Beven, K. (1994). The sensitivity of hydrological models to spatial rainfall patterns: An evaluation using observed data. *Journal of Hydrology*, 159(1-4), 305–333.
- Ochoa-Rodriguez, S., Wang, L.-P., Gires, A., Pina, R. D., Reinoso-Rondinel, R., Bruni, G., Ichiba, A., Gaitan, S., Cristiano, E., van Assel, J., Kroll, S., Murlà-Tuyls, D., Tisserand, B., Schertzer, D., Tchiguirinskaia, I., Onof, C., Willems, P., & ten Veldhuis, M.-C. (2015). Impact of spatial and temporal resolution of rainfall inputs on urban hydrodynamic modelling outputs: A multi-catchment investigation. *Journal of Hydrology*, 531, 389–407.
- Ochoa-Rodriguez, S., Wang, L.-P., Willems, P., & Onof, C. (2019). A Review of Radar-Rain Gauge Data Merging Methods and Their Potential for Urban Hydrological Applications. *Water Resources Research*, 55(8), 6356–6391.
- Olsen, R., Rogers, D., & Hodge, D. (1978). The aRb relation in the calculation of rain attenuation. *IEEE Transactions on Antennas and Propagation*, 26(2), 318–329.
- Ostrometzky, J., Raich, R., Bao, L., Hansryd, J., & Messer, H. (2018). The Wet-Antenna Effect—A Factor to be Considered in Future Communication Networks. *IEEE Transactions on Antennas and Propagation*, 66(1), 315–322.
- Overeem, A., Leijnse, H., & Uijlenhoet, R. (2011). Measuring urban rainfall using microwave links from commercial cellular communication networks. *Water Resources Research*, 47(12).
- Overeem, A., Leijnse, H., & Uijlenhoet, R. (2013). Country-wide rainfall maps from cellular communication networks. *Proceedings of the National Academy of Sciences*, 110(8), 2741–2745.

- Pastorek, J. (2014). *Návrh a kalibrácia zrážko-odtokového modelu urbanizovaného povodia Praha Letňany v prostredí SWMM* [Design and calibration of a dynamic rainfall-runoff model of an urbanized catchment using the SWMM simulator]. Bachelor Thesis, Czech Technical University in Prague.
- Pastorek, J. (2016). The effect of different rainfall information on uncertainty in urban runoff modelling. Master's thesis, Czech Technical University in Prague.
- Pastorek, J., Fencl, M., & Bareš, V. (2019a). Calibrating microwave link rainfall retrieval model using runoff observations. In *Geophysical Research Abstracts*, volume 21.
- Pastorek, J., Fencl, M., Rieckermann, J., & Bareš, V. (2019b). Commercial microwave links for urban drainage modelling: The effect of link characteristics and their position on runoff simulations. *Journal of Environmental Management*, 251, 109522.
- Pastorek, J., Fencl, M., Rieckermann, J., & Bareš, V. (2022). Precipitation Estimates From Commercial Microwave Links: Practical Approaches to Wet-Antenna Correction. *IEEE Transactions on Geoscience and Remote Sensing*, 60, 1–9.
- Pastorek, J., Fencl, M., Rieckermann, J., Sýkora, P., Stránský, D., Dohnal, M., & Bareš, V. (2018). Posouzení srážkových dat z mikrovlnných spojů v městském povodí pomocí analýzy nejistot hydrologického modelu [The Evaluation of CML Rainfall Data in Urban Catchment by Means of Hydrologic Model Uncertainty]. *SOVAK: Časopis oboru vodovodů a kanalizací*, 27, 16–22.
- Pastorek, J., Fencl, M., Stránský, D., Rieckermann, J., & Bareš, V. (2017). Reliability of microwave link rainfall data for urban runoff modelling. In *Proceedings of the 14th IWA/IAHR International Conference on Urban Drainage* (pp. 1340–1343). Prague, Czech Republic.
- Peleg, N., Ben-Asher, M., & Morin, E. (2013). Radar subpixel-scale rainfall variability and uncertainty: Lessons learned from observations of a dense rain-gauge network. *Hydrology and Earth System Sciences*, 17(6), 2195–2208.
- Reichert, P. & Schuwirth, N. (2012). Linking statistical bias description to multiobjective model calibration. *Water Resources Research*, 48.
- Rico-Ramirez, M., Liguori, S., & Schellart, A. (2015). Quantifying radar-rainfall uncertainties in urban drainage flow modelling. *Journal of Hydrology*, 528, 17–28.
- Rios Gaona, M. F., Overeem, A., Leijnse, H., & Uijlenhoet, R. (2015). Measurement and interpolation uncertainties in rainfall maps from cellular communication networks. *Hydrology and Earth System Sciences*, 19(8), 3571–3584.
- Rios Gaona, M. F., Overeem, A., Raupach, T. H., Leijnse, H., & Uijlenhoet, R. (2018). Rainfall retrieval with commercial microwave links in São Paulo, Brazil. *Atmospheric Measurement Techniques*, 11(7), 4465–4476.
- Roversi, G., Alberoni, P. P., Fornasiero, A., & Porcù, F. (2020). Commercial microwave links as a tool for operational rainfall monitoring in Northern Italy. *Atmospheric Measurement Techniques*, 13(11), 5779–5797.

Bibliography

- Saltikoff, E., Friedrich, K., Soderholm, J., Lengfeld, K., Nelson, B., Becker, A., Hollmann, R., Urban, B., Heistermann, M., & Tassone, C. (2019). An Overview of Using Weather Radar for Climatological Studies: Successes, Challenges, and Potential. *Bulletin of the American Meteorological Society*, 100(9), 1739–1752.
- Salvadore, E., Bronders, J., & Batelaan, O. (2015). Hydrological modelling of urbanized catchments: A review and future directions. *Journal of Hydrology*, 529, 62–81.
- Scheidegger, A. (2012). adaptMCMC: Implementation of a generic adaptive monte carlo markov chain sampler. R package version 1.1.
- Schellart, A., Shepherd, W., & Saul, A. (2012). Influence of rainfall estimation error and spatial variability on sewer flow prediction at a small urban scale. *Advances in Water Resources*, 45, 65–75.
- Schilling, W. (1991). Rainfall data for urban hydrology: What do we need? *Atmospheric Research*, 27(1), 5–21.
- Schleiss, M. & Berne, A. (2010). Identification of Dry and Rainy Periods Using Telecommunication Microwave Links. *IEEE Geoscience and Remote Sensing Letters*, 7(3), 611–615.
- Schleiss, M., Olsson, J., Berg, P., Niemi, T., Kokkonen, T., Thorndahl, S., Nielsen, R., Ellerbæk Nielsen, J., Bozhinova, D., & Pulkkinen, S. (2020). The accuracy of weather radar in heavy rain: A comparative study for Denmark, the Netherlands, Finland and Sweden. *Hydrology and Earth System Sciences*, 24(6), 3157–3188.
- Schleiss, M., Rieckermann, J., & Berne, A. (2013). Quantification and Modeling of Wet-Antenna Attenuation for Commercial Microwave Links. *IEEE Geoscience and Remote Sensing Letters*, 10(5), 1195–1199.
- Schütze, M., Campisano, A., Colas, H., Schilling, W., & Vanrolleghem, P. (2004). Real time control of urban wastewater systems - Where do we stand today? *Journal of Hydrology*, 299(3-4), 335–348.
- Segond, M.-L., Wheater, H. S., & Onof, C. (2007). The significance of spatial rainfall representation for flood runoff estimation: A numerical evaluation based on the Lee catchment, UK. *Journal of Hydrology*, 347(1-2), 116–131.
- Sikorska, A. & Seibert, J. (2018). Value of different precipitation data for flood prediction in an alpine catchment: A Bayesian approach. *Journal of Hydrology*, 556, 961–971.
- Sikorska, A. E., Scheidegger, A., Banasik, K., & Rieckermann, J. (2012). Bayesian uncertainty assessment of flood predictions in ungauged urban basins for conceptual rainfall-runoff models. *Hydrology and Earth System Sciences*, 16(4), 1221–1236.
- Smiatek, G., Keis, F., Chwala, C., Fersch, B., & Kunstmänn, H. (2017). Potential of commercial microwave link network derived rainfall for river runoff simulations. *Environmental Research Letters*, 12(3), 034026.
- Spekkers, M. H., Kok, M., Clemens, F. H. L. R., & ten Veldhuis, J. A. E. (2013). A statistical analysis of insurance damage claims related to rainfall extremes. *Hydrology and Earth System Sciences*, 17(3), 913–922.

- Stránský, D., Fencl, M., & Bareš, V. (2018). Runoff prediction using rainfall data from microwave links: Tabor case study. *Water Science and Technology*, 2017(2), 351–359.
- Sun, Q., Miao, C., Duan, Q., Ashouri, H., Sorooshian, S., & Hsu, K.-L. (2018). A Review of Global Precipitation Data Sets: Data Sources, Estimation, and Intercomparisons. *Reviews of Geophysics*, 56(1), 79–107.
- Swan, M. (2012). Sensor Mania! The Internet of Things, Wearable Computing, Objective Metrics, and the Quantified Self 2.0. *Journal of Sensor and Actuator Networks*, 1(3), 217–253.
- Tauro, F., Selker, J., van de Giesen, N., Abrate, T., Uijlenhoet, R., Porfiri, M., Manfreda, S., Caylor, K., Moramarco, T., Benveniste, J., Ciraolo, G., Estes, L., Domeneghetti, A., Perks, M. T., Corbari, C., Rabiei, E., Ravazzani, G., Bogena, H., Harfouche, A., Brocca, L., Maltese, A., Wickert, A., Tarpanelli, A., Good, S., Lopez Alcala, J. M., Petroselli, A., Cudennec, C., Blume, T., Hut, R., & Grimaldi, S. (2018). Measurements and Observations in the XXI century (MOXXI): Innovation and multi-disciplinarity to sense the hydrological cycle. *Hydrological Sciences Journal*, 63(2), 169–196.
- Thorndahl, S., Beven, K., Jensen, J., & Schaarup-Jensen, K. (2008). Event based uncertainty assessment in urban drainage modelling, applying the GLUE methodology. *Journal of Hydrology*, 357(3-4), 421–437.
- Thorndahl, S., Einfalt, T., Willems, P., Nielsen, J. E., ten Veldhuis, M.-C., Arnbjerg-Nielsen, K., Rasmussen, M. R., & Molnar, P. (2017). Weather radar rainfall data in urban hydrology. *Hydrology and Earth System Sciences*, 21(3), 1359–1380.
- Tsihrintzis, V. A. & Hamid, R. (1997). Modeling and Management of Urban Stormwater Runoff Quality: A Review. *Water Resources Management*, 11(2), 136–164.
- Uhlenbeck, G. E. & Ornstein, L. S. (1930). On the theory of the Brownian motion. *Physical review*, 36, 823.
- Uijlenhoet, R., Overeem, A., & Leijnse, H. (2018). Opportunistic remote sensing of rainfall using microwave links from cellular communication networks. *Wiley Interdisciplinary Reviews: Water*, 5(4), e1289.
- Valtr, P., Fencl, M., & Bareš, V. (2019). Excess Attenuation Caused by Antenna Wetting of Terrestrial Microwave Links at 32 GHz. *IEEE Antennas and Wireless Propagation Letters*, 18(8), 1636–1640.
- van der Pol, T., van Ierland, E., Gabbert, S., Weikard, H.-P., & Hendrix, E. (2015). Impacts of rainfall variability and expected rainfall changes on cost-effective adaptation of water systems to climate change. *Journal of Environmental Management*, 154, 40–47.
- van Leth, T. C., Overeem, A., Leijnse, H., & Uijlenhoet, R. (2018). A measurement campaign to assess sources of error in microwave link rainfall estimation. *Atmospheric Measurement Techniques*, 11(8), 4645–4669.
- Vezzaro, L. & Grum, M. (2014). A generalised Dynamic Overflow Risk Assessment (DORA) for Real Time Control of urban drainage systems. *Journal of Hydrology*, 515, 292–303.

Bibliography

- Vihola, M. (2012). Robust adaptive Metropolis algorithm with coerced acceptance rate. *Statistics and Computing*, 22, 997–1008.
- Villarini, G., Mandapaka, P. V., Krajewski, W. F., & Moore, R. J. (2008). Rainfall and sampling uncertainties: A rain gauge perspective. *Journal of Geophysical Research*, 113(D11), D11102.
- Vrugt, J. A., ter Braak, C. J. F., Clark, M. P., Hyman, J. M., & Robinson, B. A. (2008). Treatment of input uncertainty in hydrologic modeling: Doing hydrology backward with Markov chain Monte Carlo simulation: FORCING DATA ERROR USING MCMC SAMPLING. *Water Resources Research*, 44(12).
- Wang, L.-P., Ochoa-Rodríguez, S., Onof, C., & Willems, P. (2015). Singularity-sensitive gauge-based radar rainfall adjustment methods for urban hydrological applications. *Hydrol. Earth Syst. Sci.*, 19(9), 4001–4021.
- Wang, L.-P., Ochoa-Rodríguez, S., Simões, N. E., Onof, C., & Maksimović, Č. (2013). Radar–raingauge data combination techniques: A revision and analysis of their suitability for urban hydrology. *Water Science and Technology*, 68(4), 737–747.
- Wang, Q., Shrestha, D. L., Robertson, D., & Pokhrel, P. (2012). A log-sinh transformation for data normalization and variance stabilization. *Water Resources Research*, 48.
- Willems, P., Arnbjerg-Nielsen, K., Olsson, J., & Nguyen, V. (2012). Climate change impact assessment on urban rainfall extremes and urban drainage: Methods and shortcomings. *Atmospheric Research*, 103, 106–118.
- Wood, S. J., Jones, D. A., & Moore, R. J. (2000). Accuracy of rainfall measurement for scales of hydrological interest. *Hydrology and Earth System Sciences*, 4(4), 531–543.
- Xiang, Y., Gubian, S., Suomela, B., & Hoeng, J. (2013). Generalized Simulated Annealing for Efficient Global Optimization: The GenSA Package for R. *The R Journal*, 5(1).
- Zinevich, A., Messer, H., & Alpert, P. (2010). Prediction of rainfall intensity measurement errors using commercial microwave communication links. *Atmospheric Measurement Techniques*, 3(5), 1385–1402.